DESIGN AND PERFORMANCE ANALYSIS OF MULTISTAGE CENTRIFUGAL PUMP USING CFD

A Thesis submitted

in Partial Fulfilment of the Requirements for the

Degree of

DOCTOR OF PHILOSOPHY

in

the Department of

MECHANICAL ENGINEERING

Submitted

By

DURVESH

(2K19/PHDME/504)

Under the Supervision of

Prof. Rajkumar Singh **Dr. Manjunath K.**

Department of Mechanical, Production & Industrial Engg. and Automobile Engg.

DELHI TECHNOLOGICAL UNIVERSITY

(Formerly Delhi College of Engineering)

Shahbad Daulatpur, Main Bawana Road Delhi-110042, India

August, 2025

DELHI TECHNOLOGICAL UNIVERSITY

Shahbad Daulatpur, Main Bawana Road

Delhi-110042 (India)

CANDIDATE'S DECLARATION

I **Durvesh (2K19/PHDME/504)** hereby declare that thesis entitled **"Design and Performance Analysis of Multistage Centrifugal Pump using CFD"** submitted by me in fulfillment of the requirement for the degree of Doctor of Philosophy to Delhi Technological University (Formerly Delhi College of Engineering) is a record of bona fide work carried out by me under the supervision of **Dr. Rajkumar Singh,** Professor, Department of Mechanical Engineering, Delhi Technological University and **Dr. Manjunath K.,** Associate Professor, Department of Mechanical Engineering, Delhi Technological University.

I further declare that the work reported in this thesis has not been published and will not be submitted, either in part or in full, for the award of any other degree or diploma in any other Institute or University.

Candidate's Signature

DELHI TECHNOLOGICAL UNIVERSITY

Shahbad Daulatpur, Main Bawana Road

Delhi-110042 (India)

CERTIFICATE

This is to certify that the work embodied in the *Thesis* entitled **"Design and Performance Analysis of Multistage Centrifugal Pump using CFD"** is a record of bona fide research work carried out by **Ms. Durvesh** (**2K19/PHDME/504**) in fulfillment of requirements for the award of the degree of **Doctor of Philosophy** in **Mechanical Engineering** specialization in **Thermal Engineering**. She has worked under our guidance and supervision and has fulfilled the requirements to reach the requisite standard for submitting the thesis.

The results in this thesis have not been submitted in part or in full at any other University or Institute for the award of any degree or diploma. This is to certify that the student has incorporated all the corrections suggested by the examiners in the thesis, and the statement made by the candidate is correct to the best of our knowledge.

(**Dr. Rajkumar Singh**)
Professor
Mechanical Engineering Department
Delhi Technological University
Delhi-110042 (India)

(**Dr. Manjunath K.**)
Associate Professor
Mechanical Engineering Department
Delhi Technological University
Delhi-110042 (India)

This Thesis is
Dedicated to My Loving Family

DELHI TECHNOLOGICAL UNIVERSITY

Shahbad Daulatpur, Main Bawana Road

Delhi-110042 (India)

ACKNOWLEDGEMENT

Firstly, I would like to express my gratitude to my Supervisors**, Prof. Rajkumar Singh and Dr. Manjunath K.,** for their pertinent support of my Ph.D. study and related research, for their patience, motivation, and immense knowledge. Their valuable guidance and mentorship helped me throughout the research and thesis writing. This thesis could not have attained its present form without their supervision, academic support, and interest in the research work.

Besides my supervisors, I would like to thank Prof. Atul Kumar Agarwal, DRC Chairman, Department of Mechanical Engineering, for his valuable suggestions and encouragement. I am extremely thankful to **Prof. R.C Singh**, **Prof. Amit Pal**, **Prof Vijay Gautam**, **Prof R.S. Mishra, Dr. Sanjay Kumar, and Dr. M.S. Niranjan of the Department of Mechanical Engineering, Prof. A. K. Sahu of the Department of Civil Engineering, Delhi Technological University,** for their constant encouragement.

I am extremely thankful to **Prof. B.B. Arora**, HOD, Department of Mechanical Engineering, Delhi Technological University, for his constant support. I also want to express my gratitude to **Prof. Prateek Sharma**, the honorable Vice Chancellor, Delhi Technological University, for giving me this opportunity.

I would like to express my sincere appreciation to **Prof. Vishnu Prashad**, Dr. Charu Parashar, and Dr. Ruchi Khare, Department of Civil Engineering, MANIT, Bhopal, for teaching me the subject Computational Fluid Dynamics, which is an integral part of my PhD work. I would like to thank the technical staff, Mr. Narendra Bist, for helping me during lab engagements.

I always got constant encouragement from **Mr. Subodh Kumar Yadav,** a very good friend of mine. I am extremely thankful to **Mr. Anant Bhardwaj, Mr. Bandla Sheshvenkat Naidu**, and **Mr. Gaurav Kumar** for their constant support and help during my experimental and writing work, and for providing moral support. I am thankful to my friends **Dr. Jyoti Rani, Dr. Km. Komal,** and **Dr. Priya Yadav** for there with me in my PhD journey whenever I need them. Your friendship and solidarity have made the challenges more manageable and the victories sweeter. A special thanks to my Warden, Dr. Anamika Chauhan, and all the attendants in the hostel for being there and for their full support during my stay in the hostel, and serving as assistant warden.

I am indebted to my father, **Mr. Vijendra Pal**, and mother, **Mrs. Kanta Devi**, for their encouragement. Their patience, support, and sacrifices have been a constant source of motivation and strength. This achievement is as much yours as it is mine. I am extremely thankful to my elder sister, Mrs. **Hirdesh Yadav**, my brother-in-law, **Mr. Vipin Yadav**, and my brothers, **Mr. Jay Yadav**, for creating an amicable environment at the domestic front such that I would be able to concentrate on my work. I gratefully acknowledge my cousins, **Mr. Sunil Yadav, Mr. Sushil Yadav, Mr. Arvind Yadav, Mr. Kushlendra Yadav, Mr. Sumit Yadav**, **Mrs. Neelam Yadav, Ms. Priya Yadav, and Ms. Anamika Yadav** for their constant support, understanding, and encouragement. I also express my sincere thanks to my fellow Ph.D. friends for their constant encouragement.

Last but not least, my two lovely nieces **Nimmi** and **Naina**, for their beautiful smile, infectious laughter, boundless energy, curiosity, and unconditional affection throughout the duration of my doctoral thesis journey. Their presence, as a beacon of my joy and innocence, brought warmth and inspiration to my daily life. I would like to thank the Almighty for giving me constant patience, keeping me calm during my Ph.D. journey.

Lastly, I would like to thank all the countless individuals, institutions, and resources that have contributed to this research in various ways, directly or indirectly. Your collective efforts have been indispensable in the completion of this doctoral thesis.

Thank you all for being an integral part of this remarkable journey.

Durvesh

2K19/PHD/ME/504

Table of Contents

LIST OF FIGURES

LIST OF TABLES

NOMENCLATURE

C	Absolute velocity	b_1	Impeller inlet width
C_1	Absolute velocity at impeller inlet	Ac	Cross-sectional area
C_2	Absolute velocity at impeller outlet	V_f	Flow velocity
C_3	Absolute velocity in the volute	V_3	Diffuser inlet velocity
W	Relative velocity	V_4	Diffuser outlet velocity
W_1	Relative velocity at impeller inlet	d	Diffusion coefficient
W_2	Relative velocity at impeller outlet	α_1	Inlet flow angle to impeller
C_{u1}	Whirl velocity at impeller inlet	α_2	Outlet flow angle to impeller
C_{u2}	Whirl velocity at impeller outlet	β_1	Inlet blade angle
C_{m1}	Meridional velocity at impeller inlet	β_2	Outlet blade angle
C_{m2}	Meridional velocity at impeller outlet	R_c	Radius of curvature
C_{m3}	Meridional velocity in the volute	R_1	Impeller inlet radius
U_1	Peripheral velocity at impeller inlet	R_2	Impeller outlet radius
U_2	Peripheral velocity at impeller outlet	γ	Specific weight of water
P_{in}	Input Power	H_e	Euler's head
P_{out}	Output Power	H^*	Head coefficient
η	Hydraulic efficiency	P^*	Power coefficient
N	Rotational speed of impeller	H	Head generated
ω	Angular velocity of impeller	Ψ	Flow coefficient
N_S	Specific speed of centrifugal pump	Φ	Speed coefficient
Q	Flow rate	g	Gravity

Abstract

A multistage centrifugal pump is a specific type of centrifugal pump featuring multiple impellers arranged in series on a single shaft. While a typical centrifugal pump uses a volute casing, a multistage pump employs a diffuser that serves a similar function. To guide the flow to the next impeller, a return passage channel is utilized.

To conduct numerical flow simulations for multistage pumps, it is necessary to first perform an analysis of a single-stage pump and then further for the multistage pump. A single-stage model is created in Creo-parametric software, where each domain, i.e., impeller, diffuser, and return passage, is modeled separately. The model is then imported into ANSYS 22R1 for part meshing of each domain. Subsequently, the model is imported into CFX –PRE, where boundary conditions at the inlet and the outlet are applied, and the domains are interfaced with each other. The flow simulation is carried out using the k-ε turbulence model. The flow analysis is performed for different numbers of blades (5, 6, and 7) at varying speeds from 1450 rpm to 1900 rpm while maintaining a constant discharge. The results show that the pump performance increases with speed, with the highest efficiency observed for 1900 rpm. The response surface approach was employed to enhance the hydraulic performance of the pump at the rated point. Specifically, an approximate link between the design head and efficiency of the single-stage centrifugal pump and the parameters of the impeller's design was established. The first step in creating a one-factor experimental design involved selecting significant geometric variables as factors. Decision variables such as the number of blades, flow rate, and rotation were chosen due to their significant impact on hydraulic performance, while head and efficiency were considered as responses. Subsequently, the best-optimized values for each level of the parameters were identified using response surface analysis and a central composite design. The impeller schemes of the Design-Expert software were evaluated for head and efficiency using Computational fluid dynamics, and a total of 20 experiments were conducted. The simulated results were then validated with experimental data. Through the analysis of the individual parameters and the approximation model, the ideal parameter combination that increased head and efficiency by 7.90% and 2.06%, respectively, at the rated value was discovered. It is worth noting that in cases of a high rate of flow, the inner flow was also enhanced.

After analyzing the single-stage pump, the three best-performing configurations based on speed are selected for further flow simulation of a two-stage centrifugal pump for different blades, varying from 5, 6, and 7, with the speed and mass flow kept constant at 1900 rpm and 128.8 kg/s, respectively. It is observed that the two-stage pump with a 7-blade impeller rotating at 1900 rpm provides the highest head among all configurations. It is also observed that losses in the diffuser of the 1st stage and 2nd stage are almost the same, but head losses in the return passage of the 1st stage and 2nd stage have differences of 19.99%, 28.5%, and 23.59% for 5, 6, and 7 blades, respectively. For compacting the design structure of the Centrifugal Pump, three different types of return guide vanes (mixed return guide vane, radial return guide vane, and distorted return guide vane) are modeled and analyzed using ANSYS 22R1 with the same configurations used in a two-stage pump. The results show that the radial return guide vanes give the best vane efficiency and lower loss coefficients. Further, the analysis is done on a radial guide vane with varying vane outlet angles (20, 25, and 30). From this analysis, we found that the radial guide vane with 25 degrees gives the best vane efficiency and less loss coefficient. This thesis provides valuable insights for optimizing multistage centrifugal pump designs, enhancing efficiency and performance in industries like water treatment, oil and gas, and chemical processing. By applying these findings, engineers can achieve higher energy efficiency, reduced operational costs, and improved reliability in pump systems.

CHAPTER 1. INTRODUCTION

This chapter defines the introduction of centrifugal pumps and multistage pumps, the classification of pumps, the components of the multistage pump, and the thesis layout.

1.1 GENERAL

A centrifugal pump is a work-absorbing turbo machinery device that converts mechanical

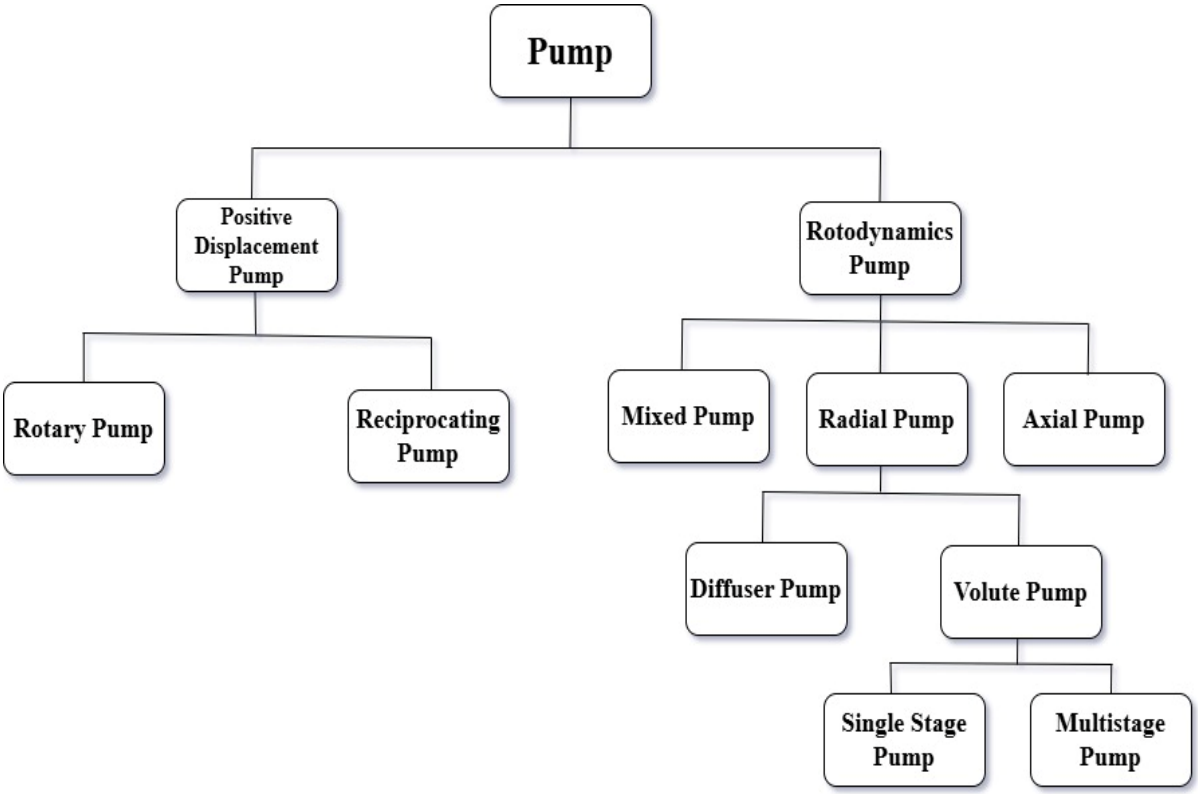

energy into pressure energy of the water being pumped, which results in raising the water from a lower elevation to a higher elevation. This is attained by creating a suction pressure at the inlet and a higher pressure at the outlet [1]. The system has two parts: one rotating part (impeller) and another stationary part (volute or diffuser). As the impeller rotates, it forces the liquid outward, creating a centrifugal force that converts the driving energy into kinetic energy. The function of a volute or diffuser is to convert kinetic energy into pressure energy.

1.2 CLASSIFICATION OF PUMPS

Fig. 1.1 Classification of Pump [1]

1.3 CLASSIFICATION OF CENTRIFUGAL PUMPS

Pumps can be classified according to the different features:

1.3.1 Working Head

The working head is a head where the pump delivers the fluid at a certain height. According to the range of working heads, they are further classified into three types. [2].

(a) Low lift centrifugal pump: are the pumps capable of having a working head up to 15m. It consists of a volute casing and no guide vanes.

(b) Medium lift centrifugal pump: is a pump that has a working head as high as 40m. This pump basically contains a guide vane system.

(c) High Lift centrifugal pump: is applied to build a head above 40m. These pumps are mainly multistage centrifugal pumps containing more than one impeller. This may be in horizontal type or vertical type. The above shown figure, Fig. 1.1, shows the classification of pumps.

1.3.2 Type of Casing

The casing is the main part of the pump, having a gradually increasing cross-section, where the velocity of fluid decreases and pressure increases. According to shape, it is classified into

(a) Volute casing: it's a spiral form of casing having a gradually increasing cross-sectional area from the tongue till the delivery pipe. The delivery exit may be tangential to the spiral or may be at the center of the pump axis. The volute casing may be a cross-section of circular, rectangular, or trapezoidal shape. Among these three,the circular gives the best efficiency and minimum hydraulic losses. The function ofthe spiral casing is to collect fluid from the impeller and deliver it to the outlet pipe at a constantvelocity. From the discharge equation,

$$Q = A_c . V_f \quad (1.1)$$

Cross-sectional area is inversely proportional to the velocity of flow; therefore, in casing, Ac increases, which causes the velocity of flow to reduce, thus resulting in a risein pressure.

(b) Diffuser pump: A Vaned diffuser is a stationary part surrounding the impeller. Its function is the same as that of volute casing, i.e., conversion of velocity head into pressure head. It consists of stationary vanes called diffuser vanes. The inlet flow section is smaller compared to the outlet, which means an increase in flow passage.

Due to this, the water flowing in a diffuser passage causes a decrease in velocity as the cross section is inversely proportional to flow velocity, which results in a rise in pressure.

1.3.3 Types of impeller

Depending on the viscosity of the fluid, the pump impeller is categorized into,

(a) Open impeller: The impeller consists only of blades and no shroud. Such pumps are basically used in dredgers and fluid containing solid particles. The impeller has to work under rough duty, so it is mostly made up of forged steel.

(b) Semi-open impeller: The impeller has only a single shroud, and this is used for viscous fluids like sewage water, paper pulp, etc. The impeller has less number of blades and their height is somewhat more.

(c) Closed impeller: The impeller blades are enclosed between the shrouds, and such an impeller is used to handle non-viscous fluids like water, oil, chemicals, etc. Fig. 1.2 shows the types of impellers

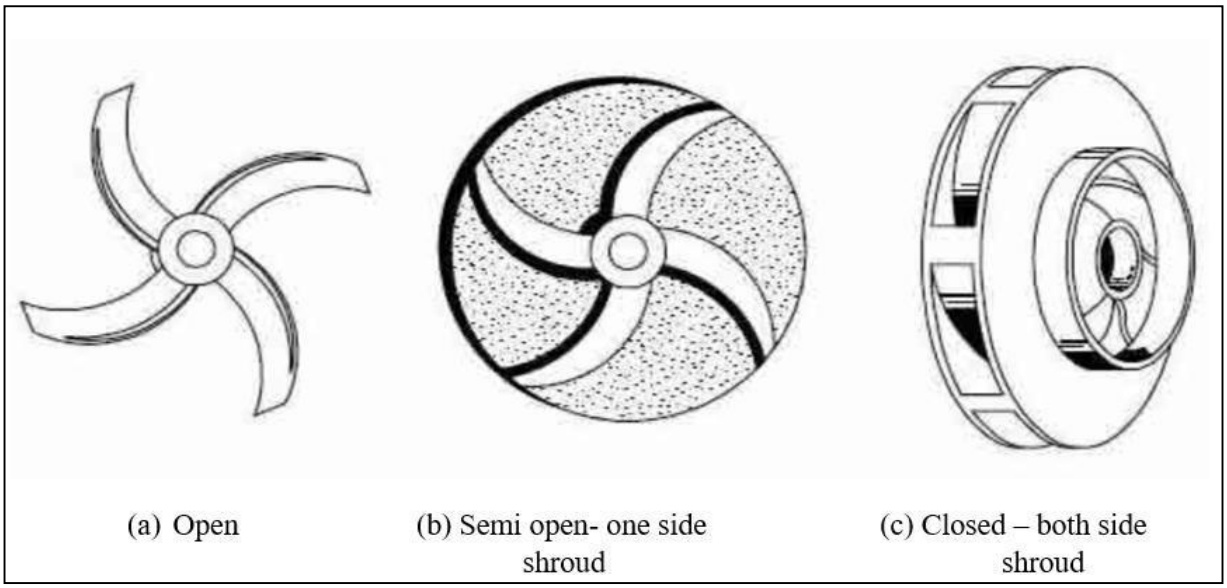

Fig. 1.2 Types of impellers

1.3.4 Number of Stages

(a) Single-Stage Centrifugal Pump: The pump consists of a single impeller keyed tothe shaft.

(b) Multistage Centrifugal Pump: A multistage centrifugal pump is basically a classification of general centrifugal pumps; it consists of two or more impellers arranged in series and mounted on the same shaft of the rotor. The purpose of mounting an impeller in series is to achieve a high head. Fig. 1.3 shows the number of stages of a centrifugal pump.

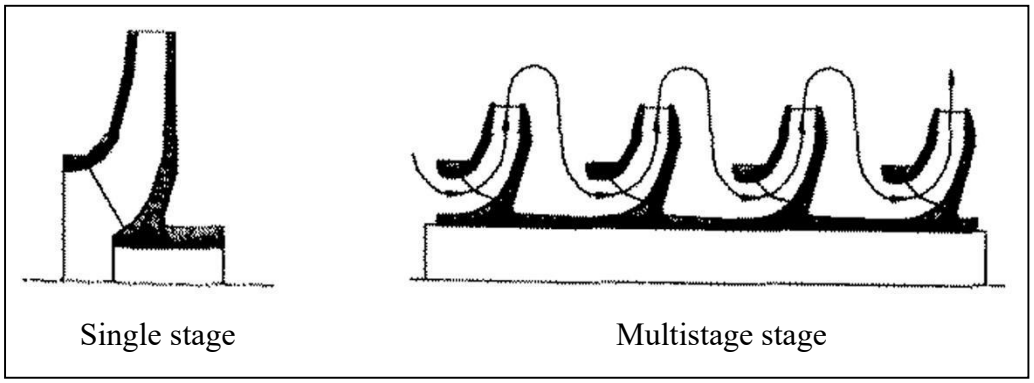

Fig. 1.3 Number of stages

1.3.5 Direction of flow through impeller:

(a) Radial flow pump: In this pump, fluid enters axially and discharges radially. This pump has a low specific speed.

(b) Mixed flow Pump: It's a combination of radial flow and axial flow pump. The impeller acts like the propeller of a ship. Such a type of pump is mostly used in irrigationfields where the requirement of discharge is higher at low heads.

(c) Axial flow pump: It consists of an aerofoil blade. The impeller is the same as that of the propeller or Kaplan turbine, which is run in reverse order. Water flows axially inward and axially outward. These are used to deliver large quantities of water atlow heads. The specific speed of such a pump is high among all pumps. The figure Fig. 1.4 shows different flow through the impeller.

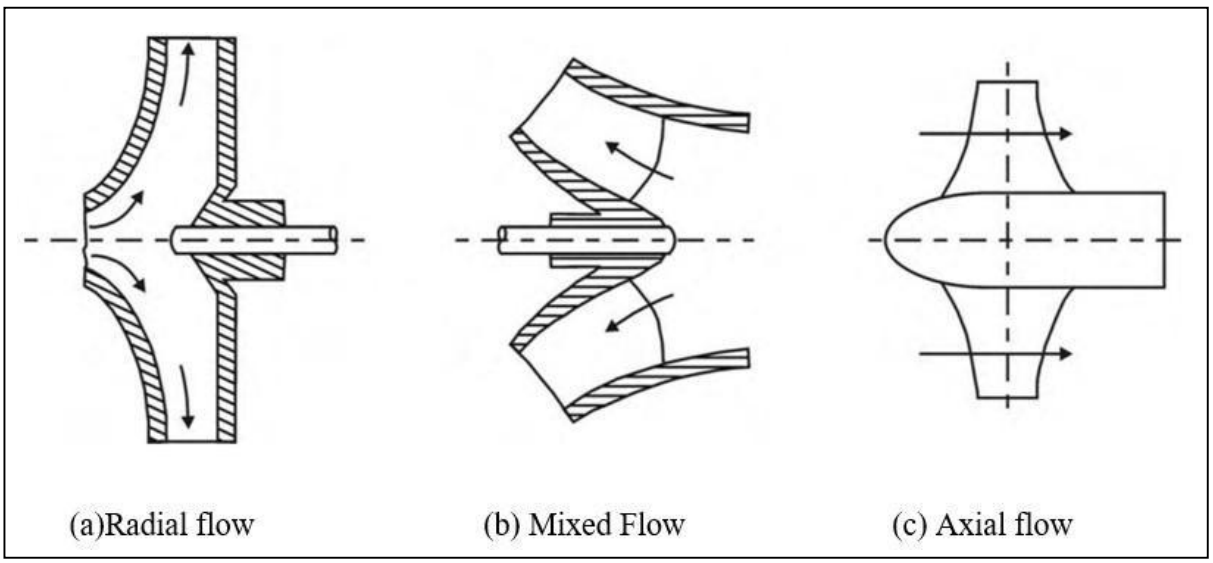

Fig. 1.4 Different flow through Impeller

1.3.6 Number of Entrances to the Impeller:

(a) Single suction pump: In a single suction pump, the impeller has only one eye i.e., liquid enters only from one side.

(b) Double Suction Pump: In a double suction pump, the impeller has two eyes, i.e., liquid enters from both sides of the impeller. The pump has a split-type casing. This is shown in Fig. 1.5, which shows the number of entrances to the pump.

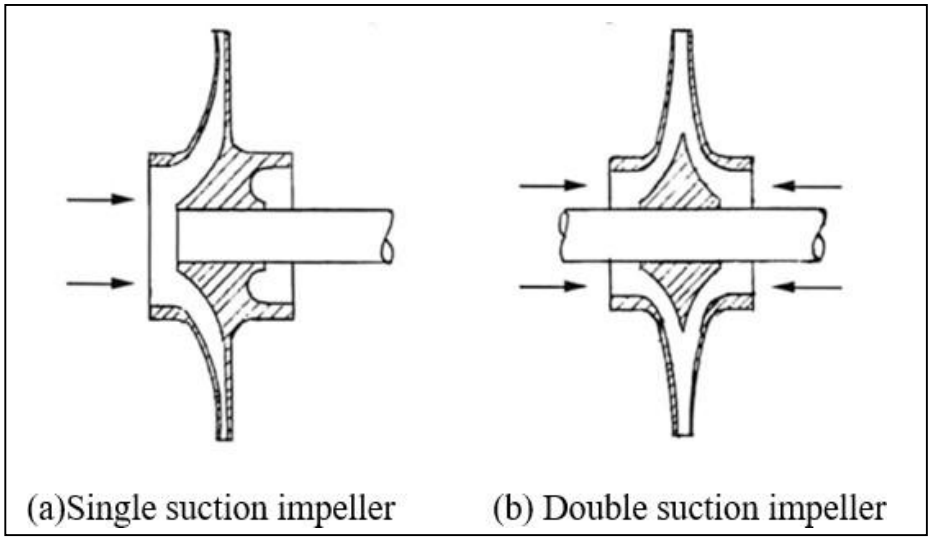

Fig. 1.5 Number of entrances to the pump

1.4 MULTISTAGE CENTRIFUGAL PUMP

A multistage centrifugal pump is a classification of a general centrifugal pump; it consists of two or more impellers arranged in series and mounted on the same shaft of the rotor.The purpose of mounting the impeller in series is to achieve a high head. Fluid enters into the first impeller then passes through the vane diffuser which is just attached peripheral to the impeller after passing over diffuser fluid takes a sharp turn to back side of impeller and enters into return channel where the return vane guides the fluid to the next eye of the the impeller and thus in such a way fluid passes from each stage in multistage centrifugal pump. [2].As the machine contains more impellers and has to produce greater pressure, the speed required for such a type is more than 1000 rpm. It is to be noted that the volumetric flow is the same through each impeller. The application of a multistage centrifugal pump is found in reverse osmosis, spray, boiler feed, pressure boosting, snow making, high-pressure draining, and mine dewatering. Fig. 1.6 and Fig. 1.7 show the sectional view of a multistage centrifugal pump, and the principle of a centrifugal pump, respectively.

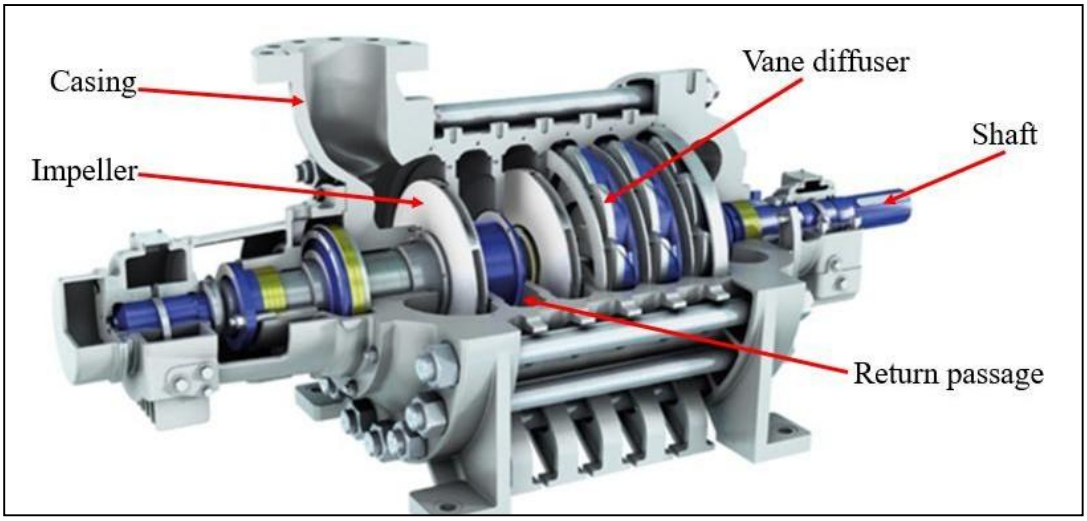

Fig. 1.6 Sectional view of multistage centrifugal pump

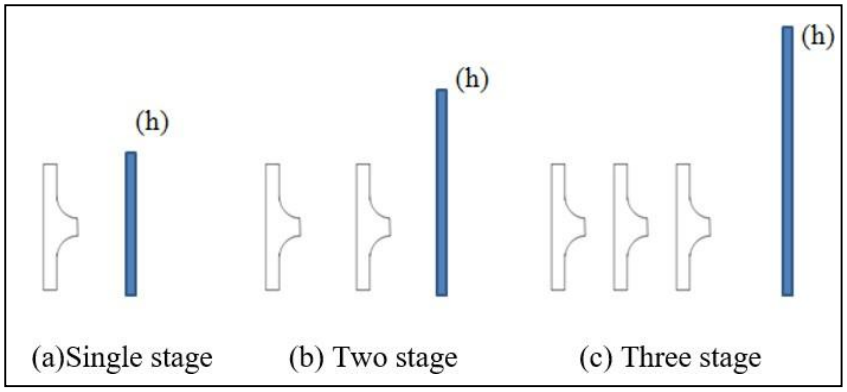

Fig. 1.7 Principle of multistage pump

1.4.1 Impeller

The impeller is a rotating part of a multistage centrifugal pump. The function of the impeller is toapply a whirling motion to the liquid with the help of back-curved blades. Liquid enters the eye of the impeller and discharges into the diffuser and casing. If we say in thermodynamics, an impeller is a system that has some boundary and an inlet and an outlet. The impeller impartscentrifugal force to the liquid, which results in the conversion of the velocity head into pressure head. Fig. 1.8 shows energy transfer in the impeller.

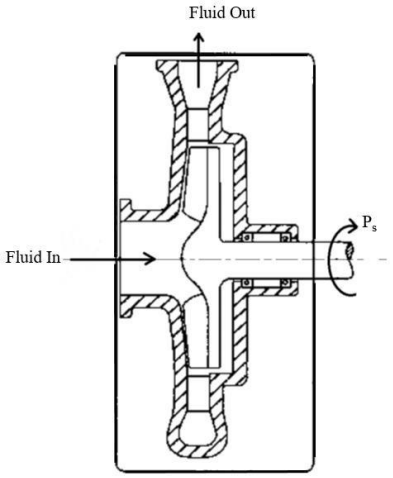

Fig. 1.8 Energy transfer in impeller

1.4.2 Vane diffuser

A Vane diffuser is a stationary part surrounded by the impeller. Its function is the same as that of volute casing, i.e., conversion of velocity head into pressure head. It consists of stationary vanes called diffuser vanes. The inlet flow section is smaller than the outlet, which means an increase in flow passage. Due to this, the water flowing in a diffuser passage causes a decrease in velocity as the cross section is inversely proportional to flow velocity, which resultsin a rise in pressure. While designing the diffuser vanes, it should be noted that the vanes' inletcoincides with the absolute velocity of impeller outlet C_2.

According to the expert, the gap provided between the diffuser and impeller will increase the efficiency of the pump by 16%.

The diffusion coefficient is the ratio of the inlet velocity (v_3) to the outlet velocity (v_4) of the diffuser.

$$d = \frac{v_4}{v_3} \tag{1.2}$$

The greater the diffusion coefficient, the better the performance.

1.4.3 Return channel

The main purpose is to increase the pressure over the pump, which is possible only when more impellers are arranged in series, but the main function is to guide the fluid from one stage to the next stage, and it is possible only by providing a return channel (a stationary device) having return guide vanes. This system is assembled at the backside of the impeller. Its function issame as that of a volute casing to convert dynamic pressure to static pressure. Before entering the next stage, the fluid is de-swirled wholly. To accomplish this, a return channel with guide vanes is introduced, which results in an undistorted flow into the flowing impeller. Due to the presence of vanes, the fluid accelerates as it approaches the next impeller eye. There is asharp turn in the flow from the diffuser outlet and at the return channel exit. Therefore, the fluid causessome pressure losses, which do not affect the pump efficiency so much.

1.5 THESIS LAYOUT

In this thesis titled "**Design and Performance Analysis of Multistage Centrifugal Pump using CFD",** the effect of the number of impeller blades and rotational speed on the performance of the Multistage Centrifugal Pump is analyzed. The thesis includes modeling and simulation, along with experimentation with a different number of blades and rotational speeds, and a novel shape of return guide vane is proposed.

Chapter 1 includes the introduction of centrifugal pumps and multistage pumps, the classification ofpumps, and the components of the multistage pump of centrifugal pumps.

Chapter 2 compiles the accounts of various research works on the design optimization of centrifugal pumps and their applications. The accounts describing the design of the impeller, diffuser, and volute casing, mathematical modeling, and the industrial application of the same are highlighted. The chapter is concluded with the research gap, followed by the objectives of the present study.

Chapter 3 narrates Computational Fluid Dynamics (CFD), its need to study, governing equations, and various flow models.

Chapter 4 gives theoretical knowledge about the multistage pump and its components, the velocity triangles for the impeller and diffuser were discussed, and Euler's head equation was derived. It also contains a detailed description of the experimental setup, including the equipment's ratings, functions, and the dimensions of the single-stage centrifugal pump.

Chapter 5 deals with the solid modelling of various elements of the Centrifugal Pump, such as the impeller, diffuser, and return passage. The impeller blade profile design method is defined and shown, and the 3D model of impeller, diffuser, and return passage with their dimensions is shown, the meshing of all these domains showing their nodes and elements, and inlet and outlet boundary details are specified.

Chapter 6 describes the optimization technique (Response Surface Methodology) used for the optimization of a single-stage centrifugal pump.

Chapter 7 relates to the results obtained after flow simulation for a single-stage pump with different no. of impeller blades and rotational speed, the performance parameters are discussed with tables and charts. A simulation for a two-stage pump is discussed for constant speed with various impeller blades, and the velocity streamlines pattern and pressure contour are shown, and head losses in the two-stage pump are tabulated.

Chapter 8 discusses the conclusions inferred from the above results and discussions.

Summary

1. **This chapter introduces centrifugal and multistage pumps, detailing their components, classifications, and applications.**
2. **It emphasizes the importance of these pumps in converting kinetic energy from a prime mover into pressure energy, thereby raising water from lower to higher elevations.**
3. **Key classifications include working head, casing type, impeller type, number of stages, flow direction, and impeller entrances.**
4. **Multistage centrifugal pumps, with their multiple impellers in series, are highlighted for their ability to achieve high head and are vital in applications such as reverse osmosis, boiler feed, and mine-dewatering. The chapter underscores the roles of the impeller, vane diffuser, and return channel in enhancing pump efficiency and performance.**

CHAPTER 2. LITERATURE REVIEW

Many researchers[3–12] have done a literature survey for enhancing the performance of the multistage centrifugal pump and concluded the various design parameters that affect the efficiency of the pump. The study was carried out on 3 different types of impellers by Weidong Zhou et al. [13] of them have 6 twisted blades, while one has four straight blades. The problem was modelled using the k-ε two-equation turbulence model. The result predicted that the twisted blades were more efficient than the straight blades. Jianjun Feng et al. [14] Investigated impeller-diffuser interaction, numerical simulation, pressure fluctuation, and radial gap. The impeller experienced pressure variation caused by the diffuser, which grew with the increasing diffuser radius. Pressure fluctuation dramatically decreased by roughly 60% when the radial gap rose from 3% to 10%.

A 2-stage pump with 7 impeller blades, 11 diffuser vanes, and 11 return channel guide vanes was chosen for CFD analysis on return channel guide vanes by M. Miyano et al. [15]; the k-model was used to solve the issue. They demonstrated that when the return vane trailing edge is set to this condition, the fluid will no longer be swirled before entering the subsequent stage, causing the next impeller to suck in more fluid and exert more force on the fluid.

Centrifugal pump CFD analysis using FLUENT by Chakraborty et al. [16] using the k-ε turbulence model was performed. They varied the number of impeller blades from 4 to 12 and concluded that as the number of blades increased, the area of low-pressure increased, and static pressure gradually increased. It was found that an impeller having a number of blades 10 has better efficiency and head out of all.

The interaction between the stator and rotor and pressure fluctuation in the impeller and return guide vane (RGV) section were studied by Q. Zhang et al.[17] for a two-stage multistage centrifugal pump. They proposed a new Return Guide Vane with a twisted segment that produces better outcomes than the traditional one.

The first stage of a multistage centrifugal pump is numerically investigated by Nicolas et al. [18]. It is comprised of a casing, an impeller, a diffuser, and return vanes. The analysis is carried out with five parameters, i.e., varying impeller blade height by 16, 23, and 29 mm, varying impeller a number of blades by keeping diffuser and return vane constant, varying diffuser vanes by 7,8,12, varying return vanes by 3,8,11 and roughness with 0 mm, 0.002 mm and 2 mm by the parameter, i.e., changing blades and diffuser height 16, 23 and 29 mm for impeller with 6 number blades, diffuser vane 1 and return vane 8. The head produced

was found to be highest when the height was 29 mm, and efficiency, i.e., the best efficiency point, was highest for a height of 23 mm.

The different design methods of radial-type vane profile design were represented by Bowade et al. [19]. There are many studies that have been done on impeller-diffuser interaction.[20–26]. Alawadhi et al. [27] investigated the design and optimization of a centrifugal pump. To move slurry at a flow rate of 120 m^3/hr to a head of 20 m, they undertook this study specifically for that purpose. They employed response surface methodology (RSM) and a multi-objective genetic algorithm (MOGA) for optimization. The shape of the pump was optimized using a combination of five different software programs, including ANSYS Vista, ANSYS Design Modeler, response surface optimization tools, and ANSYS CFX.

According to extensive studies,[28–33] The impeller, a crucial part of the centrifugal pump, is highly influential to how well the same performs. The aim of Bogarassa's [34] research is to determine how a centrifugal pump's performance parameters are impacted by its rotating speed. He has used an impeller with eight blades and a range of varying the operating speed from 1500 to 3000 rpm with intervals of 500 rpm. The influence of speed variation on centrifugal pumps' total head, output power, and efficiency was examined.

Zhai et al.[35] Computationally examined a 10-stage centrifugal pump's operational capacity, unsteady flow characteristics, generation of vortices, and pressure pulsation characteristics. They concluded that by enhancing the rotor-stator contact, energy dissipation brought on by backflow, jet-wake, and rotor-stator interference might be reduced. Although many researchers[32,36,45–47,37–44] have examined the optimization of impellers using various methodologies; the impeller, a key component of pumps, directly affects pump performance, as presented by Wu et al.[48].

As was already noted, the optimization of impellers is a multi-factor optimization problem, and more research is needed to determine how to achieve a balance between various factors. Efficiency, shaft power, and pump net positive suction head were used in Wang and Huo’s [49] multi-objective optimization mathematical model. They employed CFD to numerically simulate the flow field, utilizing four parameters as independent variables: impeller outlet width, blade inlet angle, blade outlet angle, and cape angle. To increase the hydraulic efficiency of the pump, they analyzed the impact of the key design factors of the impeller on the head, efficiency, shaft power, and NPSHr of the pump. The ideal set of parameters is then computed using a weight matrix.

Jafarzadeh et al. [50] took the coefficient of the head, the hydraulic performance, and the required NPSHr as design variables and the tip blade angle at the inlet, the tip blade angle at the outlet, and the ratio of the outlet hub radius to the inlet hub radius as objective functions to optimize the performance of an inducer. They used computational fluid dynamics (CFD) technology to model the inducer performance and compare the results to the experimental data, demonstrating the accuracy of the employed methodology and presumptions. Significant optimum design principles are revealed by recommended design points, which can only be attained by employing a multi-objective optimization strategy.

A two-stage pump with 7 impeller blades, 11 diffuser vanes, and 11 return channel guide vanes was chosen for CFD analysis on return channel guide vanes by Miyano et al. [15]; the k-ε model was used to solve the problem. They demonstrated that when the return vane trailing edge is set to this condition, the fluid will no longer be swirled before entering the subsequent stage, causing the next impeller to suck in more fluid and exert more force on the fluid.

Centrifugal pump CFD analysis using FLUENT by Chakraborty et al [51] using the k-ε turbulence model was performed. They varied the number of impeller blades from 4 to 12 and concluded that as the impeller blade number increased, the area of low pressure increased, and static pressure gradually increased. It was found that an impeller with 10 blades has better efficiency and head out of all.

Guo et al.[35] research aims to determine how a centrifugal pump's performance parameters are impacted by its rotating speed. He has used an impeller with eight blades and a range of varying operating speeds from 1500 to 3000 rpm with intervals of 500 rpm. The influence of speed variation on centrifugal pumps' total head, output power, and efficiency was examined.

Ofuchi et al. [52] numerically investigated the effect of viscosity in a multistage electrical Submersible pump (ESP) and assessed the performance degradation by analyzing the impact of viscosity on head and flow rate. The flow behavior when the pump runs at various viscosities was also compared using a flow field study. The influence of a prior stage on the upstream flow was demonstrated, and the interaction between stages was also examined.

To get the best pressure distribution inside the pump, Arumugam et al. [53] tested a five-stage vertical multistage pump at different speeds and looked into how the characteristics of pressure change in the stages of a vertical multistage pump at BEP at different rotations

related to each other. Five different pump speeds were selected at BEP, and the pressure fluctuation signals were recorded and evaluated. Results showed a nonlinear variation in the pressure fluctuation with stage and speed, and showed a similar distribution of pressure fluctuation with a variation in the level of intensity at BEP of varied operating speeds in the time domain analysis of the captured signals, and that for two cycles. The asymmetry of the flow in the impeller passages and the inter-stage effects of different stages are the main causes of this variance in the amplitude of pressure fluctuation.

Deng et al. [54] designed a multistage hybrid model that uses only the measured values for the speed and valve opening to determine the various performance indices of centrifugal pumps. They outlined two key defining characteristics. First, for better prediction performance with small sample sizes, the beneficial process information and JGPR-based modeling technique are incorporated into the prediction model. Second, the data-and-knowledge hybrid model gradually captures the properties of centrifugal pumps with a small number of input variables by successively introducing the predicted values into the input vector. The experimental results showed its feasibility and simplicity. Results showed that error propagation may worsen the reliability of the proposed multistage hybrid model as the modeling stage progresses.

Other studies have prioritized improving operational parameters such as fluid viscosity, flow rate, and rotating speed. By using surrogate models and optimization techniques, it is also possible to practically determine the best combination of design parameters [55],[56],[57],[58] For instance, Li et al.[59] optimized the operating settings of a centrifugal pump using RSM. They found that by increasing the discharge and reducing the rotation, the head of the pump and efficiency were improved. The optimization of hydraulic performance in centrifugal pumps is a critical area of research in fluid dynamics. There is a significant amount of literature related to the optimization of centrifugal pumps to improve their performance. Various studies [59] have focused on utilizing different methodologies to enhance the efficiency of single-stage and multistage centrifugal pumps. For instance, the response surface methodology (RSM) has been applied to optimize the hydraulic performance of single-stage centrifugal pumps [60], [61]. An important first step in the realm of turbomachinery optimization is the analysis of the key metrics for performance, since it helps to make the pump design apparent. Many studies concentrated on enhancing the efficiency and effectiveness of these pumps by optimizing various design modifications in the impeller, diffuser, and return passage [62], [63], [64].

2.2 RESEARCH GAPS

1. From the literature review, critical parameters of the centrifugal pump impeller are found, which highly affect the performance characteristics of the centrifugal pump: impeller outlet width, impeller outlet diameter, impeller Outlet Blade height, impeller blade outlet angle, and number of blades on the impeller. A lot of work has been done in the design optimization of these parameters in single-stage centrifugal pumps. There is still a need for further optimization of these various parameters in a multistage centrifugal pump.
2. From the literature, it was found that most previous research, especially research based on numerical approaches, had focused mainly on the numerical investigation of a liquid flow in the first stage of a multistage centrifugal pump consisting of an impeller, diffuser with return vanes, and casing. Few efforts were made to study the liquid flow in other stages of a multistage centrifugal pump. Therefore, there is still a lot of work to be done in these fields.
3. A few studies have been done on the design optimization of the pump structure of a multistage pump. So, there is a need for design optimization of a compact pump structure (Return guide vane, i.e., RGV structure) as compared to the former pump structure. The return passage at the periphery of the casing can be made into a circular shape, i.e., eliminating sudden sharpness.
4. A lot of research has been undertaken on the design optimization of single-stage centrifugal pumps by varying the following parameters, such as the shape of the impeller, by Zhou et al.[13], the no. of blades by Nicolas et al. [18] and Chakraborty et al. [16], different methods of vane profile, volute casing, and the number of diffuser vanes. Further performance can be improved by increasing the outlet width of the diffuser and by increasing the return passage casing height.

2.3 RESEARCH OBJECTIVES

From the above-mentioned research gaps, the present investigation aims to enhance the performance of multistage centrifugal pumps with the following objectives -

1. To design a two-stage centrifugal pump according to the specifications given in the literature of Nicholas et al. [18] and validate it by carrying out a numerical simulation of the 1st stage centrifugal pump by changing the number of blades and impeller speed to conclude the pump that gives the best efficiency and head.
2. To investigate the effect of rpm and the number of blades of the impeller on the 2nd stage of a multistage centrifugal pump. Then, among all the 1st stage results, the best one is selected to carry out the flow simulation of the 2nd stage centrifugal pump.

3. For the compactness of the pump, we are going to design three types of return guide vane, i.e., mixed guide vane, radial guide vane, and distorted guide vane, run flow simulation on these three to validate which one is best for enhancing efficiency.
4. We are also going to conduct a flow simulation on these three types of return guide vane, which are going to reduce the area of the Centrifugal Pump for optimizing the design by carrying out the flow simulation by varying the outlet angle of the Return Guide Vane.

2.3 NOVELTY OF THE PRESENT WORK:

The originality of this research lies in the **systematic optimization and performance analysis of a multistage centrifugal pump** using CFD integrated with Response Surface Methodology (RSM). Unlike conventional studies that focus on single-variable changes, this work applies a **multi-factor full factorial design** (impeller blade number, flow rate, and speed) to establish statistically validated performance trends. Furthermore, the study advances the state-of-the-art by extending single-stage optimization to **two-stage flow analysis**, enabling quantification of diffuser and return-passage losses. A key novel contribution is the **comparative evaluation of return guide vane (RGV) geometries**-mixed, radial, and distorted types-and the systematic variation of radial vane outlet angles (20°, 25°, 30°), revealing that the 25° radial vane offers the highest efficiency and lowest hydraulic losses. This combined methodological and design-focused approach establishes new insights for **energy-efficient pump operation** and provides a framework for industrial optimization.

Summary

1. **Twisted blades are more efficient than straight blades.**
2. **Pressure fluctuation decreases by 60% when the radial gap increases from 3% to 10%.**
3. **Need for further optimization of critical impeller parameters and comprehensive studies on liquid flow in all pump stages.**
4. **Design optimization of compact pump structures is still needed.**

CHAPTER 3.
COMPUTATIONAL FLUID DYNAMICS THEORY

This chapter deals with the introduction of Computational Fluid Dynamics (CFD) Theory and basic components of CFD, methods of discretization, and turbulence models. The CFD flow simulation process involves creating a geometric model, meshing the model into discrete elements, setting up boundary conditions, and selecting a turbulence model (e.g., k-ε). Numerical methods, such as the finite volume method, solve the governing equations. Results are then analyzed for fluid flow insights.

3.1. INTRODUCTION

One of the main problems that the researchers face is to understand the physical phenomenon that takes place over a region of interest and the influence the surrounding has on it. In the field of fluid dynamics, there are a lot of events that increase the complexity, such as turbulence, slip, dissipation, diffusion, boundary layers, and the like. Computational Fluid Dynamics, the help of a computational tool that can give detailed information about the behavior of a specific domain under consideration by solving the governing flow equations, is known as Computational Fluid Dynamics (CFD)[72]. This is capable of solving problems related to steadyand transient flows, buoyancy, and flows in multiple frames of reference, subsonic, transonic,and supersonic flows, heat transfer and thermal radiation, etc. CFD has become an essentialtool in almost all fields of engineering due to its lack of limitation on the domain size under study and the ability to simulate the conditions that cannot be created during experimentation. Another important factor that has helped in the growth of the use of CFD is its cost and time effectiveness.

3.2 BASIC COMPONENTS OF CFD

In general, the CFD analysis follows the following steps:

- Defining the geometry
- Problem definition or Pre-processing
- Solver
- Post-processing

3.2.1 Geometry Creation

The very first step is to create and define the geometry or the region on which the study is to be carried out. After the creation of geometry, the regions of interest are defined, i.e., the inflow passage and the outflow passage, along with the boundary walls. The next step is the creation of a grid which discretizes the surface of the geometry into no. of elements, and the

calculationis done on the nodes thus created.

3.2.2 Pre-processing

This is the first step involved in analyzing the problem. After the system is identified, the pre-processing stage defines the problem. First of all, the fluid properties that will flow through the domain are defined, and then appropriate boundary conditions are applied in thedefined passages.

3.2.3 Solver

Solver is an important part of the CFD analysis. It solves the problem defined by solving the governing equations in an iterative process. This stage follows the steps given below:

a. By means of the finite element or finite difference method, the derivatives in the partialdifferential equation are approximated as an algebraic expression.
b. The result obtained from the algebraic solution helps in predicting the mass, momentum, and energy transport at the discretized points in the domain.
c. The non-linear governing equations are then solved in an iterative loop until a converged solution is obtained.

Some types of solvers developed by ANSYS are FLUENT, CFX, and POLYFLOW. In general, FLUENT and CFX are both control volume-based, which gives highly accurate results and thus have a broad application. The main difference between the two is that the CFX solver uses finite elements for discretization, whereas FLUENT uses finite volumes for discretizing the domain.

3.2.4 Post-processing

It is the final stage of the CFD analysis process. It gives a visualized result of the variation of parameters like velocity, pressure, temperature, etc. Along with the animations, it also provides a quantitative interpretation of the problem.

3.3 DISCRETIZATION METHODS

The meaning of discretization is to have distinctness of the domain on which the solution is to be approximated. There are three methods of discretization in CFD:

- Finite Difference Method (FDM)
- Finite Element Method (FEM)
- Finite Volume Method (FVM)

3.3.1 Finite Difference Method

This method of discretization is a node-based solution. In this method, each derivative of the partial differential equation is replaced with an approximate difference formula, which is derived from a Taylor series expansion. The main drawback of this method is that it does not consider the variation of parameters between two nodes, which makes the solution more

unstable.

3.3.2 Finite Element Method

This discretization method involves the division of the domain into smaller sub-domains in theform of finite elements. It gives a piecewise representation of the solution constructed fromthe basic functions and then integrated over the element. After assembling the equations over all the elements in the domain, the global equation is solved to obtain the final solution.

3.3.3 Finite Volume Method

This method of discretization is a cell-based advancement of the FDM. This uses the integral form of the partial differential equation over a finite volume created between two nodes. The domain is first discretized into finite volumes, and then the governing equations are solved. Unlike FDM, the variables are placed at the centre of the cell rather than at nodes. The main advantage of this method over other methods is that it captures the curved boundaries accurately.

3.4 GRID GENERATION

This is the process that discretizes the flow domain into different elements on which the solution is based. In general, a grid has two types:

- Structured grid
- Unstructured grid

3.4.1 Structured Grid

This type of grid generation follows a particular pattern throughout the domain, i.e., the no. of elements connected to a node is always fixed. Over a flow space, a hexahedral element is used, which connects eight elements per node. This type of grid is used where more accuracy isdesired. For a structured grid, the ratio of the number of nodes to the no. of elements is 1:1.

3.4.2 Unstructured Grid

A grid where the no. of elements connected to each node varies is identified as an unstructuredgrid. In general, for a 3D element, the tetrahedral type is used over the flow space, and the ratio of the number of nodes to the no. of elements is approximately 1:5.

3.5 GOVERNING EQUATIONS

After defining the problem, an appropriate set of governing equations is to be selected to obtain an approximate solution. Generally, fluid dynamics is governed by the conservation of mass, momentum, and energy equations, which are in the form of partial differential equations and are based on the laws of physics.

3.5.1 Continuity Equation

This equation is based on the conservation of mass principle, which states that the net rate of change of mass within the control volume is equal to the net rate of mass flow into the control volume. Eqn 3.1 gives the differential conservative form of the continuity equation in an unsteady state.

$$\frac{\partial \rho}{\partial t} + \frac{\partial}{\partial x}(\rho u) + \frac{\partial}{\partial y}(\rho v) + \frac{\partial}{\partial z}(\rho \omega) = 0 \qquad [3.1]$$

3.5.2 Momentum Equation

This equation is based on the 2nd law of Newton, which states that the rate of momentum change of a fluid particle in a particular direction is equal to the sum of all the forces acting on the fluid particle in that direction. The forces acting on a fluid element are broadly classified as body forces and surface forces. Body force includes gravity force and centrifugal force, whereas surface forces include pressure force, shear force, normal force, and viscous force. The general conservative differential form of the momentum equation in an unsteady state is given in the following equations.

Momentum equation in X-direction:

$$\frac{\partial}{\partial t}(\rho u) + \nabla.(\rho u V) = -\frac{\partial p}{\partial x} + \frac{\partial \tau_{xx}}{\partial x} + \frac{\partial \tau_{yx}}{\partial y} + \frac{\partial \tau_{zx}}{\partial z} + \rho f_x \qquad [3.2]$$

Momentum equation in Y-direction:

$$\frac{\partial}{\partial t}(\rho v) + \nabla.(\rho v V) = -\frac{\partial p}{\partial y} + \frac{\partial \tau_{xy}}{\partial x} + \frac{\partial \tau_{yy}}{\partial y} + \frac{\partial \tau_{zy}}{\partial z} + \rho f_y \qquad [3.3]$$

Momentum equation in Z-direction:

$$\frac{\partial}{\partial t}(\rho \omega) + \nabla.(\rho \omega V) = -\frac{\partial p}{\partial z} + \frac{\partial \tau_{xz}}{\partial x} + \frac{\partial \tau_{yz}}{\partial y} + \frac{\partial \tau_{zz}}{\partial z} + \rho f_z \qquad [3.4]$$

3.5.3 Energy Equation

The energy equation follows the conservation of energy principle. It is derived from the first law of thermodynamics, which states that the rate of change of energy of a fluid particle is equal to the sum of the rate of heat supplied and the rate of work done on the fluid particle.

3.6 TURBULENCE MODELS

The various types of models are used to capture the full range of velocity and length scales in random and fluctuating flows, even with a slightly coarser grid size. These are transport equations to compute the turbulent quantities.

3.6.1 Zero-equation model

This type of model does not require the solution to any additional equations and is also known as the algebraic turbulence model. It is simple to use and implement, and it provides very quick approximate results. The main drawback is that it does not account for convection and diffusion of the turbulentenergy, which makes it less reliable.

3.6.2 One-equation Model

In this type of model, there is an additional turbulent transport equation related to turbulent kinetic energy (K). The Prandtl's equation is said to be the one-equation model. The main advantage of this type of model is that it provides better approximate results than the zero-equation model and requires moderate grid resolution near the boundary wall regions.

3.6.3 Two-equation Model

This model is widely used for general fluid flow problems requiring less computational time. There are two transport equations involved for turbulent kinetic energy to represent the turbulent properties of the flow. It involves two variables, out of which one is the turbulent kinetic energy (K) and the other is either the dissipation rate of turbulent kinetic energy (ε) or the specific rate of dissipation (ω).

3.6.3.1 K-ε model

This is a robust turbulence model that is widely used for general fluid flow problems where there is no pressure gradient. The first transported variable, K, governs the turbulent velocity, and the second variable, i.e., ε, gives the rate of dissipation of K. This model finds its use in most of the industries. The most commonly used K-ε model is the standard K-ε model, which has relatively less computational time than the other two-equation models.

3.6.3.2 K-ω and SST model

This is the most commonly used turbulence model for rotating flow problems where a pressure gradient is present. The first transported variable is the same as in the K-ε model, and the second variable, ω, is the specific dissipation rate. It helps in determining the scale of turbulence (length scale or time scale). The most commonly used K-ω model type is the Shear Stress Transport (SST) model. The SST model is a blend of the robust and accurate formulation of the K-ω model in the near-wall region and the free-stream independence of the K-ε model in the far field. It provides a more accurate prediction of the flow separation

occurring due to adversepressure gradient.

In the present study, **Computational Fluid Dynamics (CFD)** simulations were performed using the Reynolds-Averaged Navier–Stokes (RANS) approach with the k–ε turbulence model to achieve a balance between computational cost and accuracy. RANS-based CFD models average the effects of turbulence, thereby significantly reducing the number of equations to be solved and enabling simulations of complex turbomachinery at practical time scales. However, this comes at the expense of fine-scale accuracy in capturing unsteady vortical structures and turbulence anisotropy. In contrast, the **Large Eddy Simulation (LES)** technique resolves the larger turbulent eddies directly while modeling only the smaller subgrid scales. This allows LES to capture transient flow physics, vortex shedding, and secondary flow structures with much higher fidelity compared to RANS models. Despite this advantage, LES requires extremely fine grids and small time steps, leading to very high computational demands, especially for high Reynolds number flows typical in centrifugal pumps. Therefore, while LES is emerging as a more accurate tool for turbomachinery flow analysis, the use of RANS-based CFD remains a practical and efficient choice for performance prediction and design optimization in engineering applications such as the present work.

Summary

1. **Computational Fluid Dynamics (CFD) is a branch of fluid mechanics that uses numerical methods and algorithms to solve and analyze problems involving fluid flows.**
2. **By simulating the physical behavior of fluids, CFD allows engineers and scientists to predict how fluids will behave under various conditions.**
3. **The theory behind CFD involves the application of the fundamental principles of fluid mechanics, such as the conservation of mass, momentum, and energy, to develop mathematical models that describe fluid behavior.**
4. **These models are then discretized into a finite number of small elements or cells, and complex calculations are performed to determine fluid properties at each point in the domain.**
5. **This approach enables detailed analysis of fluid flow, heat transfer, and related phenomena, providing valuable insights for designing and optimizing engineering systems in fields such as aerospace, automotive, and environmental engineering.**

CHAPTER 4.
DESIGN ASPECTS OF MULTISTAGE CENTRIFUGAL PUMP & EXPERIMENTATION

This chapter discusses the design criteria of the impeller, diffuser, and return channel of Single-stage and two-stage Centrifugal pumps.

4.1 GENERAL

A multistage centrifugal pump is basically a type of centrifugal pump that consists of more than one impeller in series, which are keyed to a single shaft. The pump consists mainly of three main parts, namely the impeller, diffuser, and return channel. The fluid enters at the suction eyeof the impeller, where fluid is forced by the rotating rotor, i.e., impeller, and gains velocity headand leaves the impeller at the periphery. Then fluid enters the vaned diffuser section, where the velocity head of fluid is converted to pressure head. After passing through the diffuser, the fluid enters the return passage, which consists of guide vanes, where the fluid is guided to the next eye of the impeller, i.e., to the next stage.

4.2 DESIGN OF IMPELLER

The impeller is a rotor that is rotated by means of a driver that could be an I.C. engine or induction motor. The impeller consists of several blades, which are enclosed between the shrouds. As the impeller rotates, it imparts centrifugal force on fluid particles and further momentum transfer. This force causes the fluid to move with velocity, i.e., absolute velocity C_1. To design the impeller, the velocity vectors are represented graphically to carry out our blade profile design. Fig. 4.1 shows the inlet and outlet velocity triangles of the impeller.

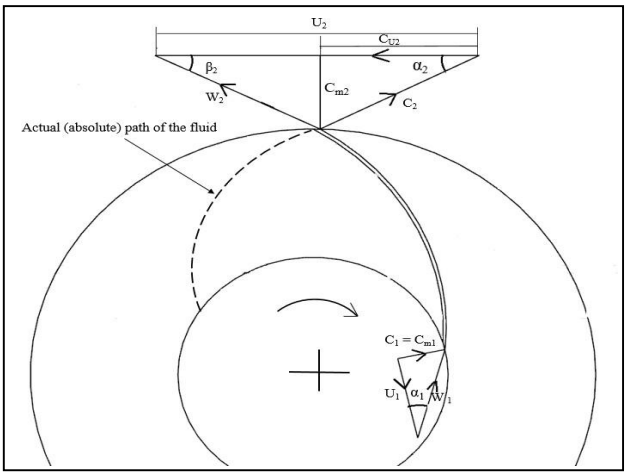

Fig. 4.1 Inlet and Outlet Velocity Triangles of Impeller.

4.2.1 Design of Blade Profile

Circular arc method:

The simple method published by G.K. Sahu for constructing a vane profile is to draw a single radius circular arc using the calculated angles β_1 and β_2 and radii R_1 and R_2, but this may have seriousimplications on the performance of the pump. In this method, the first line PQ is drawn, which makes an angle β_1 to PO as shown in the figure below. Then an angle of β_1+ β_2 is drawn at O with the radius OR and a line is drawn from P to the point R, the intersection points on radiusR_1 and is extended up to S. Then a perpendicular line is drawn in the middle of PS which intersects at Q. QP will be the radius of arc and arc PS will be the vane profile. The figures Fig. 4.2 and Fig. 4.3 show the circular arc method and blade profile, respectively.

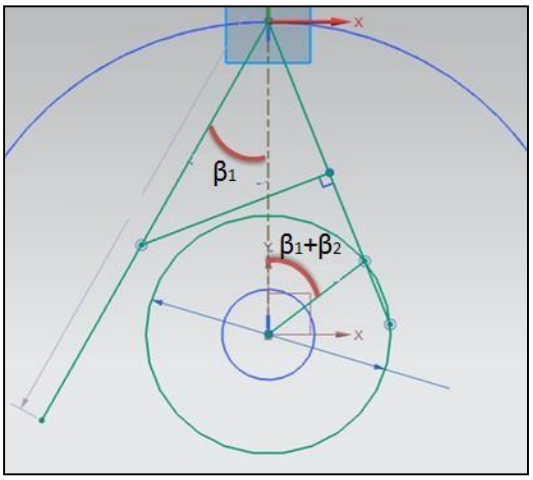

Fig. 4.2 Circular arc method

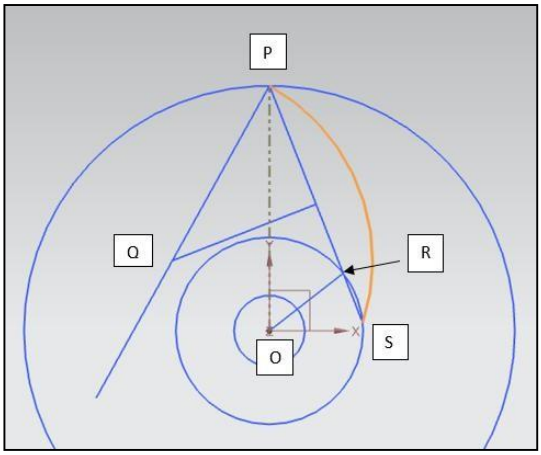

Fig. 4.3 Blade profile

The radius of curvature PS is given by

$$R_c = \frac{(R_2)^2 - (R_1)^2}{2(R_2\cos\beta_2 - R_1\cos\beta_1)} \quad (4.1)$$

4.2.2 Theoretical Head of Centrifugal Pump

The theoretical head produced by the centrifugal pump is found by the principle of angular momentum of the mass of fluid flowing within the impeller. The principle states that the rate ofchange of angular momentum of a body with respect to the rotational axis is equal to the torque(T) produced by the force on the body with the axis of rotation.

$$T = \frac{dm}{dt}(r_2 C_2 cos\alpha_2 - r_1 C_1 cos\alpha_1) \quad (4.2)$$

Where, $\frac{dm}{dt}$ = mass flow rate through the impeller, and can be written as $Q\gamma/g$

$$T = \frac{Q\gamma}{g}(r_2 C_2 cos\alpha_2 - r_1 C_1 cos\alpha_1) \quad (4.3)$$

As the power applied to the fluid is $P=T.\omega$, therefore multiplying by ω on both sides

$$T.\omega = \frac{Q\gamma}{g}.\omega(r_2 C_2 cos\alpha_2 - r_1 C_1 cos\alpha_1) \quad (4.4)$$

But $u_1=\omega r_1$ *and* $u_2=\omega r_2$, which are the peripheral velocities of the impeller and $C_{u_1} = C_1 Cos\alpha_1$ and $C_{u_2} = C_2 Cos\alpha_2$ hence above equation will be,

$$P = \frac{Q\gamma}{g}(u_2 C_2 - u_1 C_1) \quad (4.5)$$

This power will be in the form of pump output power

$$H_e = \frac{(u_2 c_{u2} - u_1 c_{u1})}{g} \quad (4.6)$$

The above equation gives the theoretical head, and the equation is called Euler's equation. Weknow that the fluid enters the eye of the impeller axially, so whirl velocity $C_{u1} = 0$ at the inlet,then Euler's equation will be

$$H_e = \frac{c_{u2} u_2}{g} \quad (4.7)$$

The velocity triangles drawn in Fig. 4.1 showing various velocity and inlet, outlet angles are known to Euler's velocity triangles and the head derived in eq. 4.7 is defined as Euler's Head.

4.3 DESIGN OF DIFFUSER

The diffuser is a stationary part of the multistage pump; it contains a number of stationary vanes. They are positioned such that the cross-sectional area of the flow passage increases gradually towards the outlet. The function of a diffuser is similar to that of a volute casing, i.e., to convert velocity head into pressure head. While considering the design point of view, the position of vanes should be such that the absolute velocity at impeller outlet should coincide with the inlet angle of diffuser vane as shown in Fig. 4.4. The inlet vane angle varies from 6° to 12°, and the outlet angle varies from 16° to 25°. It must be noted that inside the diffuser, the pressure variation must be there. As already said, the cross-sectional area should be gradually increased in nature, sothe outlet width b_3 must be greater than b_2. The number varies as small as possible, so a large flow passage will be present for fluid to flow, and thus, the head and efficiency will be higher.The presence of a gap between the impeller and diffuser showed better results, i.e., it increases the efficiency of the pump up to 16%. Fig. 4.4 shows the inlet and outlet velocity triangle for a vaned diffuser.

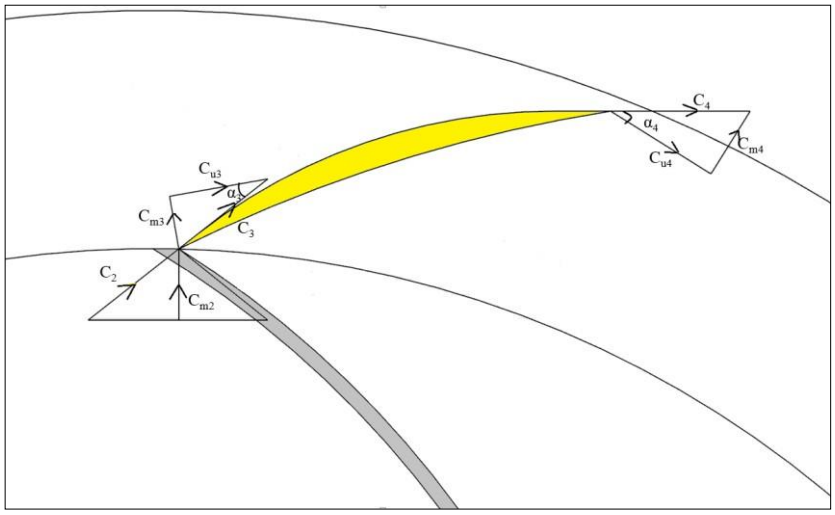

Fig. 4.4 Inlet and Outlet velocity triangle for Vaned Diffuser

4.4 DESIGN OF RETURN PASSAGE

The main purpose is to increase the pressure over the pump, which is possible only when a larger number of impellers are arranged in series, but the main function is to guide the fluid from one stage to the next stage, and it is possible only by providing a return channel (a stationary device)having return guide vanes. This system is assembled at the backside of the impeller and turns the flow 180° towards the next eye of the impeller. As discussed in section 4.3, the pressure is being varied in the diffuser. The fluid after leaving the diffuser enters the return passage, where the shape of the vanes has nothing to do with hydraulic function than to guide the fluid to the next stage. While looking at the number of guide vanes, there should be fewer in number. if more guidevanes are there, then less flow passage will be present for the fluid, also the hydraulic fluctuation

and losses will be more. The curvature of the guide vane also has an effect on head loss, i.e., the less the curvature, the more the losses. As we want to stop the swirling motion of the fluid, the guide vane curvature must be more than or equal to the impeller blade profile. If talking about the return passage casing, the casing must have more spacing, i.e., the return passage guide vanes height must be greater than the diffuser vane and impeller blade height. As the impeller forces the fluid into the casing, this large mass should be accommodated in a big space passage. If the passage is less, the pressure will be too high in its stationary parts, which may causefailure of the pump.

4.5 EXPERIMENTAL TEST RIG SETUP

The test rig utilized for the experimental validation with simulation results, as depicted in Fig. 4.5 and Fig. 4.6, is based on the previously mentioned analysis. It consists of a 3 HP AC Drive motor connected to a pump with a stepped pulley arrangement, an 80×80 cm2 measuring tank with a piezometer, a Stainless-Steel sump tank, and galvanized iron pipe connections with the required control valve, among other components. All components are mounted on a neatly painted Mild steel-structured frame made by Aarvee Industries in India. The control panel is outfitted with an energy meter for monitoring the power supplied to the motor, a pressure gauge (0-4.5 kg/cm^2) for measuring the delivery head, a vacuum gauge (0 to -760 mm Hg) for gauging the suction head, and a variable speed starter (0-5000 rpm) for speed adjustment. The line diagram of the experimental setup is illustrated in Fig. 4.5, and the experimental test configuration is presented in Fig. 4.6.

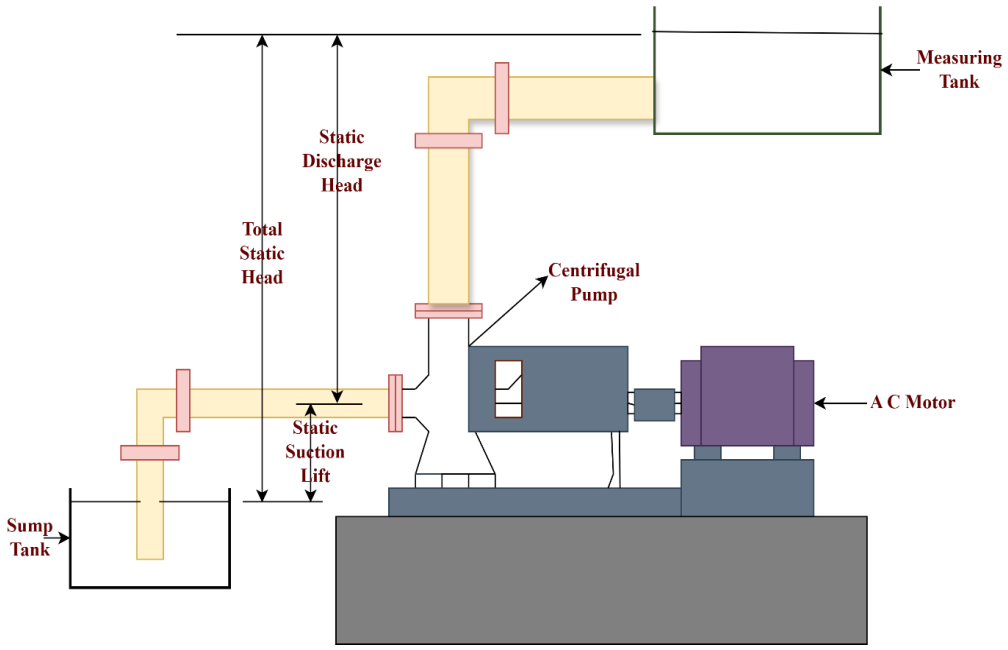

Fig. 4.5 Schematic diagram of Test Rig

Fig. 4.6 Experimental Test Rig Setup.

4.5.1. Uncertainty Analysis of Experimental Test Rig

The data provided by the manufacturers of these instruments should be utilized in calculating the standardized measurement uncertainty for various measuring systems and instruments to ensure precision. This also aids in reducing systemic measurement uncertainty within the calibration units. Regular calibration of these devices is essential. It is critical to measure uncertainty independently of the pump and guaranteed values when comparing test results with reported outcomes. One effective method for calculating uncertainty is through the propagation method [73].

$$\Delta y = \sqrt{\left(\left(\frac{\partial y}{\partial x_1}\Delta x_1\right)^2 + \left(\frac{\partial y}{\partial x_2}\Delta x_2\right)^2 + \left(\frac{\partial y}{\partial x_3}\Delta x_3\right)^2 + \cdots + \left(\frac{\partial y}{\partial x_n}\Delta x_n\right)^2\right)} \quad (4.8)$$

where y and x_1, x_2, …x_n are the responses and the independent variables, respectively. The estimated and computed degrees of uncertainty for the responses and independent variables are shown in **Table 4.1**. The result demonstrates that there is less than a 6% uncertainty error. That level of unpredictability in an engineering analysis is acceptable, according to BS EN ISO 9906:2000.

Table 4.1 Calculation of Uncertainty of Instruments

Variables	Range	Uncertainty (%)
Non-dependent variables		
Discharge pressure (kg/cm^2)	0-4.5	± 1.8
Suction pressure (mm Hg)	0 - (-760)	± 1
Flow rate (m^3/h)	0 – 850	± 0.5
Torque (N m)	0-2500	± 0.06
Rotational Speed (RPM)	0-5000	± 0.1
Dependent variables		
Head, H (m)	± 5.64 %	
Efficiency, η (%)	± 5.9 %	

4.5.2. Experimental Verification with Numerical Results

The steady-state computational study performed for 5, 6, and 7-bladed impeller centrifugal pumps in this paper is compared to the experimental analysis performed using 5-bladed impeller centrifugal pumps, as shown in [73]. Fig. 4.7 presents the validation of experimental and simulated results. It helps evaluate the performance of the system by showing how closely the simulated data aligns with the experimental measurements. This comparison is crucial for understanding the efficiency and power output at varying operational conditions, which is essential for design, analysis, and optimization in engineering and physics. The differences between experimental results and CFD results in the head are 1.92%, 4.7%, 3.2%, 7.10%, 7.02%, 6.1%, 10.6%, and 9.09% respectively. The differences between efficiency results and CFD results in efficiency are 8.4%, 5.24%, 5.01%, 5.25%, 7.4%, 7.5%, and 7.3% respectively. The differences between efficiency results and CFD results in efficiency are 6.25%, 12.5%, 8.69%, 6.89%, 5.88% 5.55%, 4%, and 7.29%. The overall average error in experimental results and CFD results for head, efficiency, and output power is 6.21%, 5.77%, and 7.13% respectively. Due to a lack of consideration during thetest for the energy loss caused by the pump itself, the test outcomes for the head and efficiencywere lower than those of the numerical calculations. The statistical results produced in this study and from other work have been gathered with reliability. As a result, the computational results reported in the research can be trusted.

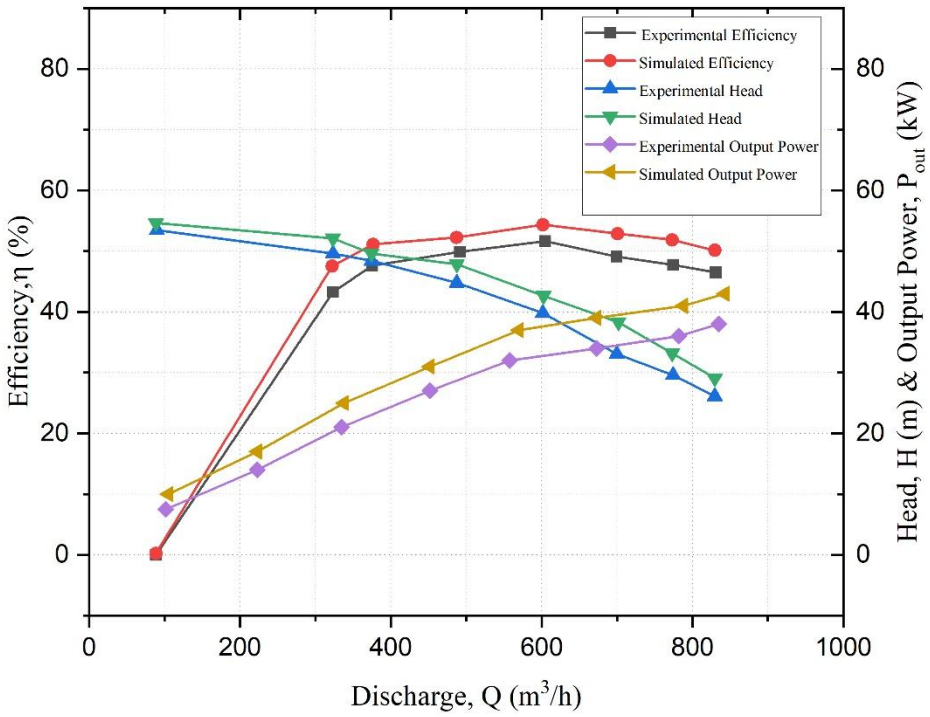

Fig. 4.7 Validation of Experimental results with CFD results.

Summary

1. **This chapter covers the design aspects of single-stage and two-stage centrifugal pumps, focusing on the impeller, diffuser, and return channel.**
2. **A multistage centrifugal pump uses multiple impellers in series to achieve high pressure.**
3. **The impeller's design involves calculating velocity vectors to create the blade profile. The diffuser, a stationary component, converts velocity head to pressure head, with vane positioning crucial for efficiency.**
4. **The return passage guides fluid between stages, maintaining pressure and reducing hydraulic losses.**
5. **Key points include the importance of accurate impeller blade design, diffuser vane angles for pressure conversion, and return channel geometry to optimize pump performance.**

CHAPTER 5.
SOLID MODELING AND SIMULATION

This chapter deals with the solid modelling of various elements of a Centrifugal Pump, such as the impeller, diffuser, and return passage. The impeller blade profile design method is defined and shown, and the 3D model of impeller, diffuser, and return passage with their dimensions is shown, the meshing of all these domains showing their nodes and elements, and inlet and outlet boundary details are specified.

5.1 INTRODUCTION

To carry out the flow simulation, we first needed to design the 3D model of a multistage pump.

The 3D model can be prepared by any CAD software, such as Creo, Unigraphics, SolidWorks, etc. For the thesis work, the 3D model of multistage centrifugal pump parts, i.e., impeller, diffuser, and return passage, is built in Ansys Design Modeler.

5.2 SOLID MODELING

The 3D model of a single-stage multistage centrifugal pump consists of three parts, as discussed in Chapter 4; therefore, each stage is divided into three domains. It is to be noted that each domain is to be separately modelled in Design Modeller and imported into ICEM CFD for meshing. The impeller domain consists of blades, impeller inlet and outlet, hub, and shroud. The diffuser contains diffuser vanes (DFV), an inlet, an outlet, and a casing. The return passage contains return guide vanes (RGV), casing, inlet, and outlet.

5.2.1 Geometrical Parameters of Impeller

Table 5.1 Dimensions of Impeller

Parameters	Values
Impeller outlet diameter	408 mm
Impeller inlet diameter	195 mm
Inlet angle β_1	40°
Outlet angle β_2	20°
Blade width at inlet and outlet	23 mm
Speed	1750 rpm
Numbers of blades	5,6 and 7

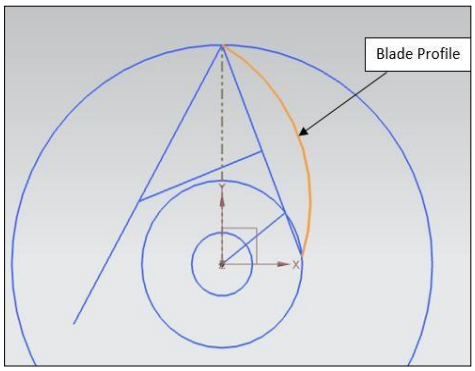

Fig. 5.1 Design of Blade Profile

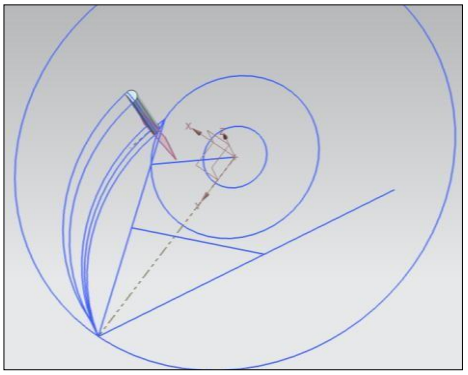

Fig. 5.2 Blade Implementation

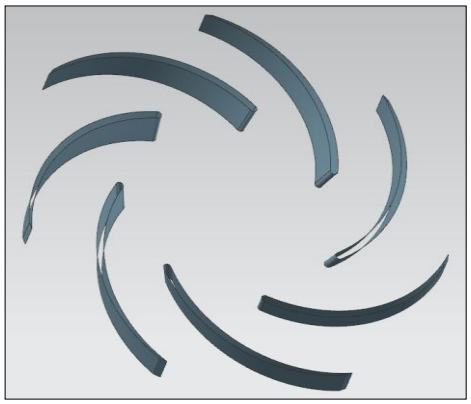

Fig. 5.3 Blades

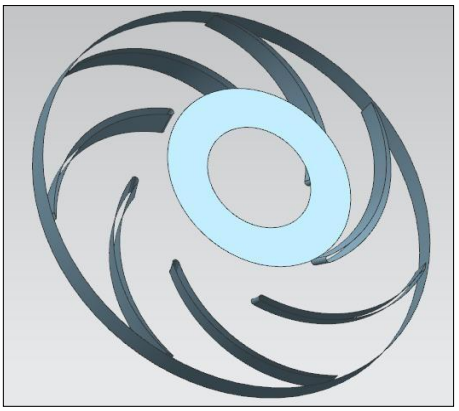

Fig. 5.4 Blades with Inlet and Outlet

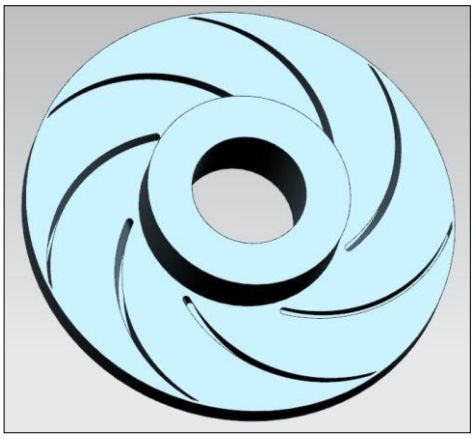

Fig. 5.5 Complete Impeller Model

Geometrical parameters of impeller, diffuser, and return passage are shown in Tables 5.1, 5.2, and 5.3, respectively. Whereas Figures 5.1, 5.2, 5.3, 5.4, and 5.5 present the design of the blade profile, the blade implementation, the blades, the blades with inlet and outlet, and the complete impeller model, respectively. Figure 5.6 shows the diffuser model.

5.2.2 Geometrical Parameters of Diffuser

Dimensions of the diffuser part are given in Table 5.2 below.

Table 5.2 Dimensions of Diffuser

Parameters	Values
Diffuser inlet diameter	408mm
Diffuser outlet diameter	502mm
Diffuser inlet and outlet width	23mm
Number of vanes	8
Inlet angle	5°
Outlet angle	25°

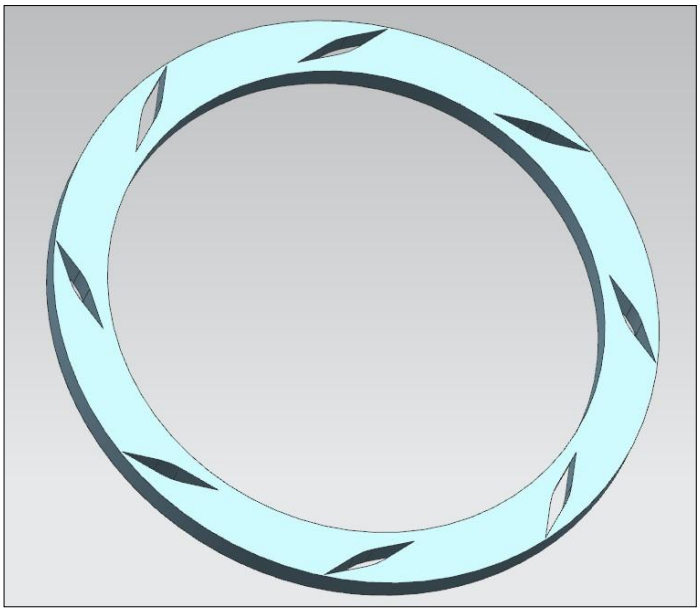

Fig 5.6 Diffuser model

5.2.3 Geometrical Parameters of Return Passage

The return passage is the last part of the single-stage pump. It is connected to the diffuser and the next impeller eye.

Table 5.3 Dimensions of Return Passage

Inlet diameter	502mm
Casing diameter	570mm
Number of guide vanes	11
Guide vane height	35mm
Casing height	58mm

5.2.4 Assembly of Multistage pump

Once all the domains are modelled, then they must be assembled properly so that the interfacing between rotor and stator parts and also between the stationary parts will be better. The following figures show the assembly of the 1st stage and the two-stage centrifugal pump. Fig. 5.7 and Fig. 5.8 show the inlet portion of the 1st stage and the outlet portion of the 1st stage, respectively.

5.2.4.1 Assembly of Single Stage Pump

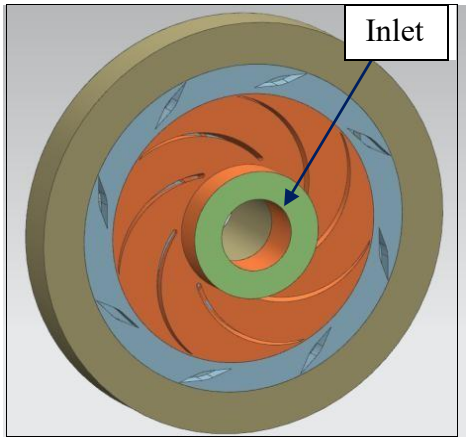

Fig. 5.7 Inlet portion of 1st stage

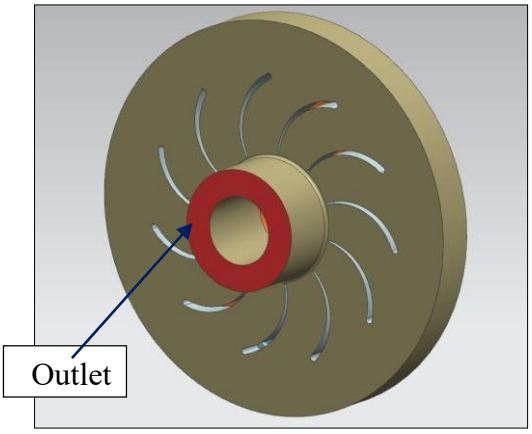

Fig. 5.8 Outlet portion of 1st stage.

The fluid enters at the inlet of the impeller and leaves the outlet through the return passage. Theinlet and outlet are defined separately to apply the boundary condition.

5.2.4.2 Assembly of Two Stage Multistage Pump

The figures below, Fig. 5.9 and Fig. 5.10, represent a two-stage centrifugal pump. The fluid enters the inlet of first-stage impeller, passes through the return passage, and enters the 2nd impeller, and then discharges from the outlet.

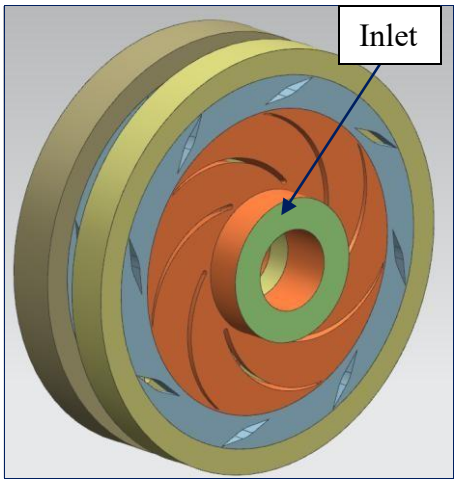

Fig 5.9 Inlet view of two stage pump

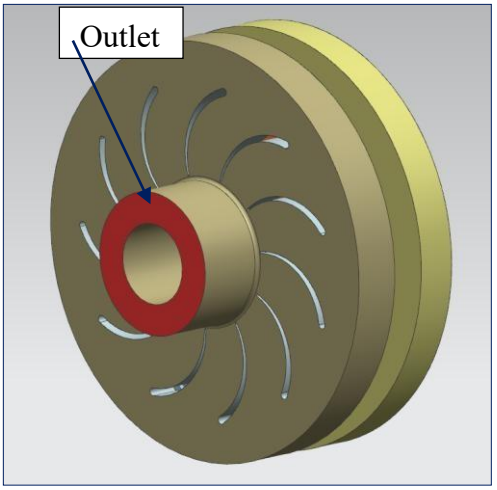

Fig 5.10 Outlet view of two stage pump

5.3 GEOMETRY PREPARATION OF MIXED, RADIAL, AND DISTORTED GUIDE VANE

5.3.1 Mixed Guide Vane

This is similar to the traditional one, but its diffuser vane and return guide vane share the identical diameter. They are used more widely in the medium and low specific speed deep well pumps. Fig. 5.11 shows (a) the 2D sketch, (b) the section of the 3D model, and (c) the mixed guide vane model, respectively.

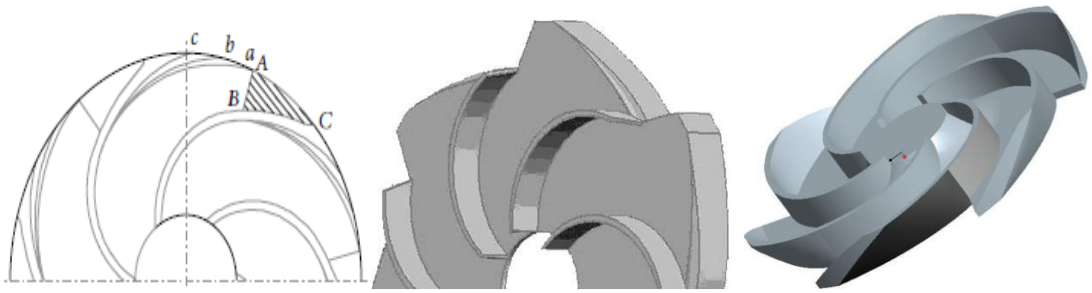

(a) (b) (c)

Fig. 5.11: Geometric model of Mixed guide vane

5.3.2 Radial Guide Vane

In this RGV, the diffuser vane is canceled, thus the liquid flowing out of the impeller is immediately transported into the triangular vane inlet. So, the suction throat of the guide vane is critical for its performance[74]. Fig. 5.12 shows (a) the 2D sketch, (b) Cross section of 3D model, (c) radial guide vane model respectively.

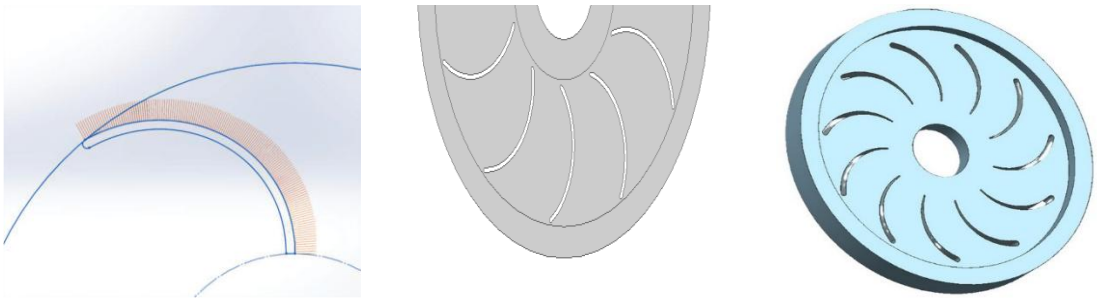

(a) (b) (c)

Fig. 5.12: Geometric model of Radial guide vane

5.3.3 Distorted Guide Vane

The structure of the distorted guide vane is directly adapted from the structure of the radial guide vane. To effectively guide the flow into the guide vane smoothly, the guide vane is designed with a distorted leading edge. Fig. 5.13 shows (a) the 2D sketch, (b) the section of the 3D model, and (c) the distorted guide vane model, respectively.

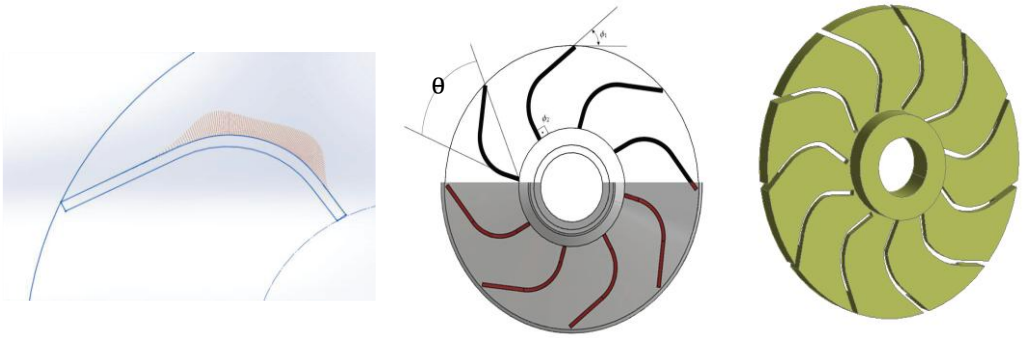

(a) (b) (c)

Fig. 5.13: Geometric model of Distorted guide vane

5.4 MESH GENERATION

The partial differential equation that governs the fluid flow is not usually used to solve for the analytical solution. To analyze fluid flow, all flow domains are divided into smaller sub-domains, which are called elements or cells. This conversion process of the domain into sub-domains is called mesh generation. Some elements will be 3D in the shape of hexahedra and tetrahedral shapes, and some will be 2D shapes of triangles and rectangular. The governing equations are then discretized and solved inside each of these subdomains. And the collection of all these 3D and 2D elements will represent a mesh or grid. The grid or mesh pattern will be unstructured or structured in a format. After completion of designing the 3D model of parts of the pump, each part of the geometry is imported to ICEM CFD, where every part of a single domain is named (i.e., parts creating), and further, the whole domain is cleaned and meshed. The domain will be divided into subdomains with a good-quality mesh. The 2D elements will represent the domain surface, and the 3D elements will show the flow domain as shown in [75].

5.4.1 Meshing of Impeller

The unstructured tetrahedral mesh for the 3D flow domain and the triangular surface mesh for the 2D domain are generated for the impeller geometry. The impeller geometry consists of the impeller inlet, impeller outlet, hub, shroud, and blades. The outlet of the impeller is connected to the diffuser inlet with proper interfacing between them. The impeller contains 398099 total no. of nodesand 2203762 no. of elements.

Fig. 5.14 3D view of impeller meshing

Fig. 5.14 and Fig. 5.15 show a 3D view of impeller meshing and an enlarged view of impeller meshing, respectively.

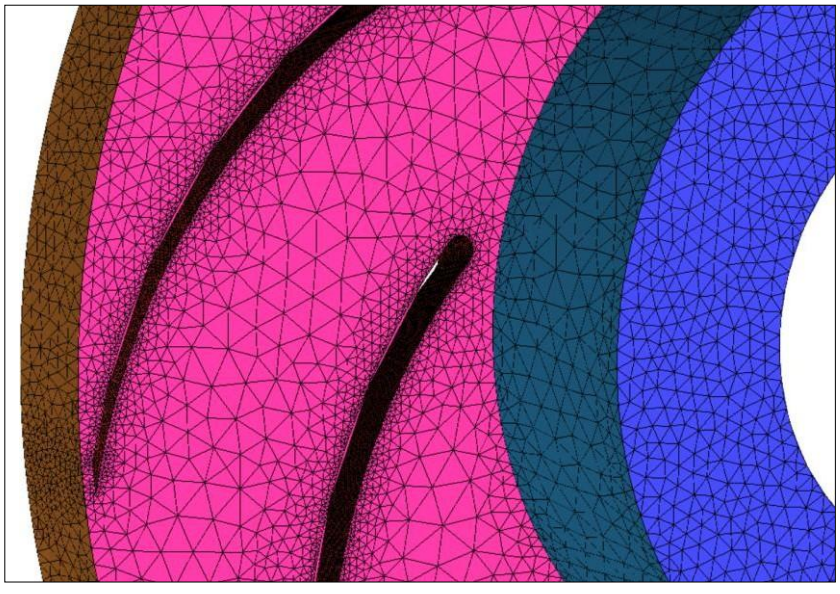

Fig. 5.15 Enlarged view of impeller meshing

5.4.2 Meshing of Diffuser

The diffuser contains its inlet, outlet, casing, and DFV. The vanes have fine edges, so the meshing of vanes is a very small size of elements. Diffuser meshing is an unstructured tetrahedral meshfor the flow domain and a triangular mesh of surfaces. The diffuser contains 181150 total no. of nodes and 1002296 no. of elements.

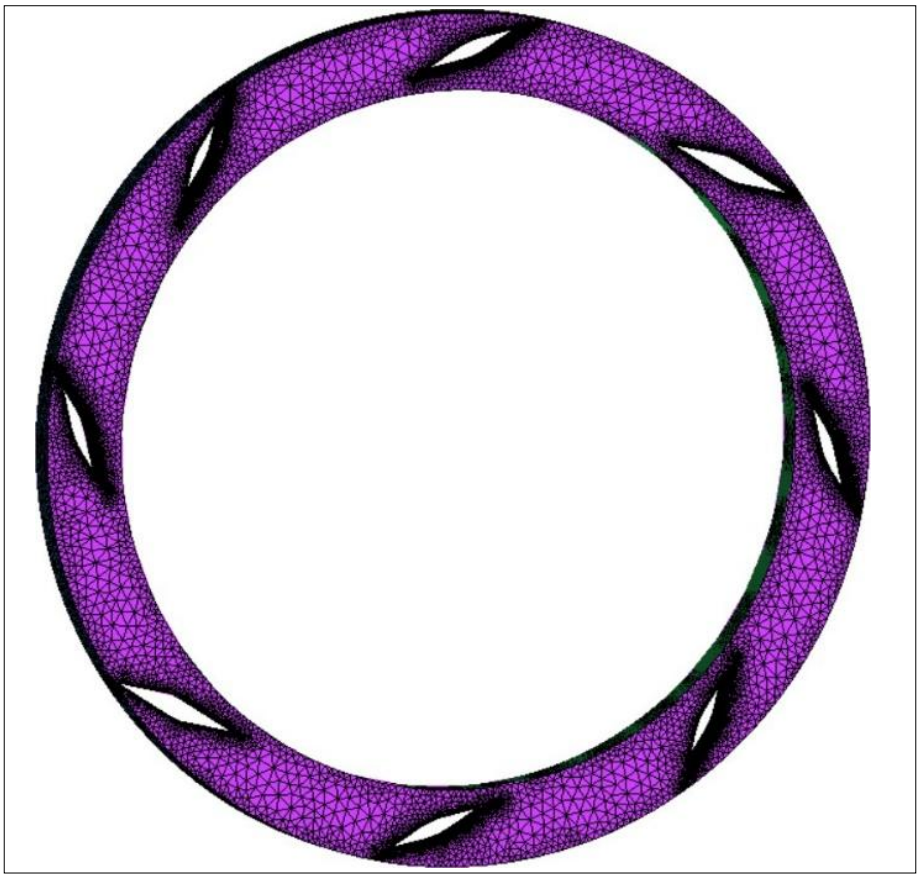

Fig. 5.16 Meshing of Diffuser

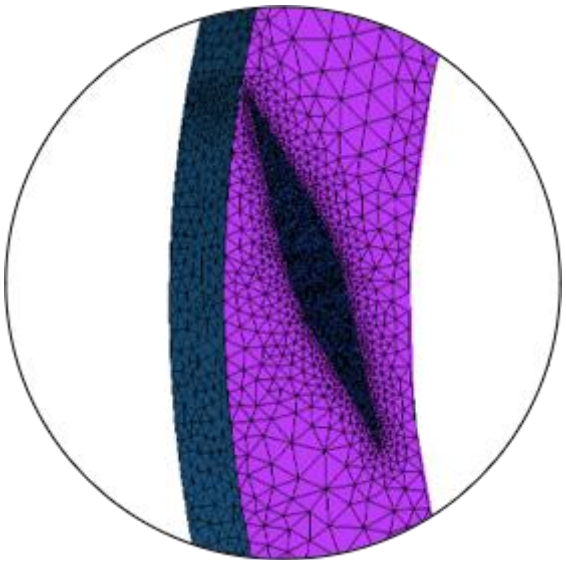

Fig. 5.17 Enlarged view of Diffuser casing and vane mesh

Fig. 5.16 and Fig. 5.17 show meshing of diffuser and enlarged view of diffuser casing and vane mesh, respectively.

5.4.3 Meshing of 1st Stage Return Passage

The return passage consists of 713657 total no. of nodes and 3975324 no. of elements.

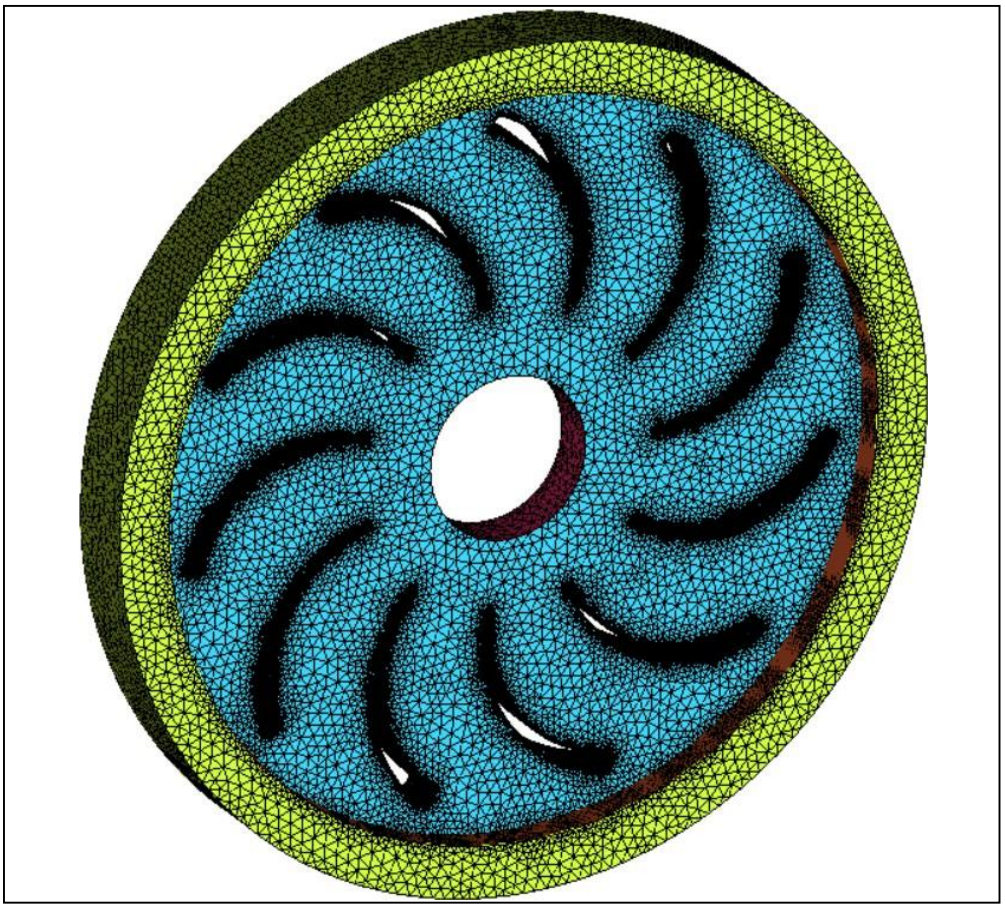

Fig. 5.18 3D view of Return passage mesh

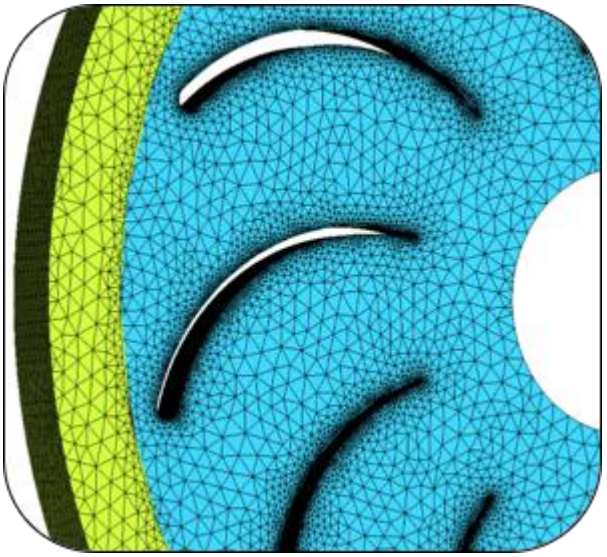

Fig. 5.19 Enlarged view of 1st stage return passage

Fig. 5.18 and Fig. 5.19 show a 3D view of the return passage mesh and an enlarged view of the 1st stage return passage, respectively.

5.4.4 Meshing of 2nd Stage Return Passage

The return passage consists of 722994 total no. of nodes and 4028811 no. of elements.

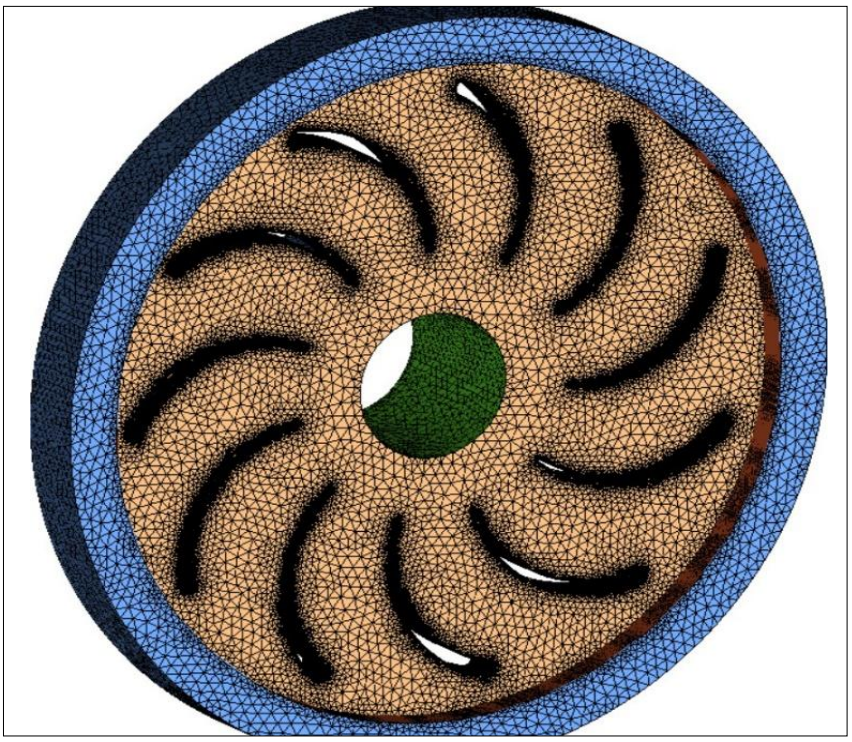

Fig 5.20 3D Front view of return passage

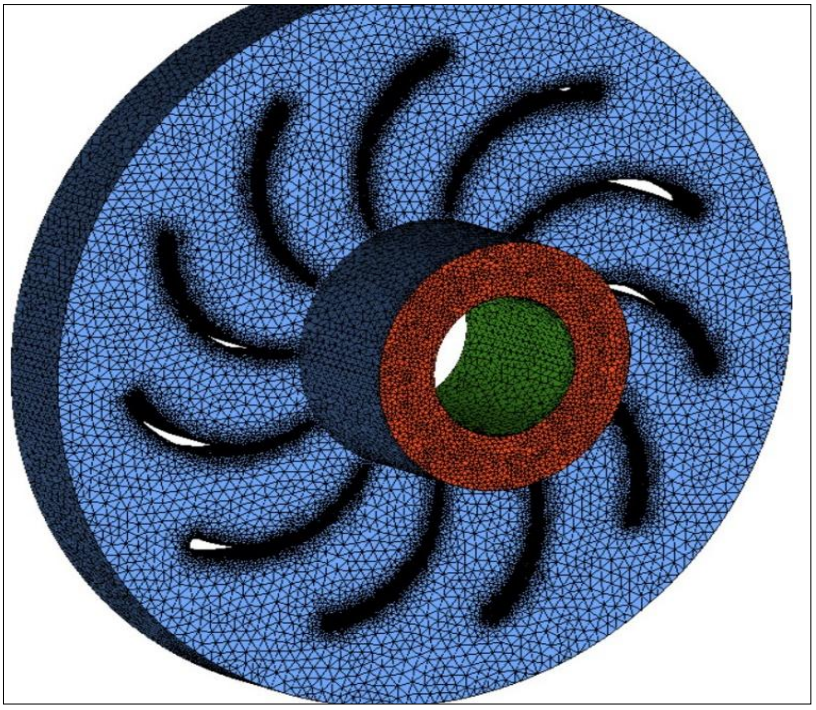

Fig. 5.21 3D Back view of return Passage

Fig. 5.20 and Fig. 5.21 show 3D front view of return passage 3D back view of return passage respectively.

Table 5.4 Mesh data of each domain

Domain	No. of Nodes	No. of Elements		Element Type
Impeller	398099	Impeller Inlet	7058	Triangle
		Hub	26343	Triangle
		Shroud	26078	Triangle
		Blades	227181	Triangle
		Impeller Outlet	7616	Triangle
		Shaft	2022	Triangle
		Flow domain	2203762	Tetrahedral
Diffuser	181150	Diffuser inlet	6061	Triangle
		Diffuser outlet	8854	Triangle
		Vanes	91357	Triangle
		Diffuser casing	26461	Triangle
		Flow domain	1002296	Tetrahedral
Return passage of 1st stage	713657	Inlet	6903	Triangle
		Outlet	3514	Triangle
		Casing	39635	Triangle
		Guide vanes	361971	Triangle
		Inner wall	32010	Triangle
		Shaft	896	Triangle
		Flow domain	3975324	Tetrahedral
Return passage of 2nd stage	722994	Inlet	6908	Triangle
		Outlet	3432	Triangle
		Casing	2750	Triangle
		Guide vanes	361934	Triangle
		Inner wall	32040	Triangle
		Shaft	2425	Triangle
		Flow domain	4028811	Tetrahedral

Table 5.4 shows the mesh data for each domain: impeller, diffuser, and return passage of the 1st stage and 2nd stage.

5.5 PRE-PROCESSING

The 3D geometry model is prepared in Ansys Design Modeler, and then the meshing of all the domains is done in ICEM CFD. From ICEM CFD, for each domain, the file is saved in .cfx format. Then, in CFX - Pre, each domain is imported as an assembly of a single-stage and a two-stage pump is carried out by translation, rotation, and copying of domains. Table 5.5 shows general input data.

Table 5.5 General Input Data

Domain type	Fluid domain	
Fluid	Water at 25°C	
Density of Fluid	997 kg/m^3	
Reference pressure	0 atm	
Domain motion	Impeller	Rotating 1. 1450 rpm 2. 1600 rpm 3. 1750 rpm 4. 1900 rpm
	Diffuser	Stationary
	Return passage	stationary
Rotation axis	Z – axis	
Turbulence model	k – ε	

5.5.1 Boundary Conditions

To obtain the final result, it is necessary first to apply boundary details, i.e., inlet and outlet conditions. The boundary details play a vital role in getting better accuracy and results.

The following boundary conditions are used,

5.5.1.1 Inlet Condition

At the inlet, the static pressure is applied of 1atm with reference pressure set as zero and shown in Fig. 5.22.

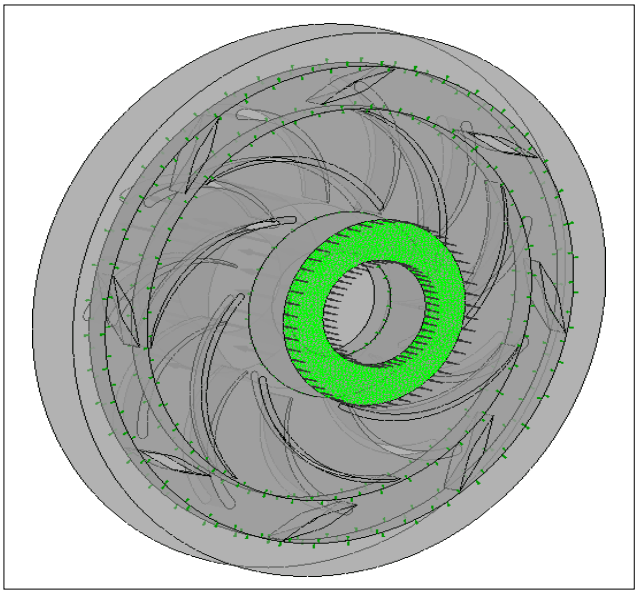

Fig. 5.22 Inlet boundary selection

5.5.1.2 Outlet Condition

At the outlet, the mass flow rate is applied of 128.88 kg/s and shown in Fig. 5.23.

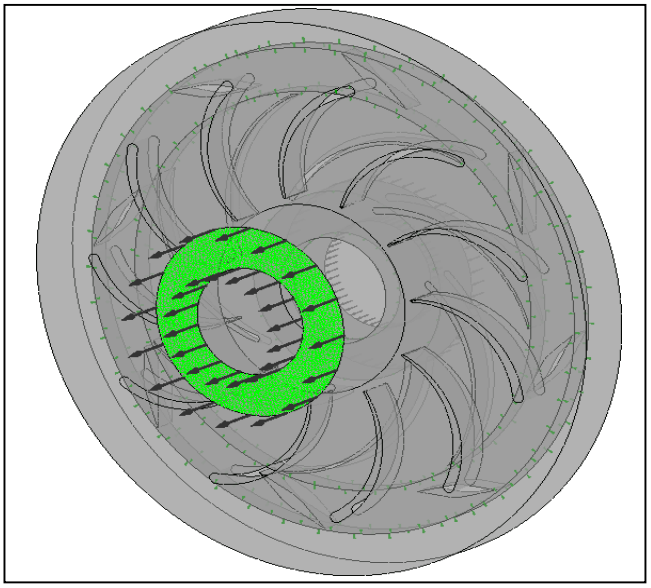

Fig. 5.23 Outlet boundary selection

5.5.2 Interface Condition between domains

As each domain is separately meshed, and then all the domains are assembled in CFX - Pre. Now each domain is to be interfaced with the others because fluid has to flow from one domain outlet to another domain inlet, i.e., representing the connectivity of the fluid domain.

Here, there are some rotating parts and some are stationary parts, so in the interference, the frame change model must be frozen rotor, having pitch change as none. Table 5.6 and Table 5.7 present domain interface data for single-stage pumps and domain interface data for two-stage pumps, respectively.

Table 5.6 Domain Interface Data for Single Stage pump

Interface Location	**Interface type**	**Interface models**	**Frame change**	**Pitch change**
Impeller - Diffuser	Fluid - Fluid	General connection	Frozen rotor	None
Diffuser - Return Passage	Fluid - Fluid	General connection	None	None

Table 5.7 Domain Interface Data for Two Stage Pump

Interface Location	**Interface type**	**Interface models**	**Frame change**	**Pitch change**
Impeller - Diffuser	Fluid - Fluid	General connection	Frozen rotor	None
Diffuser - Return Passages	Fluid - Fluid	General connection	None	None
Return passage 1 – Impeller of 2^{nd} Stage	Fluid - Fluid	General connection	Frozen rotor	None

5.6 COMPUTATIONAL METHOD FOR FLOW ANALYSIS

The flow analysis is carried out using Ansys CFX software. The flow simulation is first carriedout for a single stage by varying the number of blades by 5,6, and 7 and by changing the speed through 1450 rpm, 1600 rpm, 1750 rpm, and 1900 rpm. By varying both speed and no. of blades, a total of 12 cases are there. The discharge of 0.1288 m^3/s is kept constant for all analyses. After carrying out flow simulation for a single stage, the three best results that will give high efficiency and head will be selected, and further flow simulation for a two-

stage centrifugal pump will be carried out.

5.7 SOLVER

In the Ansys CFX, after applying boundary details, the solver control has to be run. A CFX solver involves the discretization of the flow domain into a differential equation. After discretization, the volume and surface integrals change to a system of algebraic equations. A certain number of iterations has to be applied after completion of all iterations, and a definition (.def) file will be generated. Table 5.8 shows data used in the CFX solver.

Table 5.8 Data used in CFX solver

Advection scheme	High resolution
Turbulence numeric	High resolution
Number of iterations	500
Length scale control	Conservative
Timescale control	Auto timescale
Timescale factor	1
Residual type	RMS
Residual target	10^{-06}

5.8 POST-PROCESSING

After completion of the solver, the solver creates a result file (.res), which will be analyzed in CFX – Post. In CFX – Post, the flow simulation is studied, including the streamline pattern, pressure contour,blade-to-blade analysis, etc. All the parameters, such as various velocity components, static pressure, total pressure, torque, mass flow rate, etc., can be calculated using a function calculator in various domains and at various locations.

Summary

1. **The 3D models for the impeller, diffuser, and return passage were successfully built in Ansys Design Modeler, and each domain's geometrical parameters were specified.**
2. **Detailed meshing for impeller, diffuser, and return passages was accomplished, ensuring good quality mesh for precise flow analysis.**
3. **Flow simulations were carried out in Ansys CFX, varying the number of blades and speeds, to identify the best-performing configurations.**
4. **Through simulations, the configurations that provided the highest efficiency and head were identified, which were then used for further analysis in a two-stage centrifugal pump setup.**

CHAPTER 6.

OPTIMIZATION OF SINGLE-STAGE CENTRIFUGAL PUMP USING RESPONSE SURFACE METHODOLOGY

This chapter describes the optimization technique (Response Surface Methodology) used for the optimization of a single-stage centrifugal pump.

6.1 RESPONSE SURFACE METHODOLOGY

Response surface methodology (RSM) is a statistical tool employed to simplify complex systems by examining the connection between input-independent variables and response patterns at the output. It explores the relationships between several explanatory variables and one or more response variables. Introduced by George E. P. Box and K. B. Wilson in 1951[76], RSM has become a cornerstone in experimental design and process optimization across various scientific and engineering disciplines.

RSM aims to model and analyze problems where a response of interest is influenced by several variables. The objective is to optimize this response by identifying the optimal settings of the input variables[76–85]. This is achieved by fitting a polynomial equation to the experimental data, which serves as an approximation of the true relationship between inputs and outputs.

The flowchart for the Response Surface Methodology is displayed in Fig. 6.1. The key difference between the two lies in the number of levels assigned to each input variable. Box-Behnken Design (BBD) employs three levels (-1, 0, and 1) for each input variable, which leads to a total of 15 experimental runs. The main difference between the two is the number of levels for each input variable. BBD uses three levels (-1, 0, and 1) for each input variable, resulting in a total of 15 experimental runs. This design is beneficial for detecting quadratic effects and variable interactions. Conversely, Central Composite Design (CCD) employs additional levels (-1.68, -1, 0, 1, and 1.68) for each input variable, necessitating 20 to 30 experimental runs in total. This design aids in identifying linear and quadratic effects, along with variable interactions.

6.2 EXPERIMENTAL DESIGNS IN RSM

Several different experiment design strategies were used in the response surface methodology to fit models accurately. Central Composite Design (CCD) and Box-Behnken Design (BBD) are the two most commonly utilized.

1. Central Composite Designs (CCD): These designs are used to build second-order (quadratic) models without needing to use a complete three-level factorial experiment. They are efficient for fitting a full quadratic model and are rotatable or nearly rotatable,

which means they provide constant prediction variance at points equidistant from the center.

2. Box-Behnken Designs: These are rotatable second-order designs based on three-level incomplete factorial designs. They require fewer runs than CCD and are efficient in estimating the first- and second-order coefficients.
3. Three-Level Factorial Designs: These involve experiments where each factor is tested at three levels. They are useful for detecting curvature in the response surface, but can become resource-intensive with an increasing number of factors.

6.3 METHODOLOGY

6.3.1 Model Building

The process of building a response surface model typically involves the following steps, as shown in Fig. 6.1.

1. Selection of Test Factors and Ranges: Identify the input variables (factors) that potentially influence the response and determine the feasible range for each factor. This study utilizes a face-centered Central Composite Design (CCD) with $\alpha = 1$. In a three-factor experiment, for example, the three factors chosen, A, B, and C, need to have ranges, and the upper and lower lines of the ranges are called upper and lower levels. Table 7 presents the levels of the three test factors (blade number Z (A), rotational speed N (B), and the rate of flow Q (C)). The upper, zero, and lower levels are normalized to values of 1, 0, and -1 as shown in Table 7.
2. Design of Experiments (DoE): Choose an appropriate experimental design (e.g., CCD, Box-Behnken) to systematically vary the factors and collect data. Using the response surface analysis Central Composite Design (CCD) approach in the Design Expert 12 software, the experimental design was completed with the pump head (H) and Efficiency (η) serving as responses. Table 6.1 and Table 6.2 show test factors and the levels of centre composite design and scheme, and results of central composite design, respectively. The operating speed range of 1450–1900 rpm was selected as it represents the safe working envelope of the pump. Operation beyond 1900 rpm may lead to excessive mechanical stresses and reduced cavitation margin, and was therefore excluded. In the RSM study, the flow rate was systematically varied at 350, 450, and 550 m^3/h, ensuring coverage of practical operating conditions. The constant value of 128.88 kg/s was used only for specific two-stage visualization comparisons to isolate blade-count effects, and not in the optimization process.

3. Conducting Experiments: Perform the experiments as per the design matrix and record the responses. 20 sets of schemes were produced by the experimental design, which were analyzed using the simulation technique. Table 8 shows the scheme and results of the test sites of the central composite design, where the number of experiments performed was 20 as discussed in [73]2.
4. Fitting the Model: Use regression analysis to fit a polynomial model (usually second-order) to the experimental data.
5. Model Validation: Assess the adequacy of the model using statistical tests and diagnostic plots to ensure it accurately represents the system.

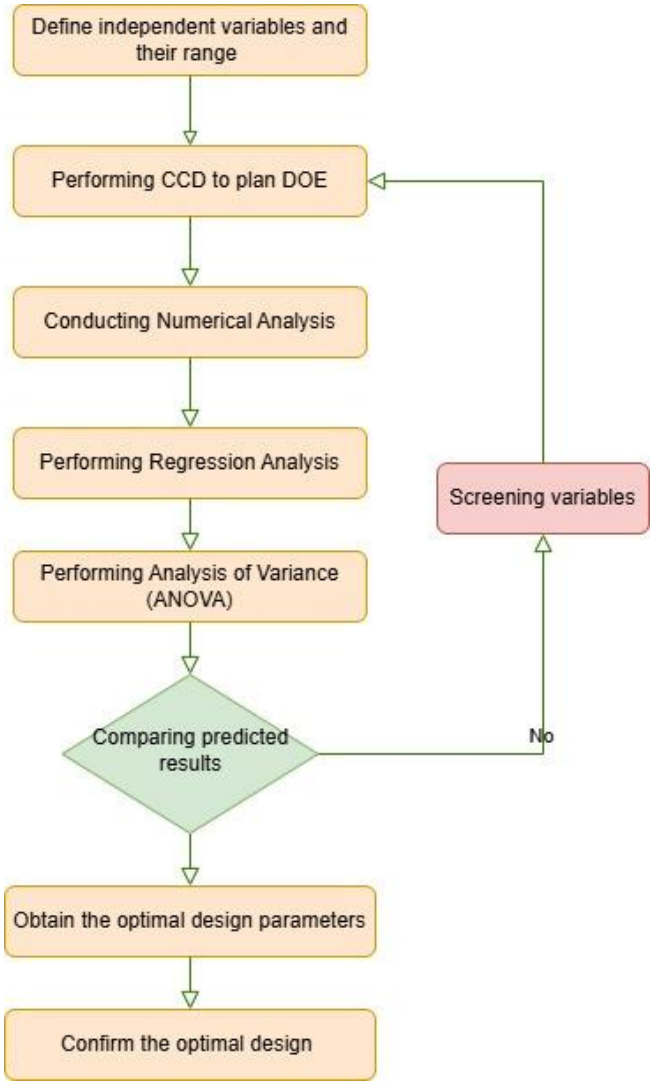

Fig. 6.1 Response surface methodology flowchart.

Table 6.1 Test factors and the levels of Centre Composite Design [86]

Factors	Code level		
	-1	0	1
A	5	6	7
B	1600	1750	1900
C	350	450	550

Table 6.2 Scheme and Results of Central Composite Design [86]

Run	**Factor1** z	**Factor 2** N (rpm)	**Factor 3** Q (m^3/h)	**Response 1** **H**	**Response 2** **η**
1	6	1750	450	32.88	47.43
2	5	1900	550	38.21	45.72
3	6	1750	450	32.88	47.43
4	5	1900	350	33.01	43.6
5	5	1750	450	26.92	41.11
6	6	1750	550	35.43	48.64
7	6	1900	450	44.01	50.93
8	7	1900	350	43.71	52.39
9	6	1750	450	27.02	47.43
10	5	1600	550	21.36	37.49
11	6	1750	450	32.88	47.43
12	7	1750	450	37.12	51.26
13	6	1750	450	32.88	47.43
14	6	1750	450	32.88	47.43
15	7	1600	350	23.21	42.68
16	6	1750	350	27.02	46.17
17	7	1600	550	28.11	46.97
18	7	1900	550	53.46	55.95
19	5	1600	350	20.01	35.08
20	6	1600	450	22.02	40.57

6.3.2 Optimization

Once a reliable model is established, optimization techniques are applied to find the factor levels that maximize or minimize the response. This involves:

1. Gradient Analysis: Determining the direction of steepest ascent or descent to move towards the optimal region.
2. Contour Plots and Surface Plots: Visualizing the response surface to identify optimal conditions and understand the interaction between factors.
3. Numerical Optimization: Employing algorithms to precisely locate the optimal settings of the factors.

6.4 APPLICATIONS

RSM is widely applied across various fields, including[87]:

- Engineering: Optimizing manufacturing processes, improving product designs, and enhancing system performance.
- Chemistry: Optimizing reaction conditions, such as temperature and pressure, to maximize yield or selectivity.
- Food Science: Developing new products and improving existing formulations by optimizing ingredient proportions and processing conditions.
- Biotechnology: Enhancing fermentation processes and optimizing culture conditions for maximum product yield.
- Agriculture: Improving crop yields by optimizing factors like fertilizer application rates and irrigation schedules.

6.5 ADVANTAGES AND LIMITATIONS[88]

6.5.1 Advantages

- Efficiency: RSM reduces the number of experimental trials needed by systematically exploring the factor space, making it cost-effective and time-saving.
- Interaction Detection: It identifies interactions between factors, providing a deeper understanding of the system under study.
- Optimization Capability: RSM not only models the response but also facilitates the optimization of processes and products.

6.5.2 Limitations

- Model Approximation: The polynomial models used in RSM are approximations and may not capture complex, nonlinear relationships accurately.
- Experimental Errors: The presence of experimental errors can affect the accuracy of the model and the optimization results.
- Factor Limitations: RSM is less effective when the number of factors is very large, as the required number of experiments can become impractical.

Summary

1. **RSM is a statistical tool that examines the relationship between input variables and response patterns.**
2. **The chapter highlights two common experimental designs: Central Composite Design (CCD) and Box-Behnken Design (BBD).**
3. **CCD uses five levels for each input variable and is effective in identifying linear and quadratic effects, while BBD employs three levels and is useful for detecting quadratic effects and interactions.**
4. **A face-centered CCD with three factors—blade number, rotational speed, and flow rate was used in the study.**
5. **Twenty experimental runs were conducted using Design Expert 12 software to analyze the pump head and flow coefficients, resulting in optimized configurations for the centrifugal pump.**

CHAPTER 7.

RESULTS AND DISCUSSIONS

This chapter relates to the results obtained after flow simulation for a single-stage pump with different no. of impeller blades and rotational speed, the performance parameters are discussed with tables and charts. A simulation for a two-stage pump is discussed for constant speed with various impeller blades, and the velocity streamlines pattern and pressure contour are shown, and head losses in a two-stage pump are tabulated.

7.1 GENERAL

A multistage centrifugal pump consists of several impellers in series. To carry out a complete flow simulation of a multistage pump, it is necessary to study the first flow simulation of a single stage of a multistage pump. So, analysis is carried out at different speeds and with different numbers of impeller blades for a single stage. The speed is varied from 1450 rpm to 1900 rpmat 150 intervals, and blades are varied as 5, 6, and 7 while keeping the 128.88 kg/s mass flowrate, diffuser vanes, and return channel vanes constant. The numerical flow simulation is carried out first for the impeller with 5 blades and only speed is varied, then for the impeller with 6 blades and varying speed, and last for those with 7 blades at various speeds. The boundary detailsare applied at the impeller inlet and return passage outlet. The objective is to carry out a numerical simulation of the multistage pump and see its performance. The results are shown in streamline and pressure contour plots and quantitatively presented in tabular and graphical forms.

7.2 STUDY OF FLOW SIMULATION FOR SINGLE-STAGE PUMP

The single stage has been analyzed by varying blades at different rotation speeds.

7.2.1. Single stage with Five Impeller Blades

The CFD simulation was carried out for a single-stage pump that has an impeller with 5 blades, a diffuser with 8 vanes, and a return passage with 11 RGV. The mass flow rate is kept constant as discussed above. The investigation is carried out by varying the speed of the impeller to 1450rpm, 1600 rpm, 1750 rpm, and 1900 rpm. The performance of the pump is represented by plotting graphs for parameters such as head, efficiency, power, head coefficient, and velocity w.r.t speed.Streamline patterns and pressure contours are shown for various speeds.

To determine the performance of a single-stage pump at different speeds, the various parameters are calculated in non-dimensional form. The parameters are

Head coefficient $$H^* = \frac{gH}{u_2^2} \quad (7.1)$$

Power coefficient $P^* = \frac{P_{in}}{\rho\omega^3 D_2^5}$ (7.2)

Head generated $H = \frac{(P_2 - P_1)\, stan.frame}{\gamma}$ (7.3)

Manometric efficiency $\eta = \frac{H_{mano}}{\frac{C_{u2}u_2}{g}}$ (7.4)

Flow coefficient $\Psi = \frac{W_2}{\sqrt{2gH}}$ (7.5)

Speed coefficient $\phi = \frac{u_2}{\sqrt{2gH}}$ (7.6)

Specific speed $N_s = \frac{N\sqrt{Q}}{H^{3/4}}$ (7.7)

Input power $P_{in} = \frac{2\pi NT}{60000}$ (7.8)

Output power $P_{out} = \frac{\gamma QH}{1000}$ (7.9)

Table 7.1 Variation of the flow parameters at different speeds for impeller with 5 blades

Speed (rpm)	**1450**	**1600**	**1750**	**1900**
P_1 (pa)	256379	246788	251630	263691
P_2 (pa)	343183	429140	515758	615133
H (m)	8.848	18.588	26.924	35.824
P_{out} (W)	11180.35	23486.93	34019.68	45265.72
P_{in}(W)	49117.38	64719.90	82740.80	101537.48
η (%)	22.76	36.29	41.11	44.58
N_s	101.43	64.142	53.135	46.566
*H**	0.0904	0.1560	0.1889	0.2133
*P**	0.1884	0.2039	0.2179	0.2268
Ψ	0.6274	0.4185	0.3459	0.2973
Φ	2.3508	1.7897	1.6265	1.5309

7.2.1.1.Variation of manometric efficiency for impeller with 5 blades

The analysis is carried out for a single-stage pump having an impeller of 5 blades. The mass flow rateis kept constant, and only the speed is varied from 1450 rpm to 1900 rpm. It is found that the variation of efficiency with speed is of an increasing type as shown in Fig. 7.1. The maximum efficiency is 44.58% at 1900 rpm. It is also found that the efficiency decreases linearly with the flow coefficient, shown in Fig. 7.2.

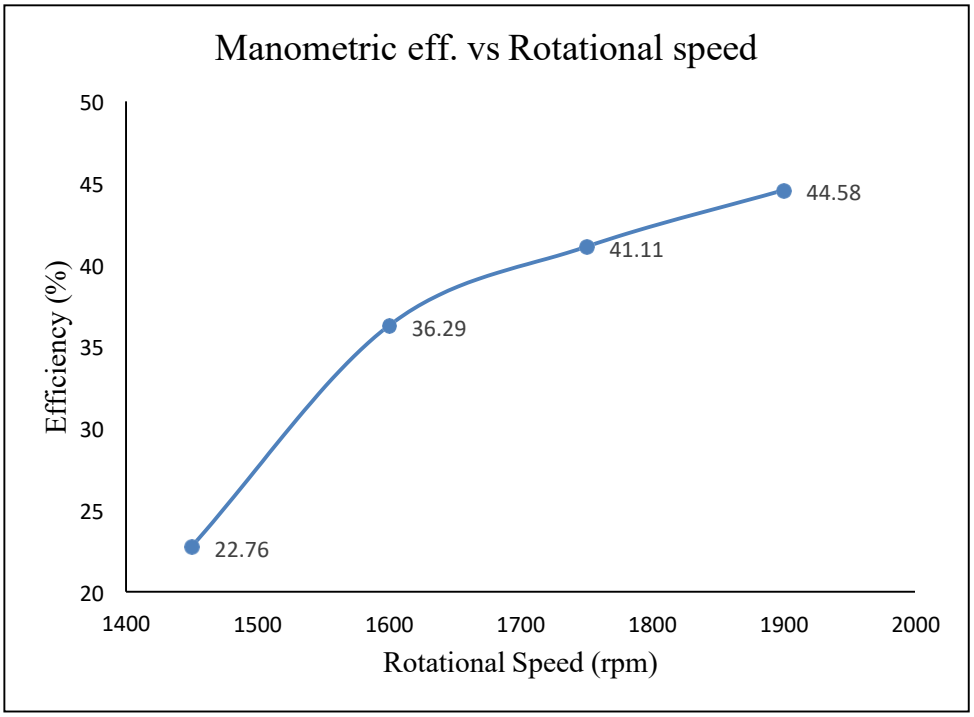

Fig. 7.1 Variation of hydraulic efficiency with the rotational speed

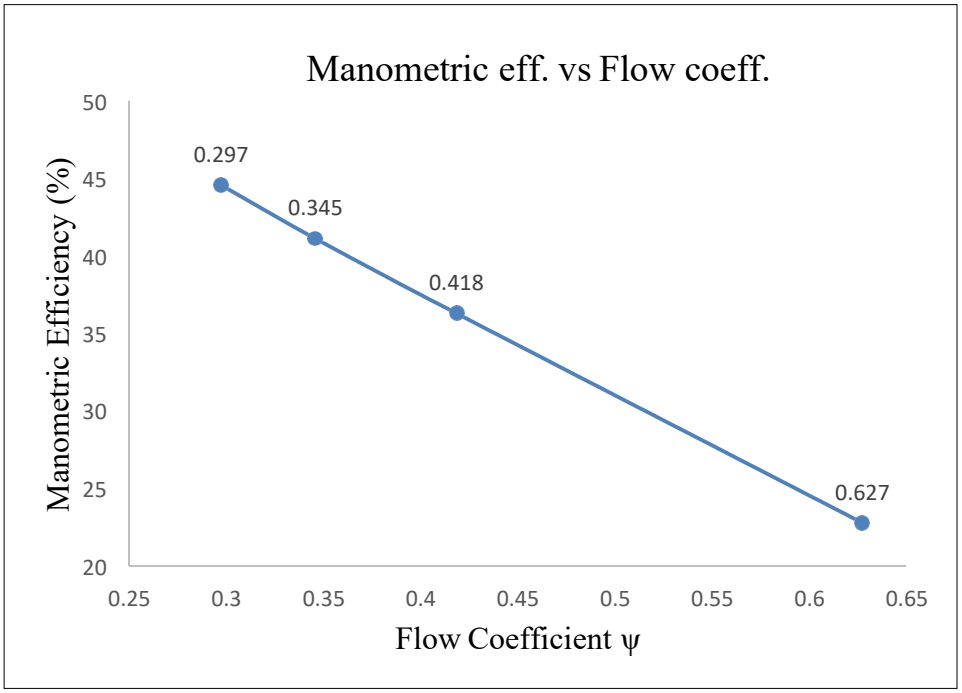

Fig. 7.2 Variation of hydraulic efficiency with flow coefficient

7.2.1.2.Variation of output power for impeller with 5 blades

The variation between the output Power with speed is shown in Fig. 7.3. It is seen that output Power increases linearly with an increase in speed.

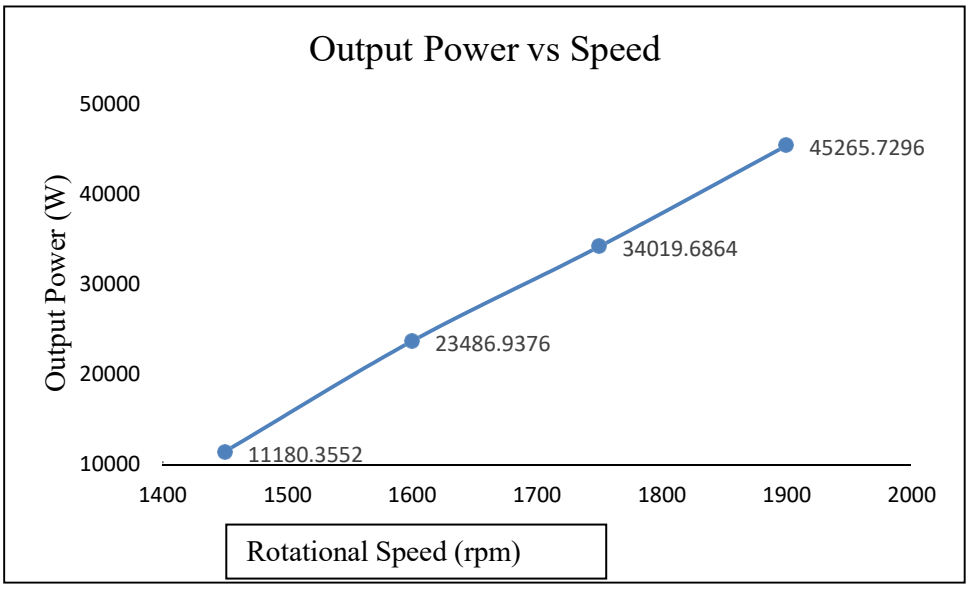

Fig.7.3 Output power variation with speed

The power coefficient varies in a straight line as speed is varied shown in figure below Fig.7.4

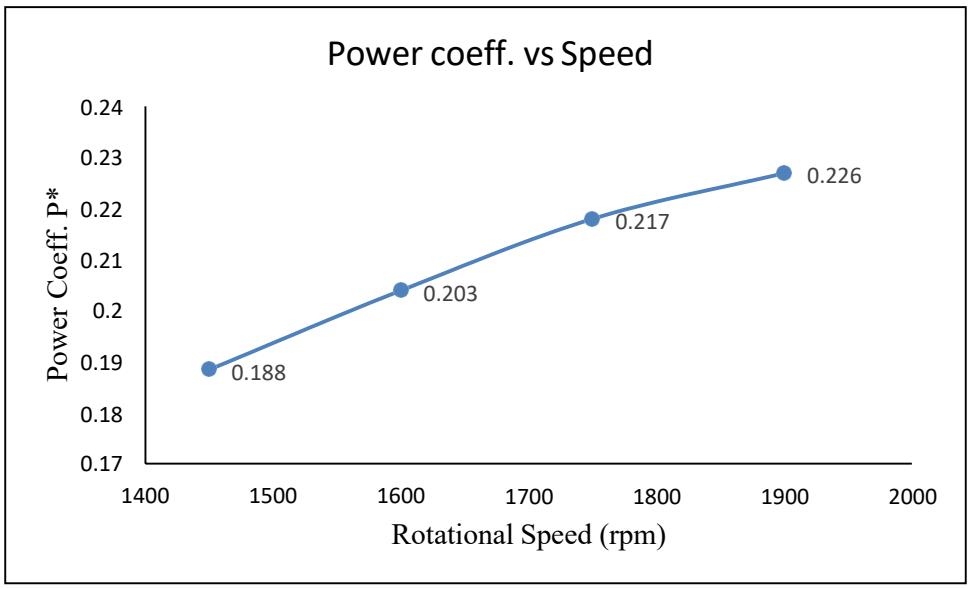

Fig. 7.4 Power Coefficient Vs Rotational speed

7.2.1.3.Variation of head for impeller with 5 blades

The head is generated by a single stage after several losses in the stationary parts. It is found that as the speed of the pump increases, the head produced by the pump also increases, as shown in Fig. 7.5.The maximum head produced by the pump is 35.82 m at 1900 rpm. It is also observed that the head coefficient varies with changing speed from Fig. 7.6.

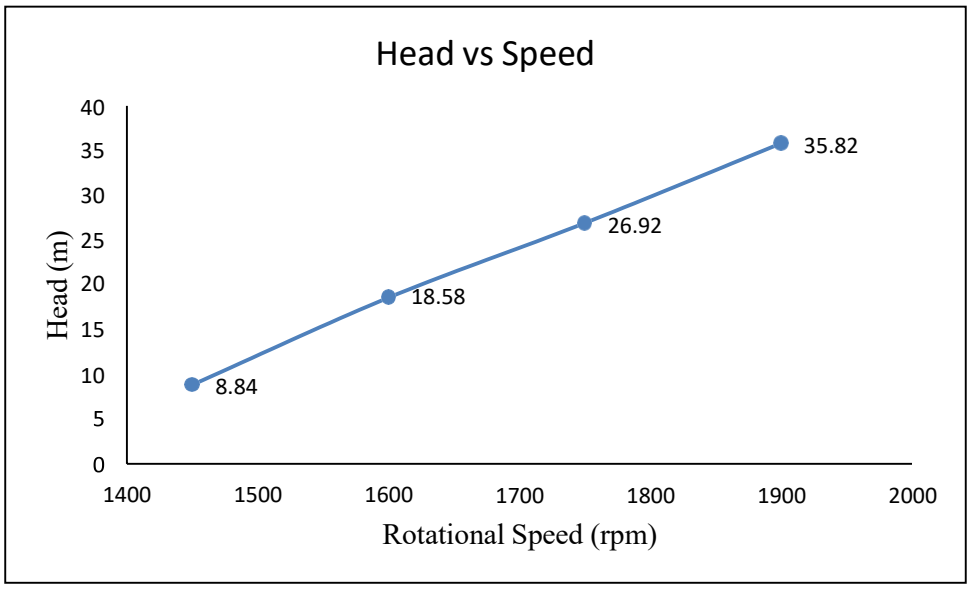

Fig.7.5 Head variation with speed

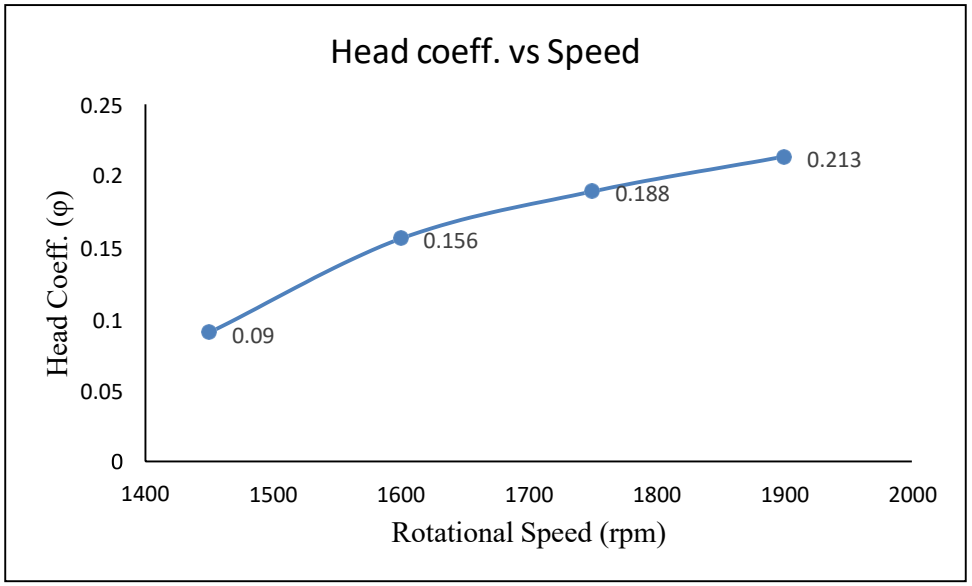

Fig. 7.6 Head coefficient Vs Speed

7.2.2. Single stage with Six Impeller Blades

After the analysis of the pump with 5 blades, the flow simulation is studied for the impeller with 6 blades, the diffuser with 8 vanes, and the return passage with 11 RGV. The mass flow rate is kept constant as discussed above. The investigation is carried out by varying the speed of the impeller to 1450 rpm, 1600 rpm, 1750 rpm, and 1900 rpm.

Table 7.2 Variation of the flow parameters at different speeds for impeller with 6 blades

Speed (rpm)	**1450**	**1600**	**1750**	**1900**
P_1 (pa)	257588	246000	231586	231963
P_2 (pa)	365527	462076	554234	663765
H (m)	11.00	22.02	32.88	44.01
P_{out} (W)	13902.54	27830.58	41557.06	55616.09
P_{in}(W)	51836.81	68588.31	87604.51	109200.86
η (%)	26.81	40.57	47.43	50.93
N_s	86.137	56.477	45.729	39.9024
H^*	0.1124	0.1849	0.2308	0.2621
P^*	0.1988	0.2161	0.2307	0.2439
Ψ	0.5470	0.3846	0.3100	0.2615
Φ	2.1081	1.6441	1.4716	1.3811

7.2.2.1.Variation of manometric efficiency for impeller with 6 blades

The analysis is carried out for a single-stage pump having an impeller of 6 blades. The mass flow rateis kept constant, and only the speed is varied from 1450 rpm to 1900 rpm. It is found that the variation of efficiency with speed is of an increasing type, as shown in Fig. 7.7, the maximum efficiency is 50.93% at 1900 rpm. It is also found that the efficiency decreases linearly with the flow coefficient, shown in Fig. 7.8

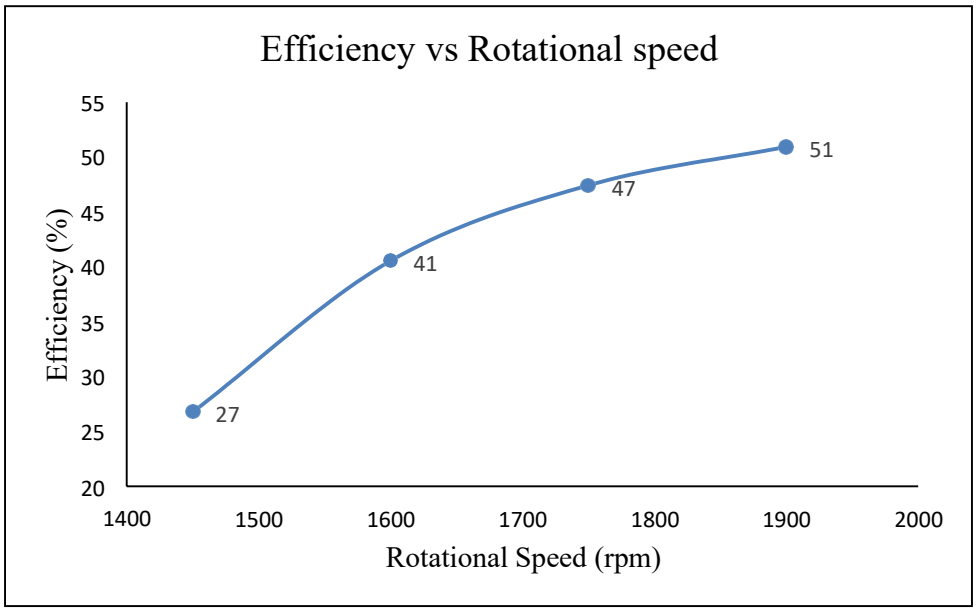

Fig. 7.7 Variation of hydraulic efficiency with the rotational speed

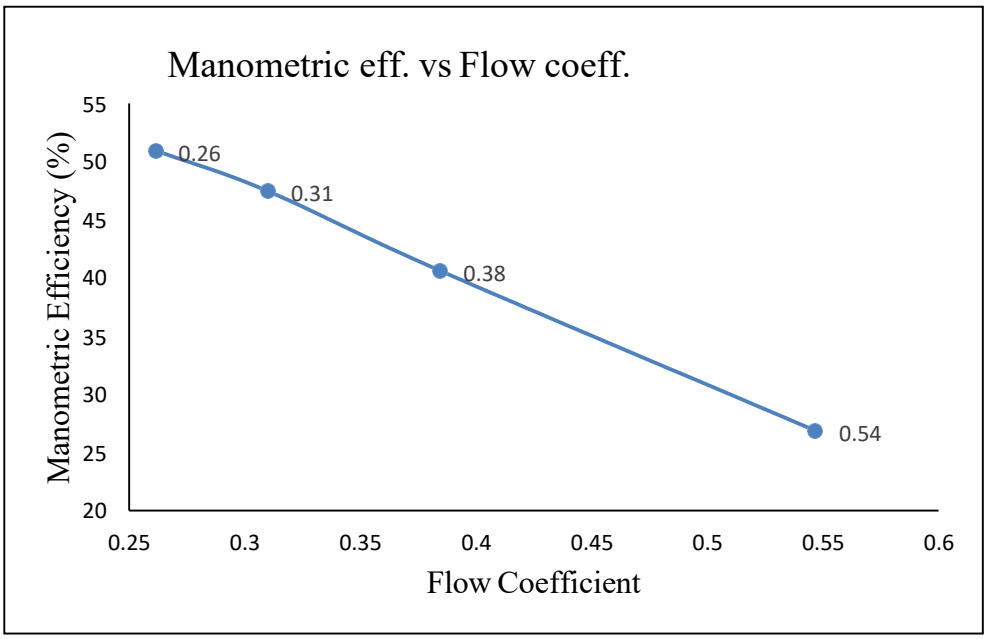

Fig. 7.8 Variation of hydraulic efficiency with flow coefficient

7.2.2.2. Variation of output power for impeller with 6 blades

The variation between output Power with speed is shown in Fig. 7.9. It is seen that output Power increases linearly with an increase in speed. The maximum power developed is 55.616 kW at 1900 rpm.

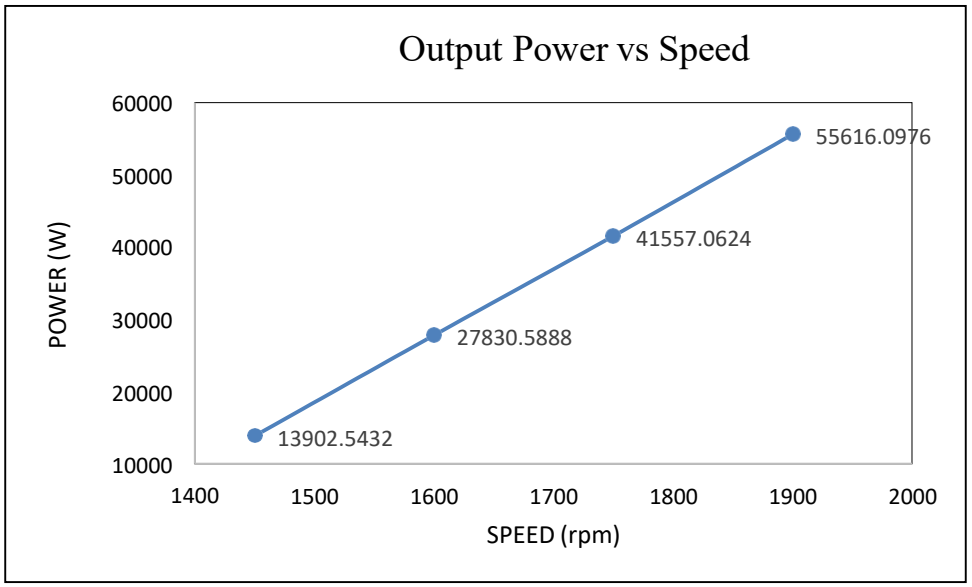

Fig.7.9 Output power variation with speed

The power coefficient varies in a straight line as speed is varied, as shown in the figure below, Fig.7.10.

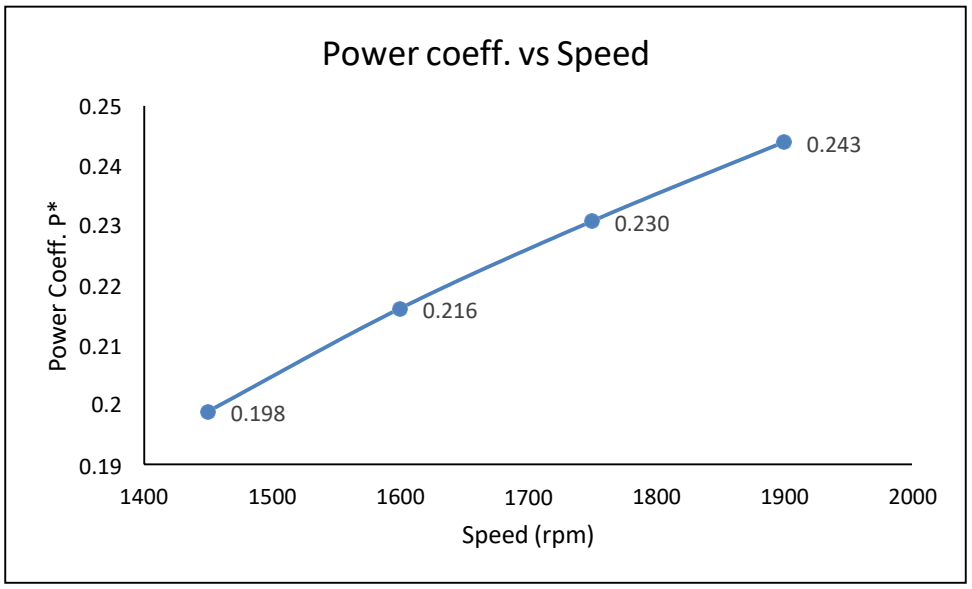

Fig. 7.10 Power Coefficient Vs Rotational speed

7.2.2.3. Variation of Head for impeller with 6 blades

The head is generated by a single stage after several losses in the stationary parts. It is found that as the speed of the pump increases, the head produced by the pump also increases, as shown in Fig. 7.11. The maximum head produced by the pump is 44.01 m at 1900 rpm. It is also observed that the head coefficient varies with changing speed, Fig. 7.12.

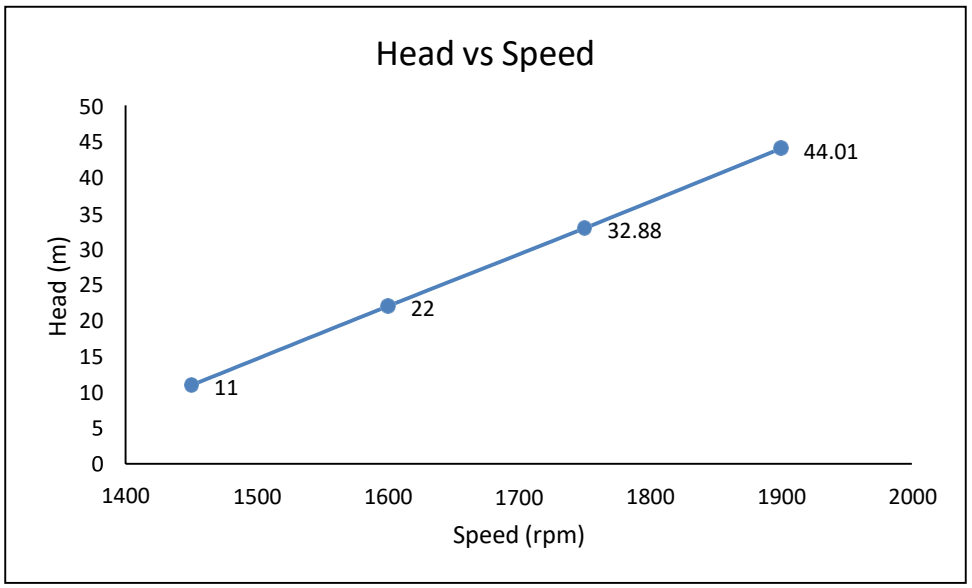

Fig.7.11 Head variation with speed

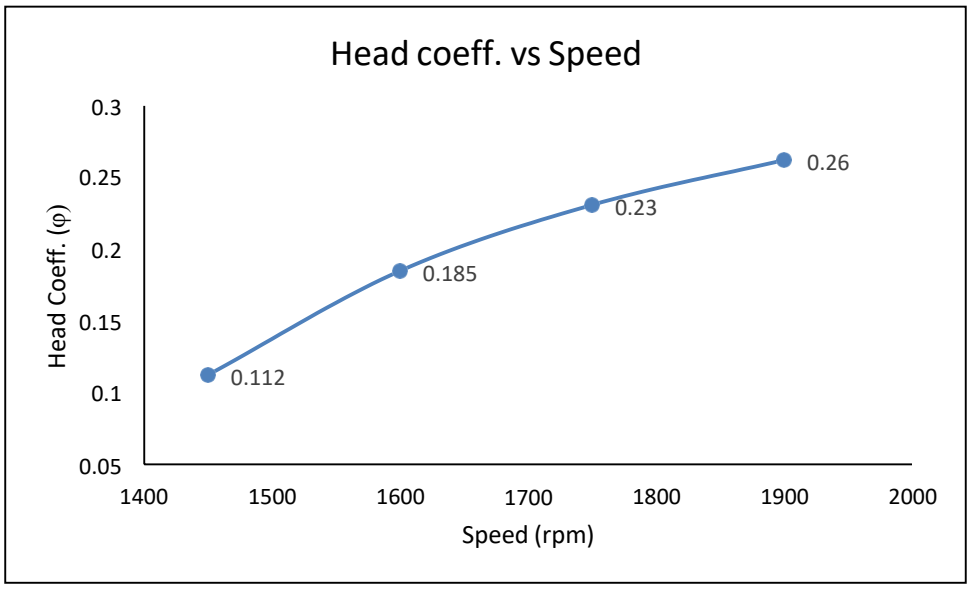

Fig. 7.12 Head coefficient. Vs Speed

7.2.3. Single stage with Seven Impeller Blades

After the analysis of the pump with 7 blades, now flow simulation is studied for the impeller with a 6-blade diffuser with 8 vanes, and the return passage with 11 RGV. The mass flow rate is kept constant as discussed above. The investigation is carried out by varying the speed of the impellerto 1450 rpm, 1600 rpm, 1750 rpm, and 1900 rpm.

Table 7.3 Variation of the flow parameters at different speeds for impeller with 7 blades

Speed (rpm)	**1450**	**1600**	**1750**	**1900**
P_1 (pa)	241515	232711	224983	223596
P_2 (pa)	386940	481350	588991	707657
H (m)	14.82	25.34	37.10	49.34
P_{out} (W)	18730.74	32024.70	46884.2	62347.05
P_{in}(W)	54260.68	71436.42	91462.60	114066.91
η (%)	34.51	44.82	51.26	54.65
N_s	68.88	50.83	41.77	36.62
H^*	0.1515	0.2128	0.2604	0.2938
P^*	0.2081	0.2250	0.2408	0.2548
Ψ	0.4695	0.3515	0.2935	0.2524
Φ	1.8162	1.5327	1.3855	1.3044

7.2.3.1. Variation of Manometric Efficiency for impeller with 7 blades

The analysis is carried out for a single-stage pump having an impeller of 7 blades. The mass flow rateis kept constant, and only the speed is varied from 1450 rpm to 1900 rpm. It is found that the variation of efficiency with speed is of an increasing type as shown in Fig. 7.13. The maximum efficiency is 54.65% at 1900 rpm. It is also found that the efficiency decreases linearly with the flow coefficient, as shown in Fig. 7.14.

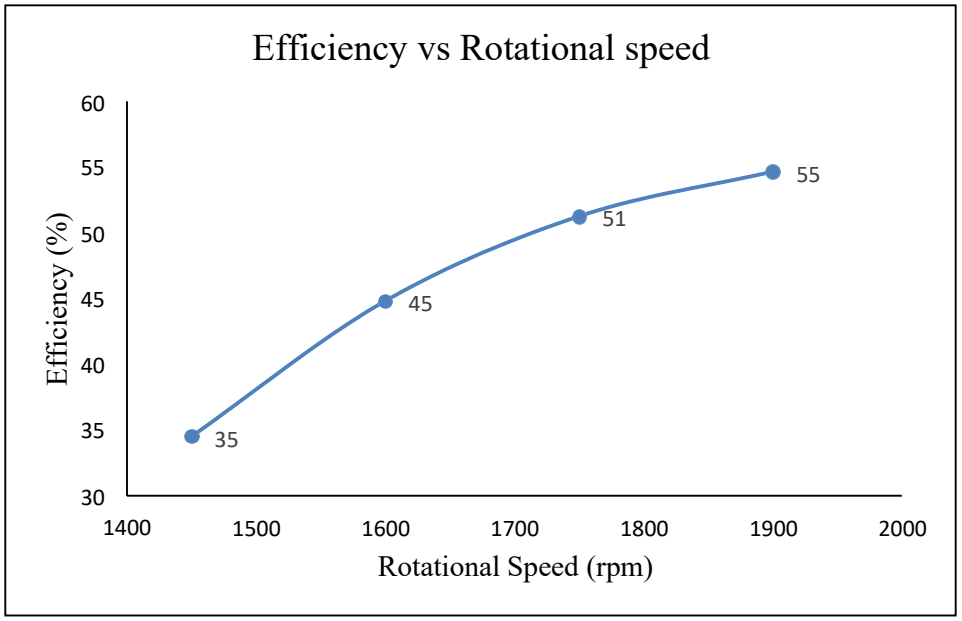

Fig. 7.13 Variation of hydraulic efficiency with the rotational speed

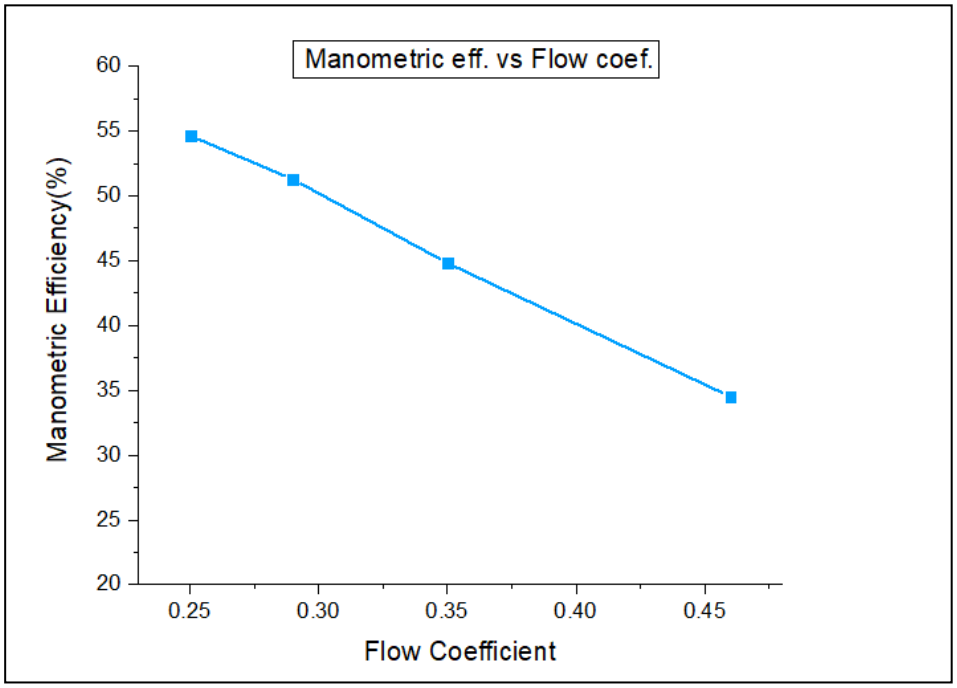

Fig. 7.14 Variation of hydraulic efficiency with flow coefficient

7.2.3.2. Variation of Output Power for impeller with 7 blades

The variation between output Power with speed is shown in Fig. 7.15. It is seen that output Power increases linearly with an increase in speed. The maximum power developed is 62.347 kW at 1900 rpm. The power coefficient varies in a straight line as speed is varied, as shown in the figure below, Fig.7.16.

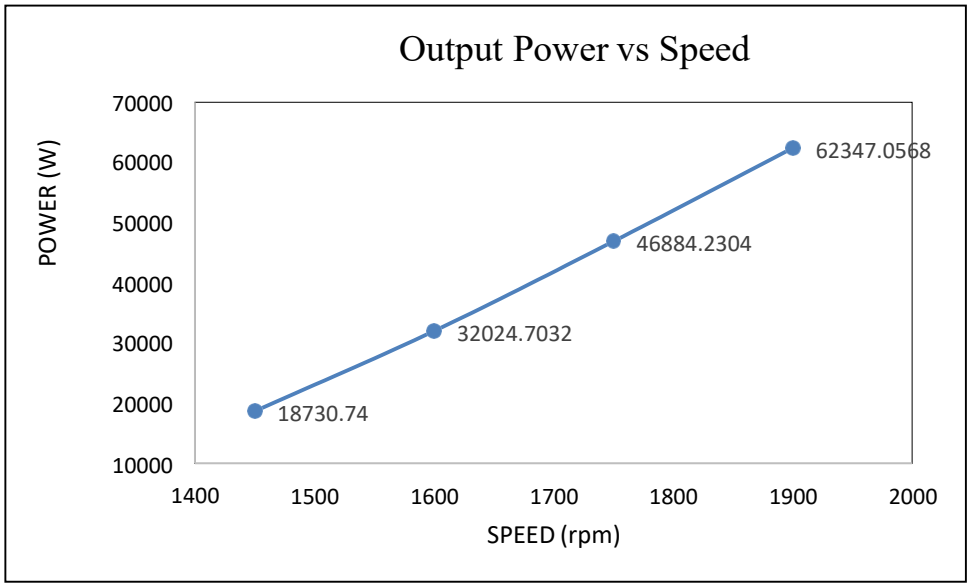

Fig.7.15 Output power variation with speed

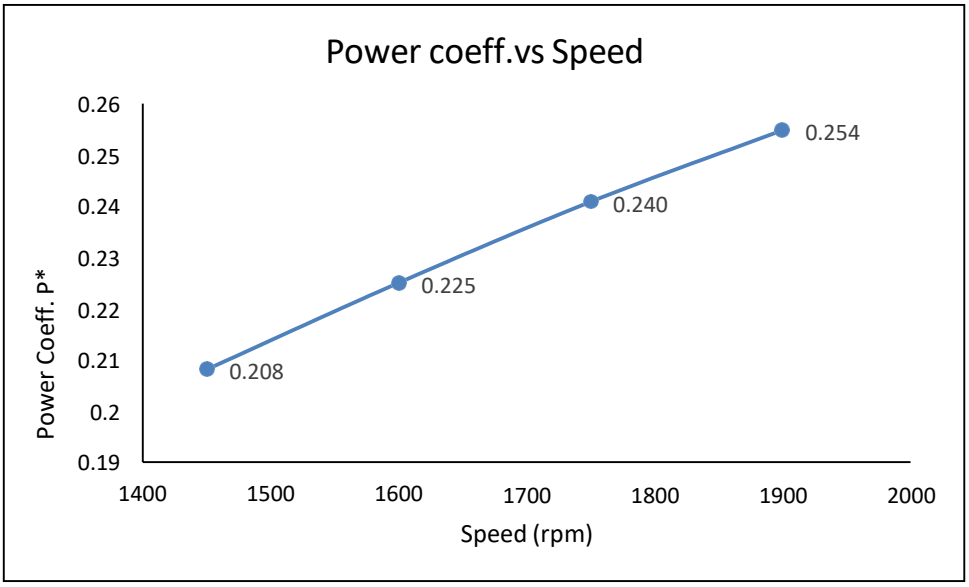

Fig. 7.16 Power Coefficient Vs Rotational Speed

7.2.3.3. Variation of Head for impeller with 7 blades

The head is generated by a single stage after several losses in the stationary parts. It is found that as the speed of the pump increases, the head produced by the pump also increases, as shown in Fig. 7.17. The maximum head produced by the pump is 49.34 m at 1900 rpm. It is also observed that the head coefficient varies with changing speed, Fig. 7.18.

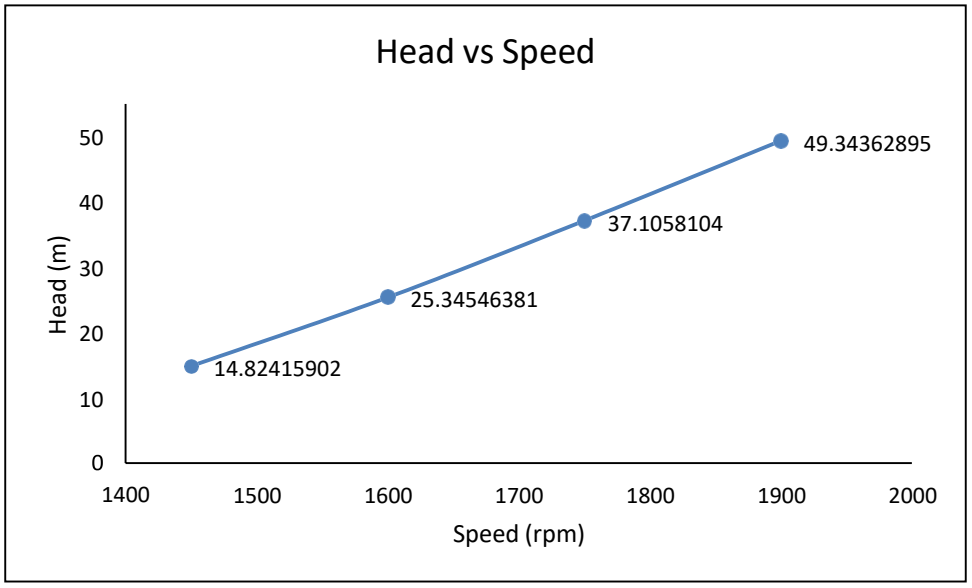

Fig.7.17 Head variation with speed

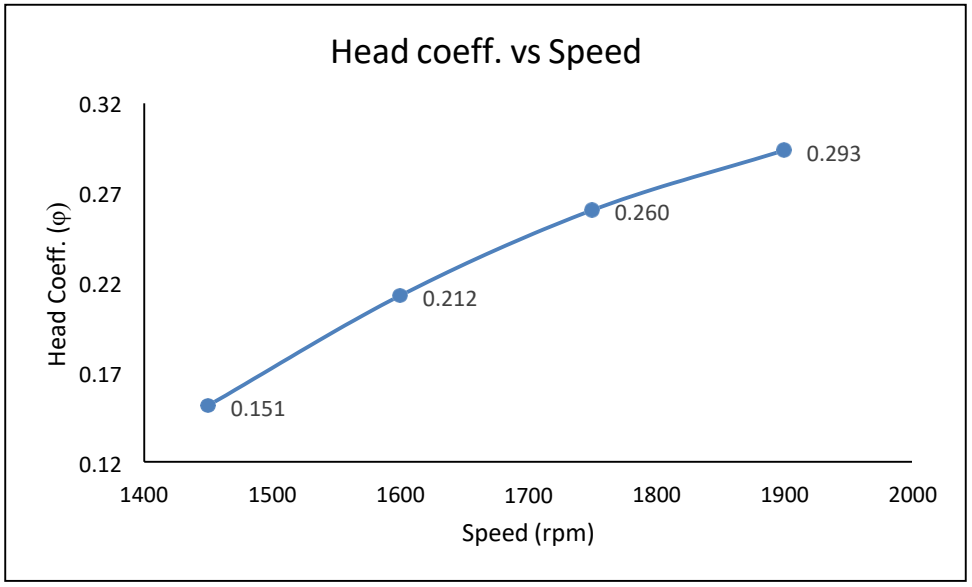

Fig. 7.18 Head coefficient Vs Speed

The above given tables, Table 7.1, Table 7.2, and Table 7.3, present the variation of the flow parameters at different speeds for impellers with 5 blades, 6 blades, and 7 blades, respectively.

7.2.4. Comparison of Performance Parameters with the different Numbers of Blades forSingle Stage Pump

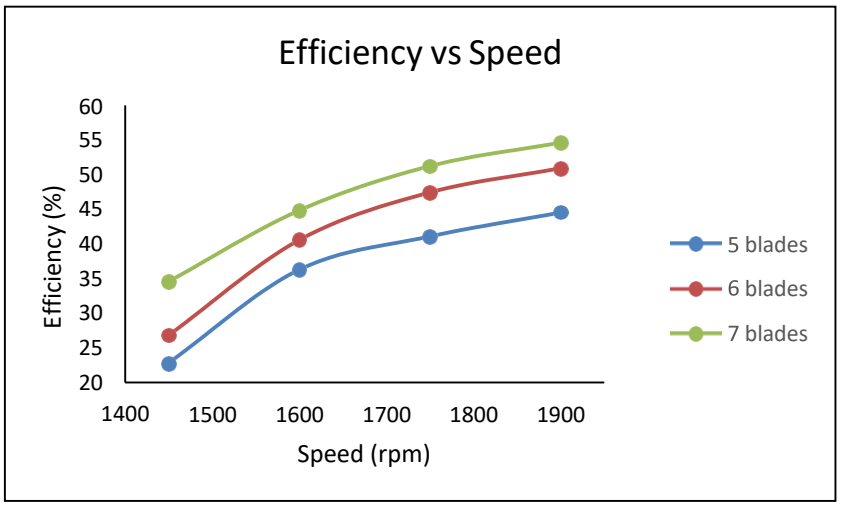

Fig. 7.19 Variation of efficiency with speed for different no. of blades

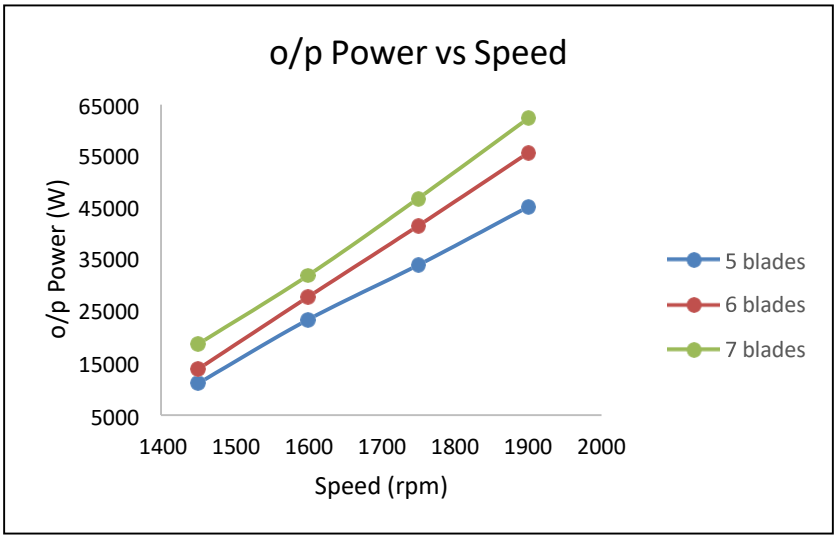

Fig. 7.20 Output power vs speed for different no. of blades

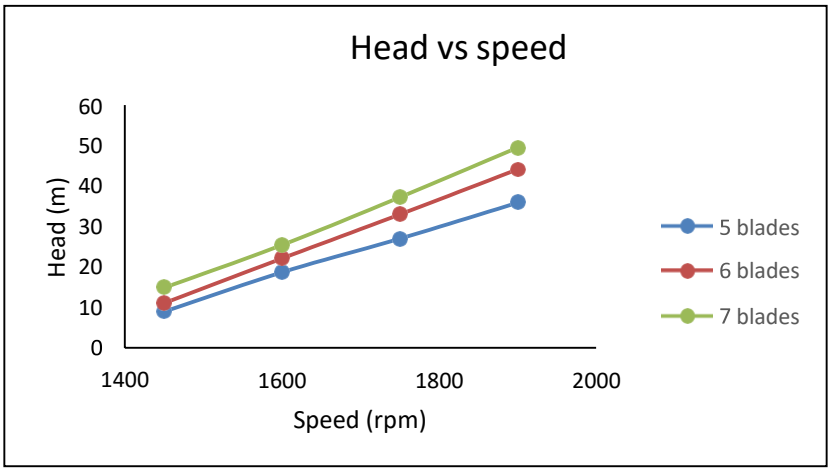

Fig. 7.21 Head vs speed for different no. of blades

From the above figures, Fig. 7.19, Fig. 7.20, and Fig. 7.21, it is observed that as the number of blades increases from 5 to 7, the pump performance parameters, i.e., head, efficiency, and output power, increase. Therefore, a single-stage pump having an impeller with 7 blades is the best pump out of all.

7.3 VELOCITY STREAMLINES

The streamline velocity for all the above cases has been prepared. Looking towards the streamline pattern, it is seen that the velocity of fluid particles at the inlet of the pump is more than the outlet because at the inlet, there is a suction of fluid, which causes the drawing of fluid at high velocity. It was also investigated that as the impeller is in rotating motion, it forces the fluid out of the domain, leading to the flow of fluid with the highest velocity at the impeller outlet.

7.3.1 Streamline Velocity for Single Stage with Five Impeller Blades

7.3.1.1 At speed 1450 rpm

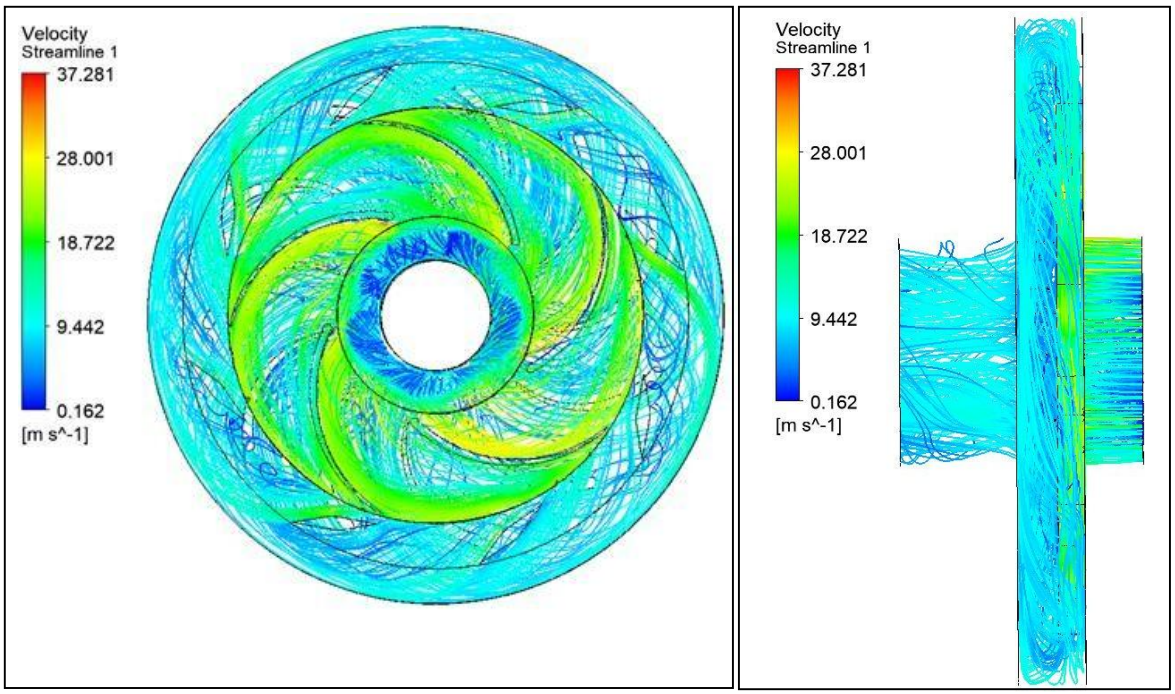

Figure 7.22 Streamlines pattern for single stage with5 blades at 1450 rpm

From the above figure, it is observed that 37.281 m/s is the highest velocity for 1450 rpm single-stage pump.

7.3.1.2 At speed 1600 rpm

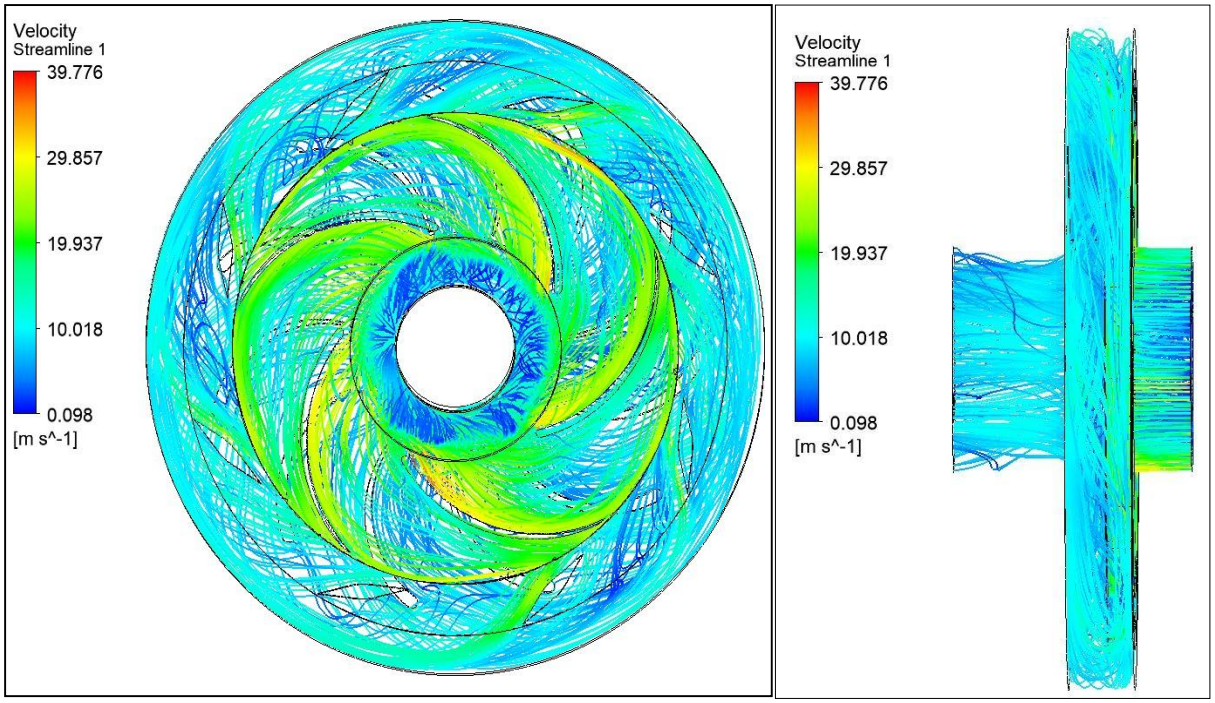

Figure 7. 23 Streamlines pattern for single stage with5 blades at 1600 rpm

From Figure 7.23, it is observed that 39.776 m/s is the highest velocity for a 1600 rpm single-stage pump.

7.3.1.3 At speed 1750 rpm

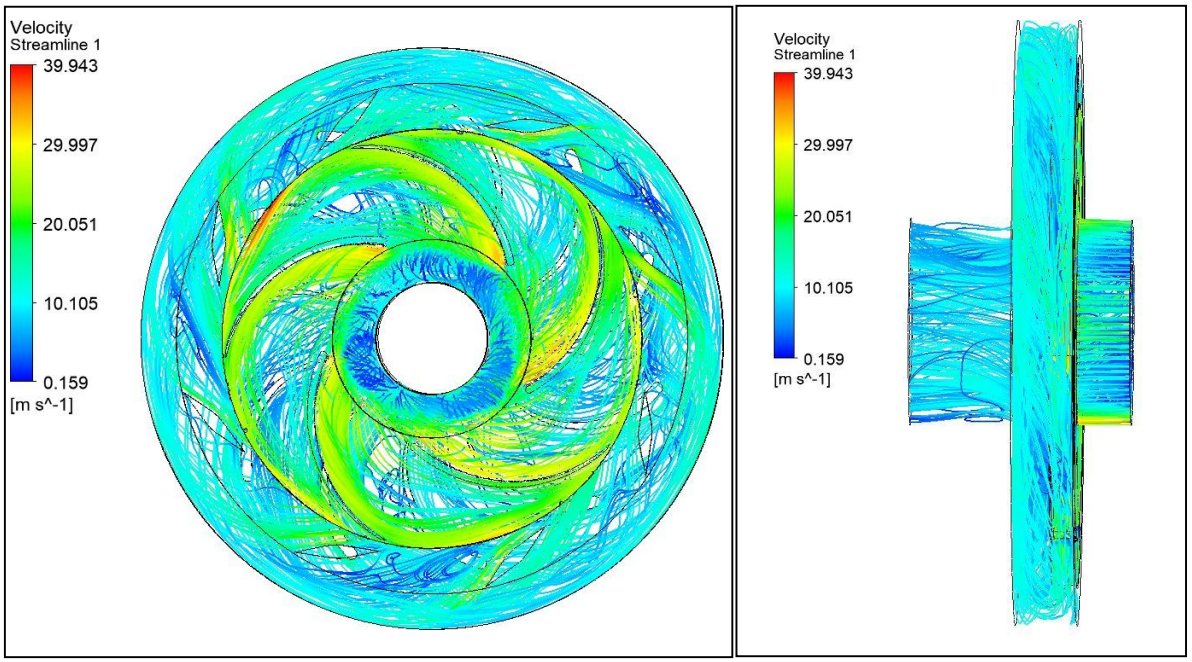

Figure 7.24 Streamlines pattern for single stage with5 blades at 1750 rpm

From Figure 7.24, it is observed that 39.943 m/s is the highest velocity for a 1750 rpm single-stage pump.

7.3.1.4 At speed 1900 rpm

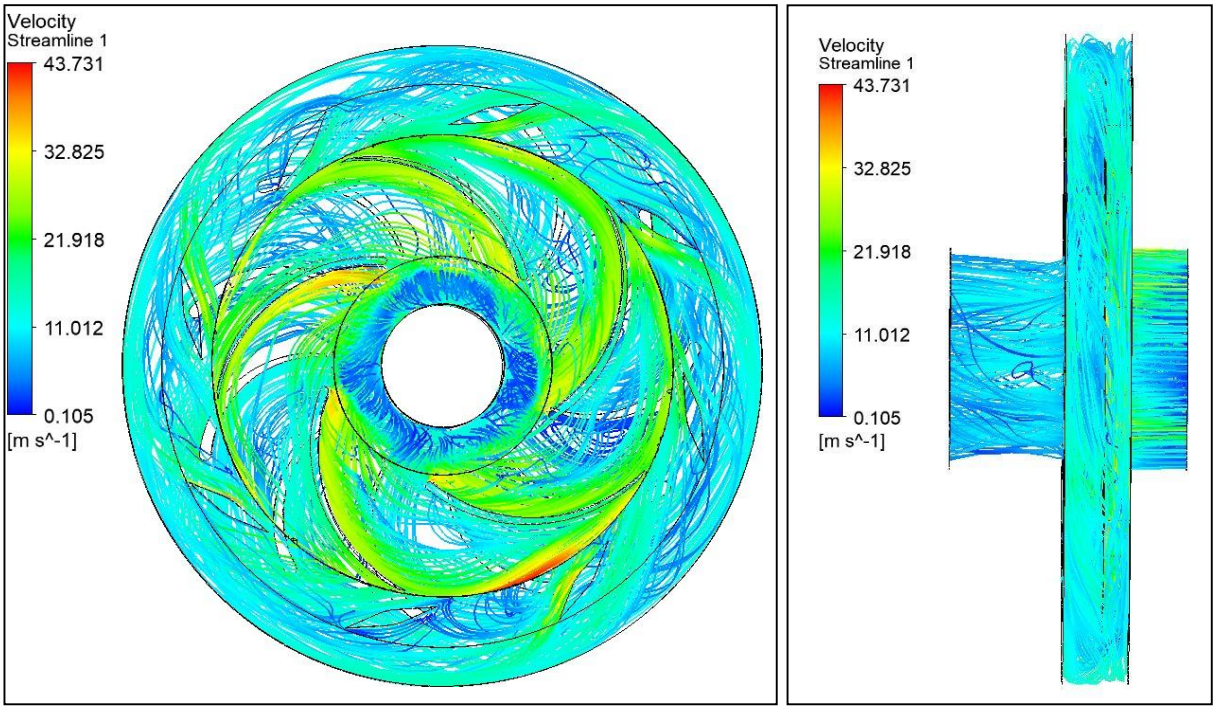

Fig. 7.25 Streamlines patternfor single stage with 5 blades at 1900 rpm

For the speed, 1900 rpm, the maximum fluid flow velocity in all flow domains is 43.731 m/s. The streamline is shown in Fig. 7.23, Fig. 7.24, and Fig. 7.25 are nearly straight along the inlet and exit pipe, i.e., parallel along the axis of rotation of the impeller. In the pump case, the whirl velocity C_{u1} at the inlet is zero; therefore, for all the above cases and further cases, $C_{u1} = 0$.

7.3.2 Streamline Velocity for Single Stage with Six Impeller Blades

7.3.2.1 At speed 1450 rpm

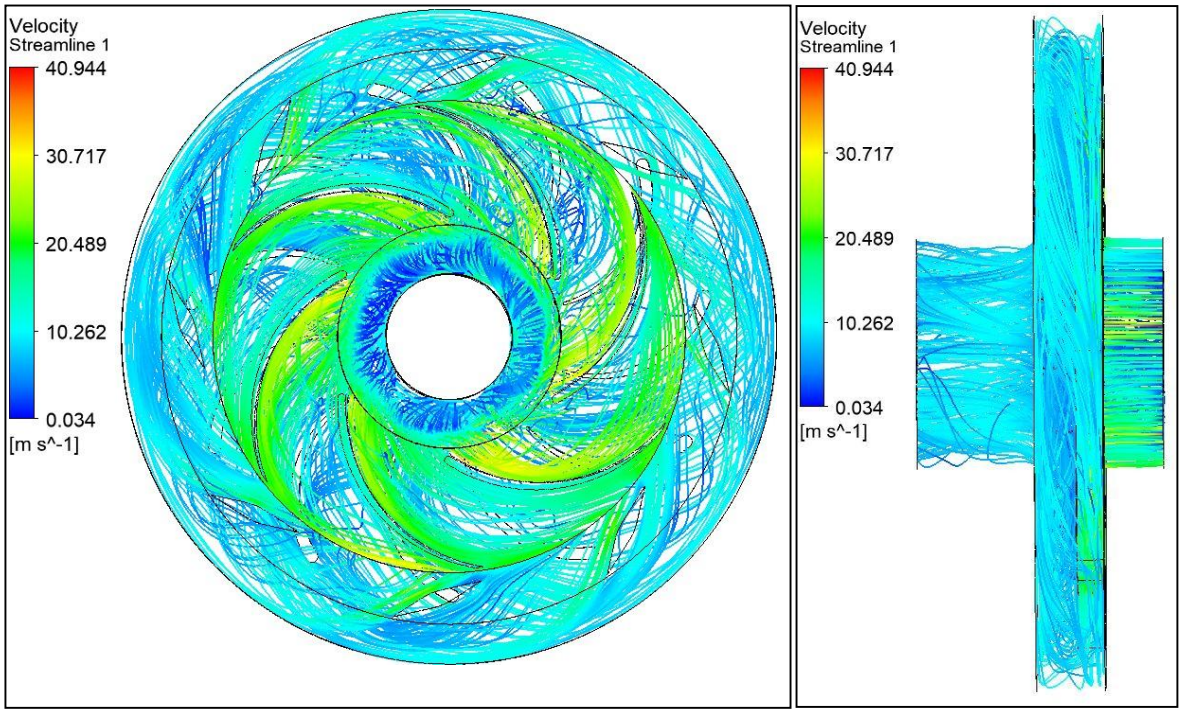

Fig. 7.25 Streamlines patternfor single stage with 6 bladesat 1450 rpm

For the speed 1450 rpm the maximum fluid flow velocity for single stage pump having 6 blades found to be 40.944 m/s.

7.3.2.2 At speed 1600 rpm

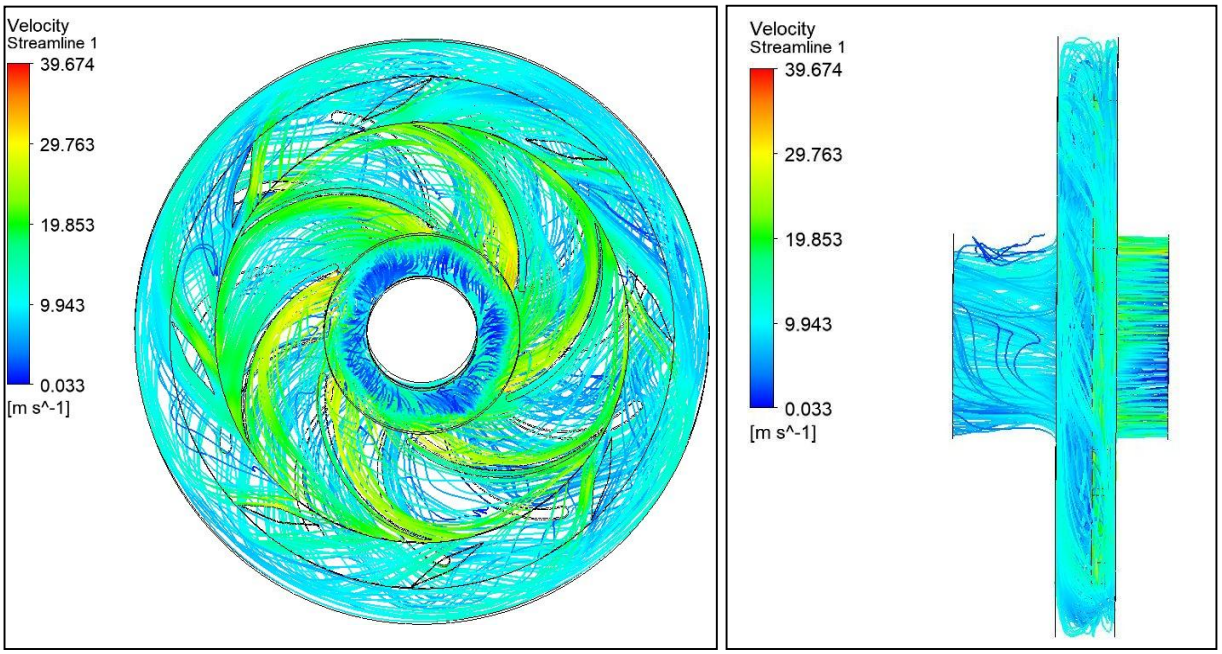

Fig. 7.27 Streamlines patternfor single stage with 6 blades at 1600 rpm

From Figure 7.27, it is observed that 39.674 m/s is the highest velocityin all domains for 1600 rpm.

7.3.2.3 At speed 1750 rpm

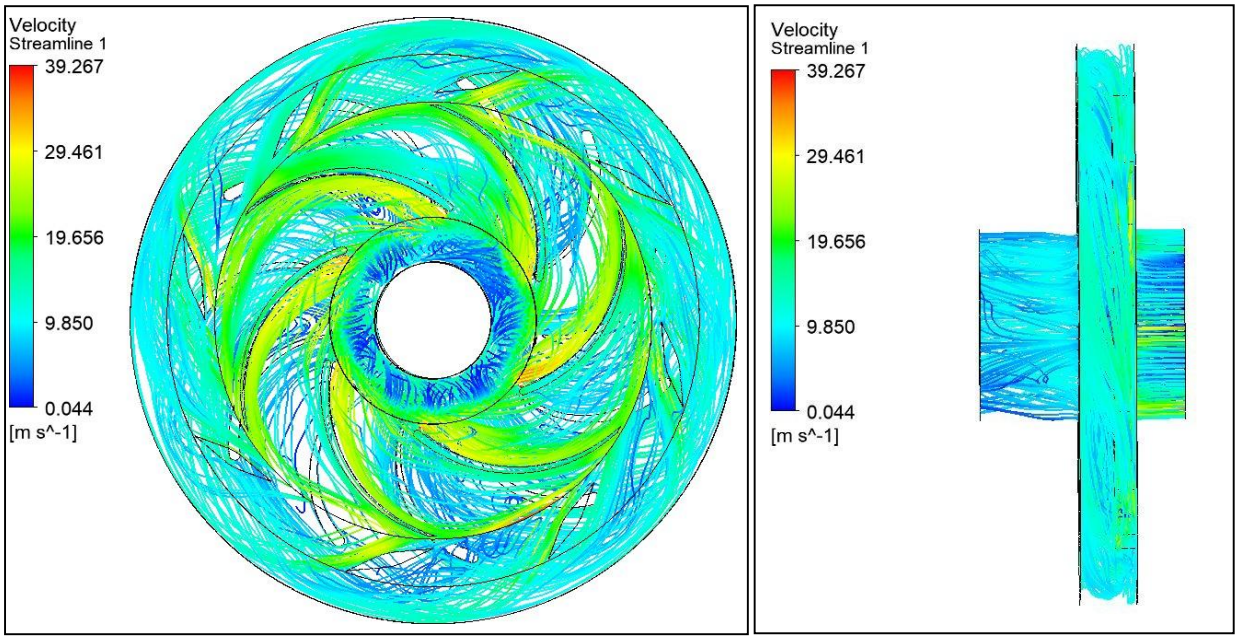

Fig. 7.28 Streamlines pattern for single stage with 6 blades at 1750 rpm

The maximum velocity for a single-stage pump domain with an impeller of 6 blades rotating at1750 rpm was found to be 39.267m/s.

7.3.2.4 At speed 1900 rpm

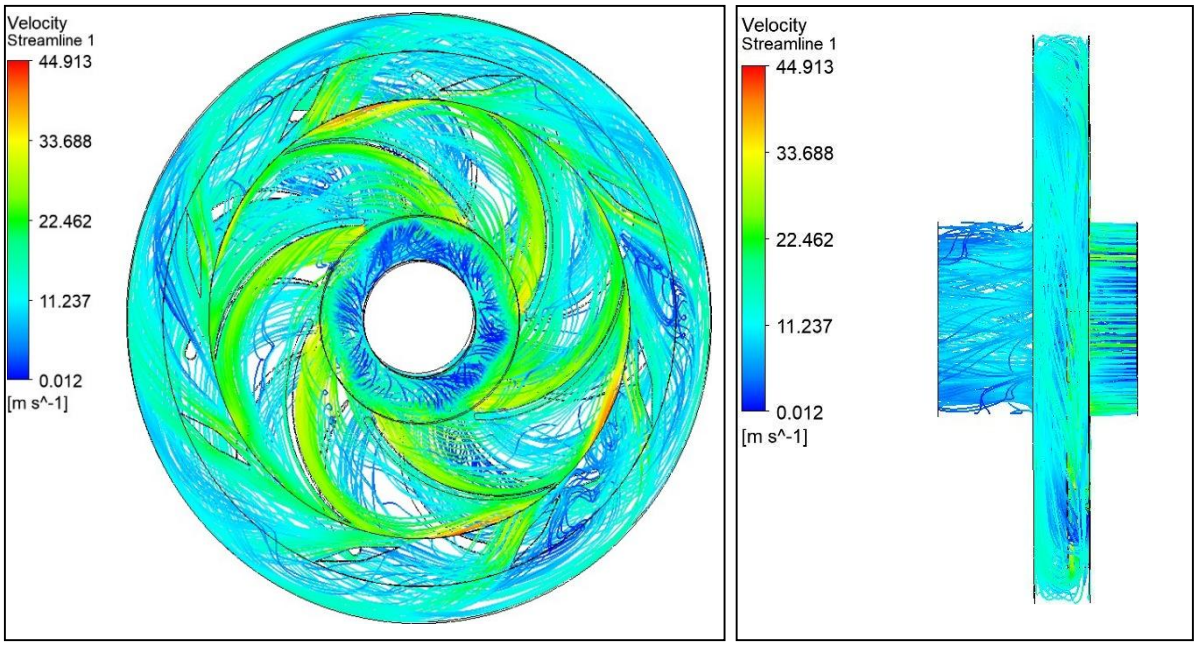

Fig. 7.29 Streamlines patternfor single stage with 6 bladesat 1900 rpm.

The maximum velocity for the single-stage pump domain with an impeller of 6 blades rotating at 1900 rpm was found to be 44.913m/s, as shown in Fig. 7.29.

7.3.3 Streamline Velocity for Single Stage with Seven Impeller Blades

7.3.3.1 At speed 1450 rpm

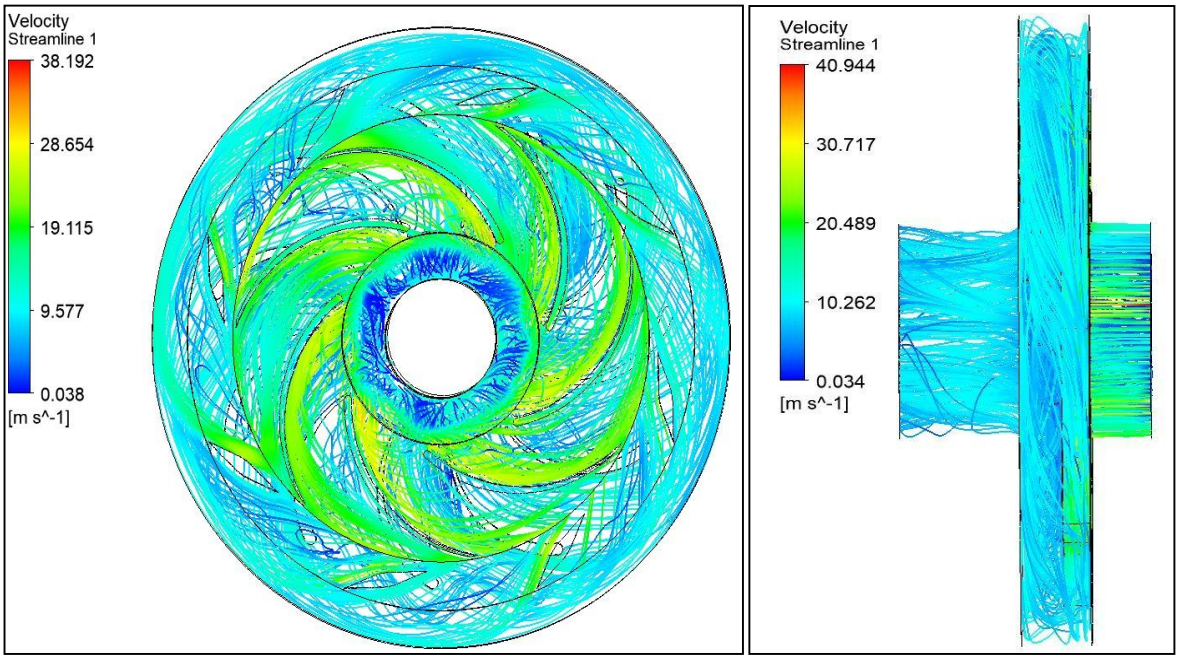

Fig. 7.30 Streamlines patternfor single stage with 7 bladesat 1450 rpm.

From the Fig.7.30, it is observed that 40.944 m/s is the highest velocityin all domains for 1450 rpm.

7.3.3.2 At speed 1600 rpm

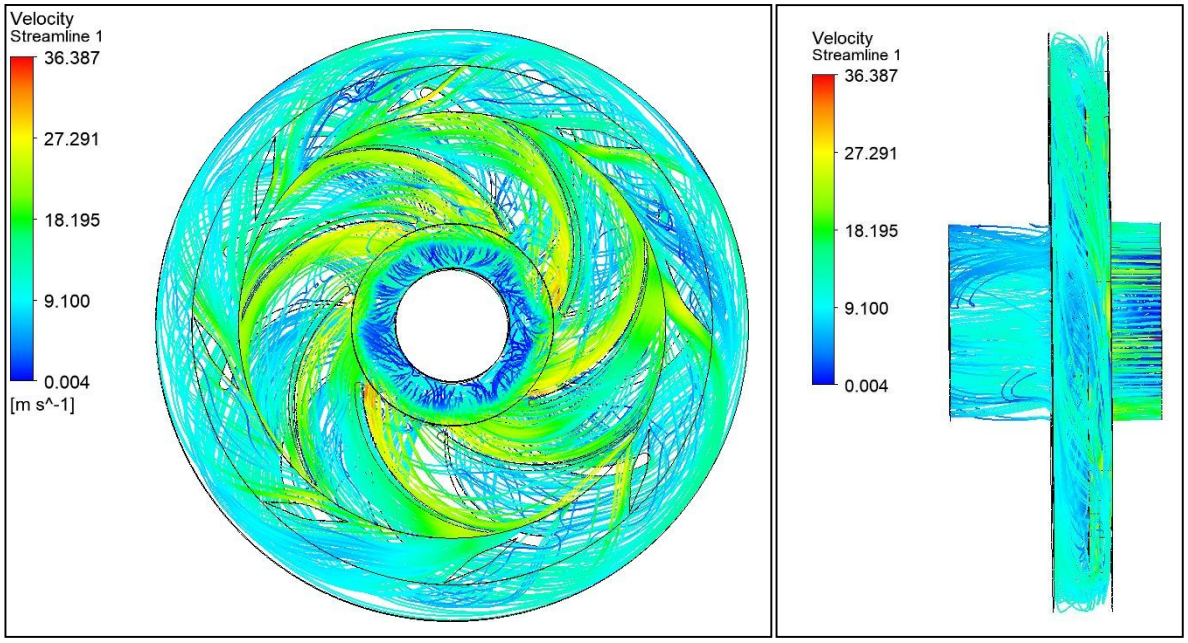

Fig. 7.31 Streamlines patternfor single stage with 7 bladesat 1600rpm.

The maximum velocity for the single-stage pump domain with the impeller of blades rotating at 1600 rpm was found to be 36.387m/s, as shown in Fig. 7.31.

7.3.3.3 At speed 1750 rpm

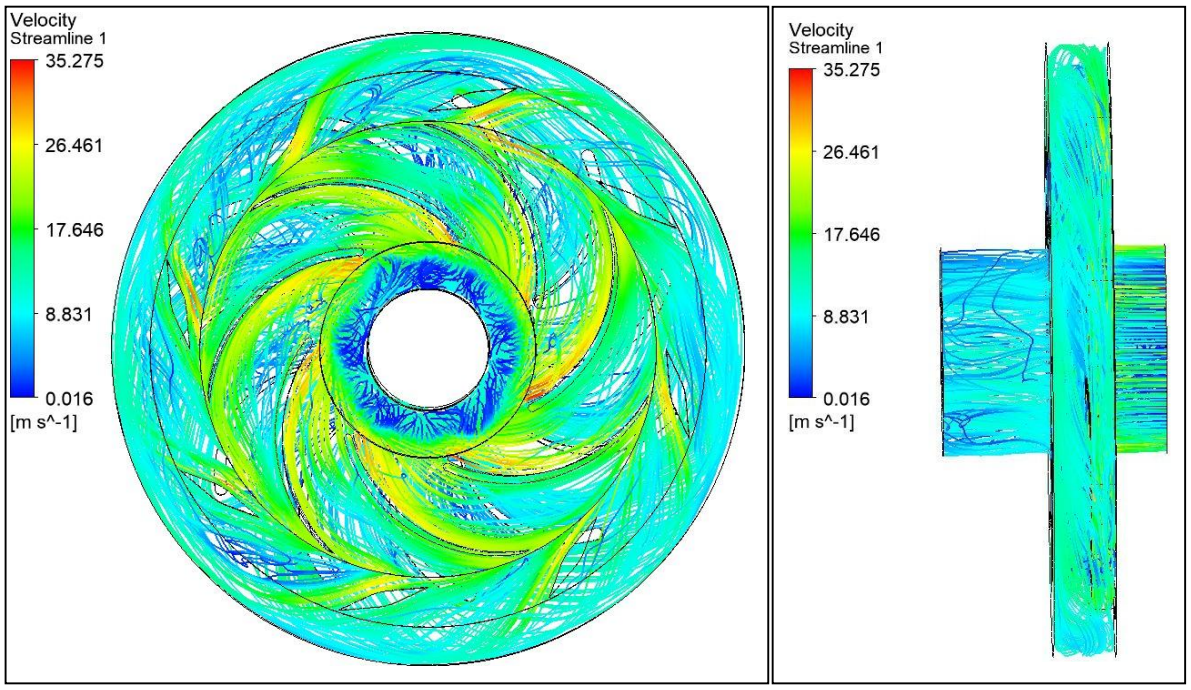

Fig. 7.32 Streamlines patternfor single stage with 7 bladesat 1750rpm.

From Figure 7.32, it is observed that 35.275 m/s is the highest velocityin all domains for 1750 rpm.

7.3.3.4 At speed 1900 rpm

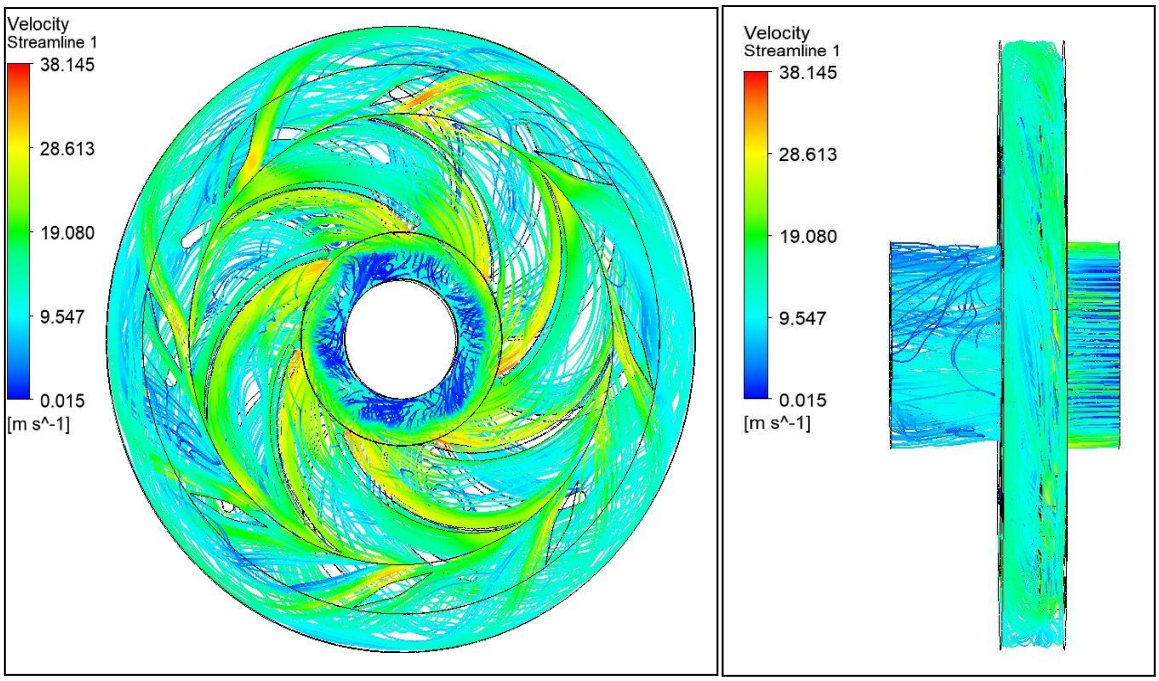

Fig. 7.33 Streamlines patternfor single stage with 7 bladesat 1900 rpm

From Figure 7.33, it is observed that 38.145 m/s is the highest velocityin all domains for 1750 rpm.

According to streamline velocity pattern figures (Fig. 7.22-Fig.7.33)**,** the maximum velocity is found near the walls of impeller blades because, near the wall of the impeller blades, there is a sudden change in the shape of the blade, causing turbulence to increase the velocity of the fluid. These figures show that velocity increases as rotational speed increases because it causes faster rotation of impeller blades, creating a greater centrifugal force, which pushes the fluid outwards and increases velocity, increasing the area of contact between, and the amount of liquid it sucked also increases. But when the blade numbers increase, it causes a reduction in velocity because the fluid has to pass through more blades, which increases the resistance to flow. From these figures, we can interpret that the function of the return guide vanes is to deswirl the fluid before moving on to the next phase, which results in an undistorted flow into the following impeller and can draw more fluid into it.

7.4 PRESSURE CONTOUR FOR SINGLE STAGE CENTRIFUGAL PUMP

The pressure distribution in a complete single-stage centrifugal pump at a constant mass flow rate of 128.88 kg/s is represented below for a pump having an impeller with blades as 5, 6, and 7 in number, and for this, the speed is varied from 1450 rpm to 1900 rpm. It is investigated that the head and hydraulic efficiency increase as the number of impeller blades and rotational speed are increased. The figures below are from Fig.7.34- Fig. 7.44 (a) Impeller and diffuser, while (b) Return passage show the pressure distribution with different impeller blades.

7.4.1 Pressure Contour for Single Stage with Five Impeller Blades

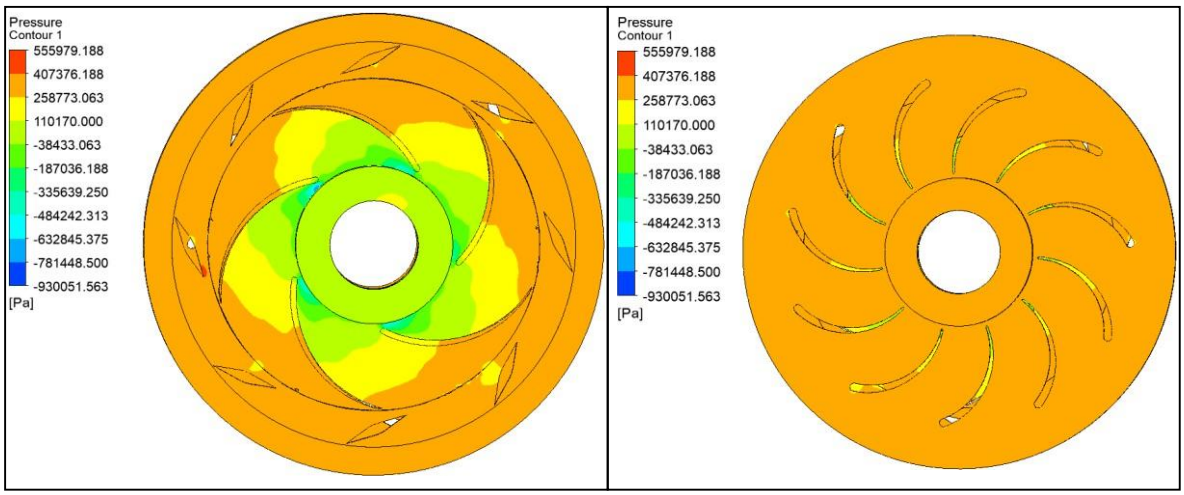

(a) (b)

Fig. 7.34 Pressure contour for single stage pump with 5 blades at 1450 rpm

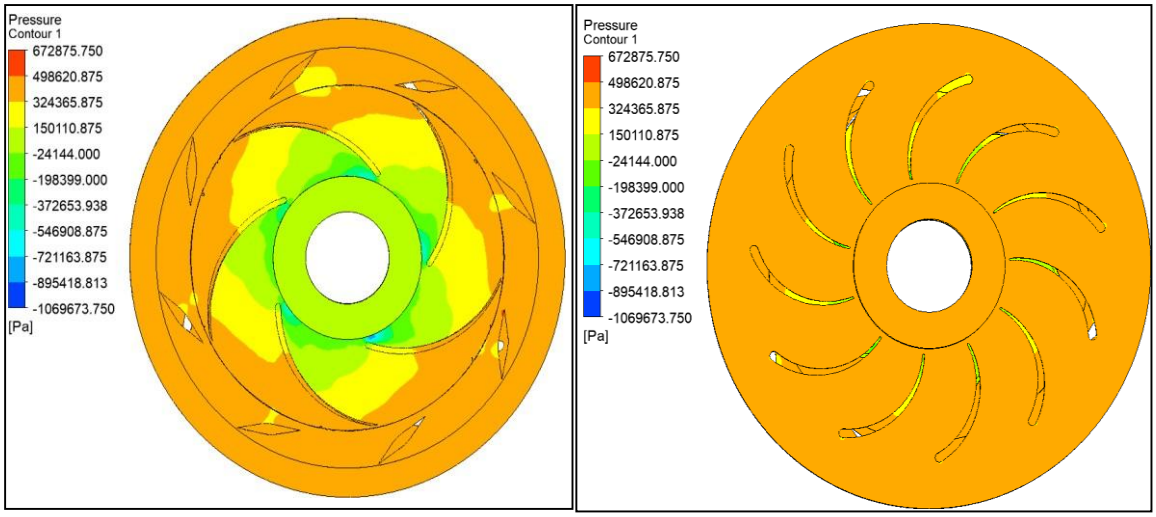

(a) (b)

Fig. 7.35 Pressure contour for single stage pump with 5 blades at 1600 rpm

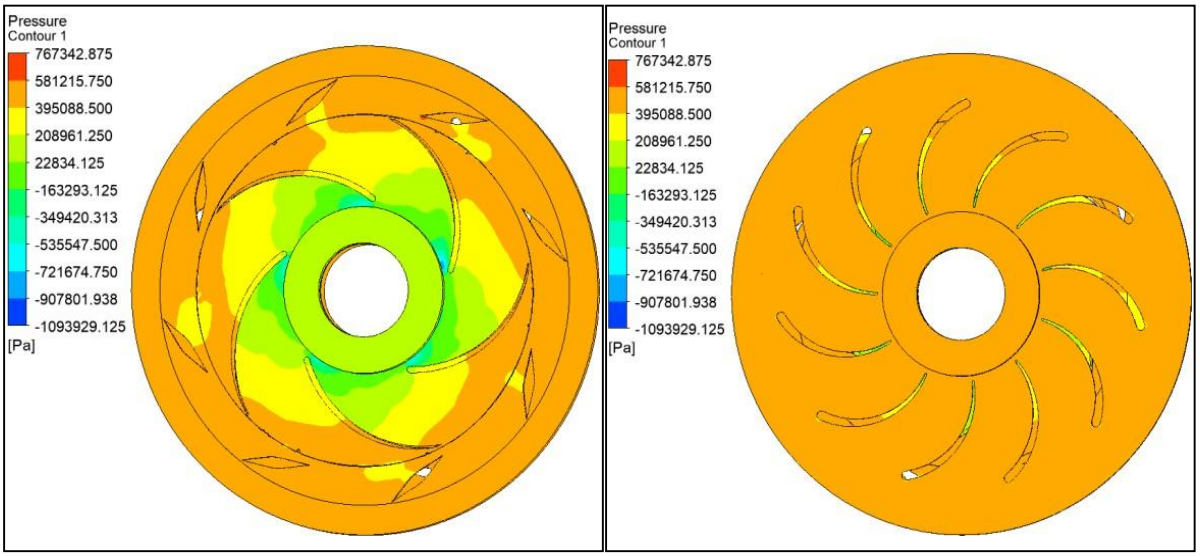

(a) (b)

Fig. 7.36 Pressure contour for single stage pump with 5 blades at 1750 rpm

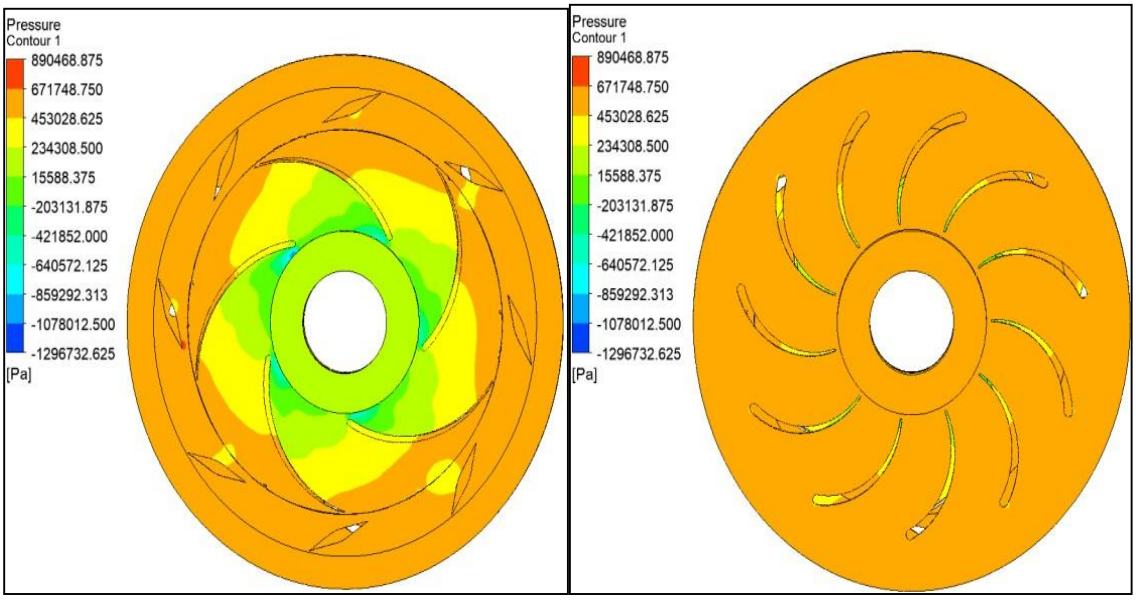

(a) (b)

Fig. 7.37 Pressure contour for single stage pump with 5 blades at 1900 rpm

7.4.2 Pressure Contour for Single Stage with Six Impeller Blades

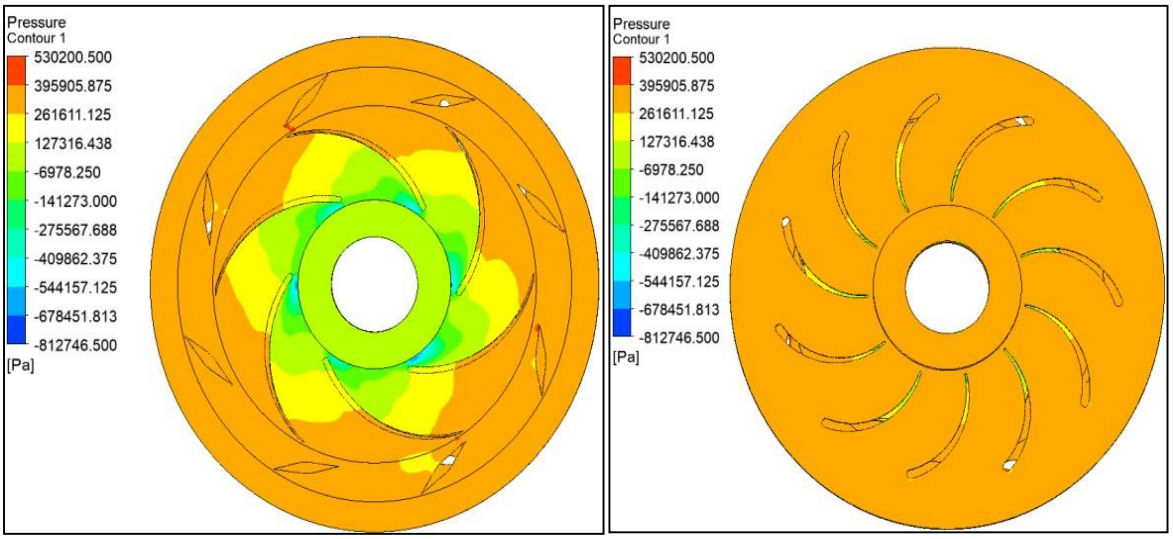

(a) (b)

Fig. 7.38 Pressure contour for single stage pump with 6 blades at 1450 rpm

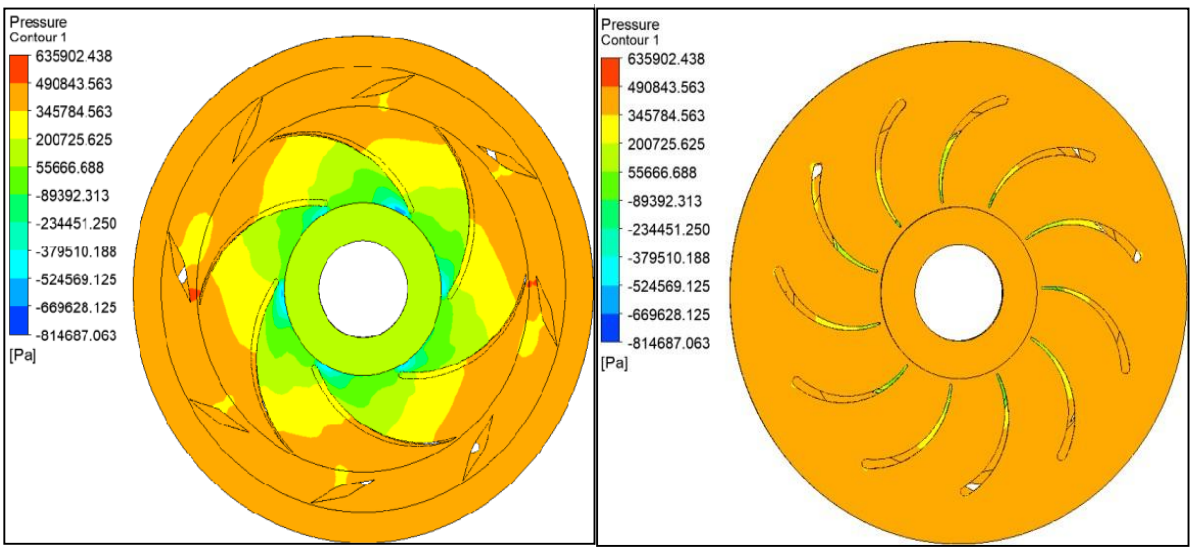

(a) (b)

Fig. 7.39 Pressure contour for single stage pump with 6 blades at 1600 rpm

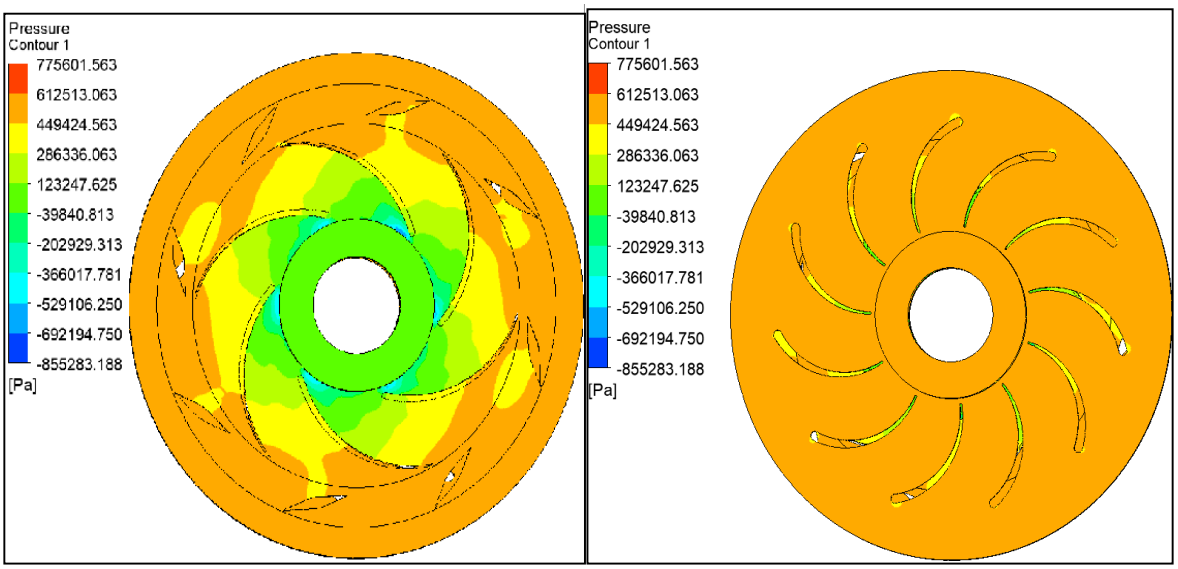

(a) (b)

Fig. 7.40 Pressure contour for single stage pump with 6 blades at 1750 rpm

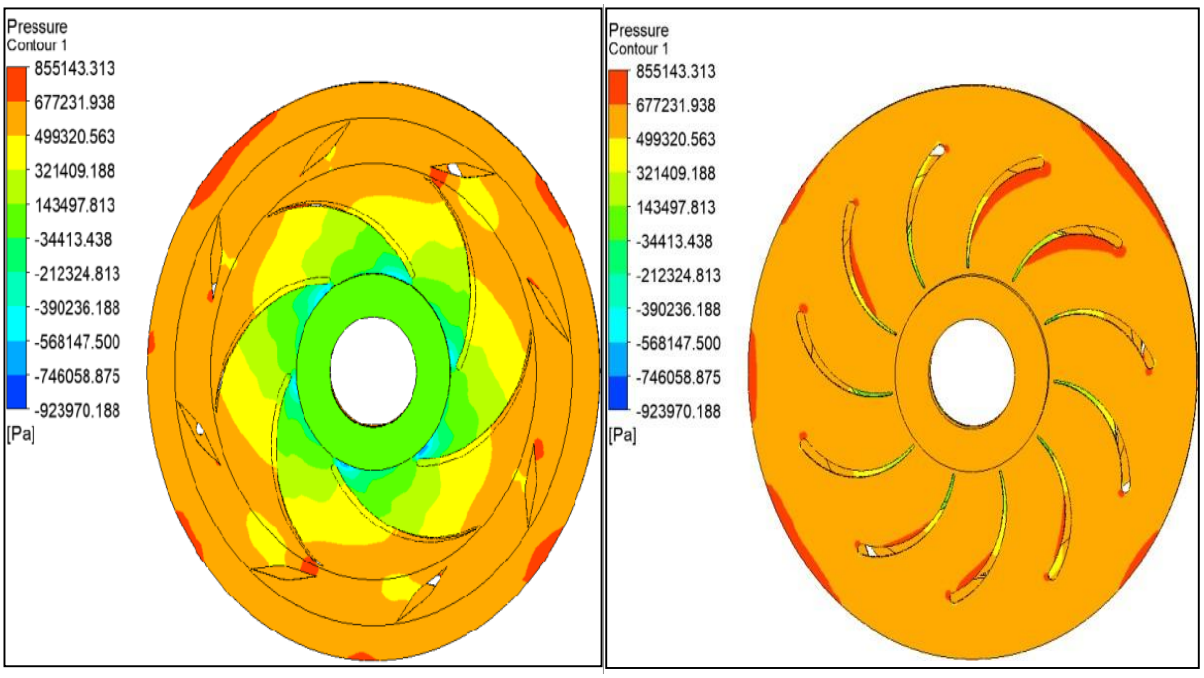

(a) (b)

Fig. 7.41 Pressure contour for single stage pump with 6 blades at 1900 rpm

7.4.3 Pressure Contour for Single Stage with Seven Impeller Blades

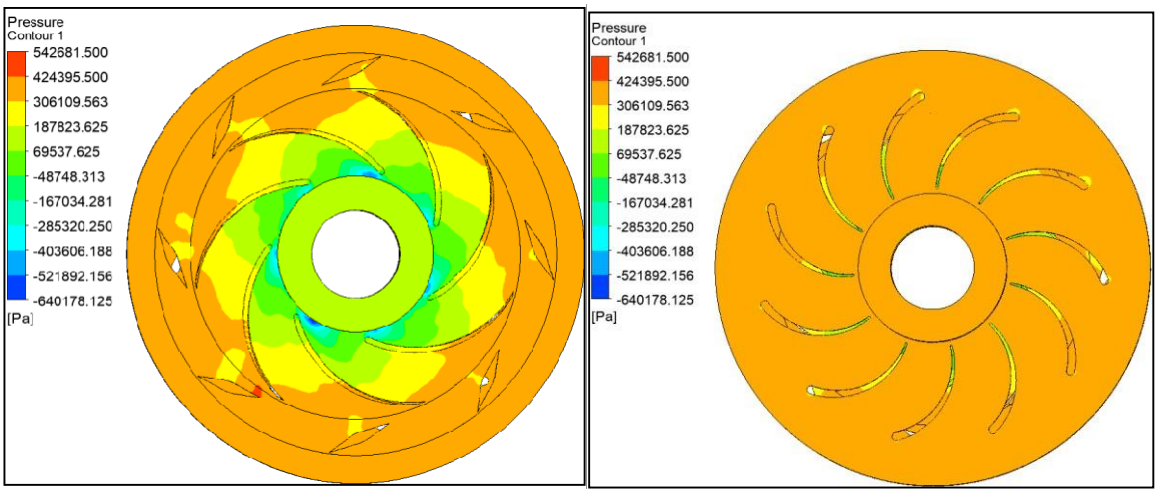

(a) (b)

Fig. 7.42 Pressure contour for single stage pump with 7 blades at 1450 rpm

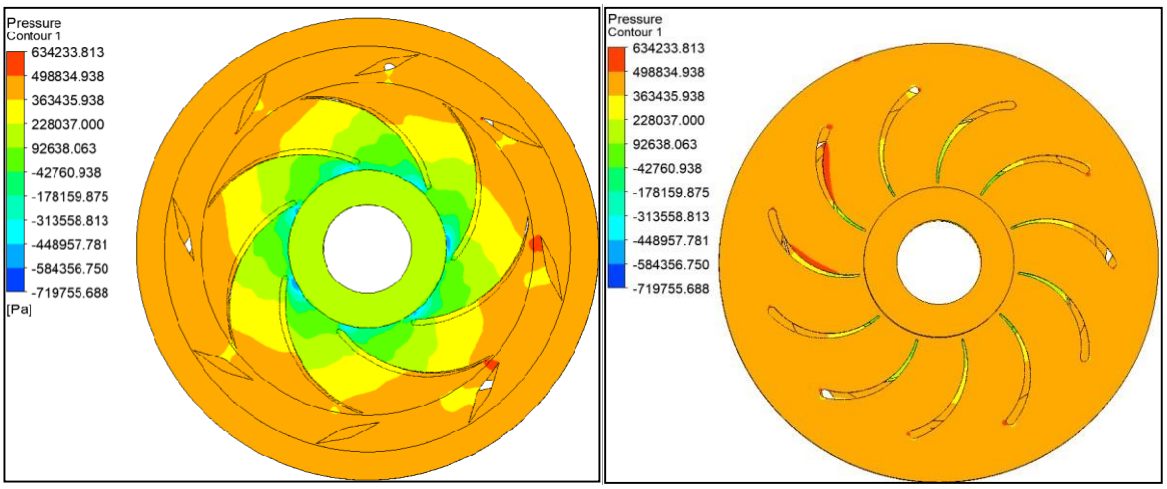

(a) (b)

Fig. 7.43 Pressure contour for single stage pump with 7 blades at 1600 rpm

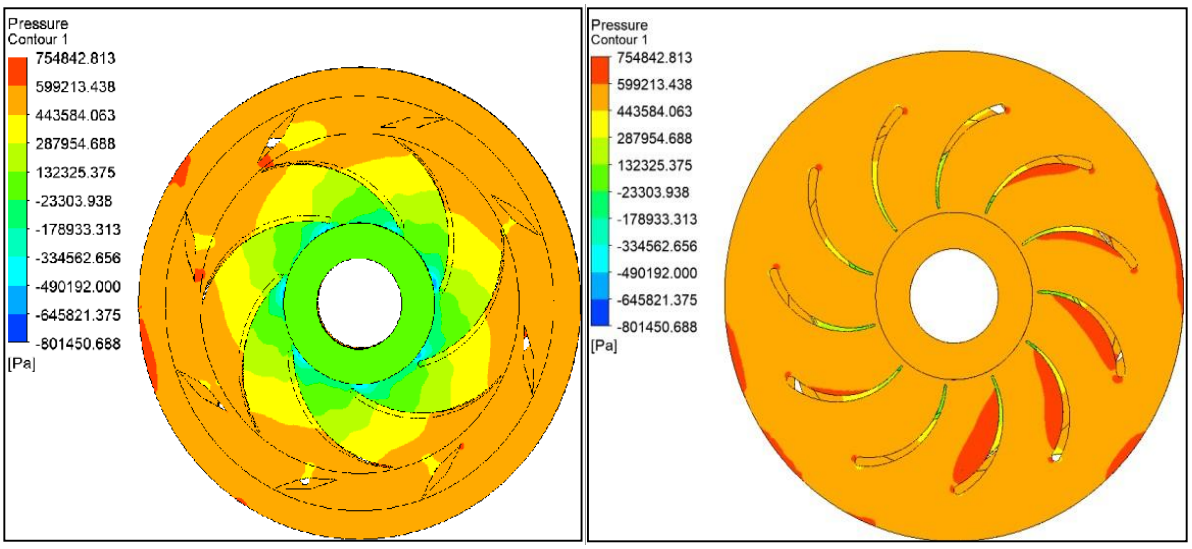

(a) (b)

Fig. 7.44 Pressure contour for single stage pump with 7 blades at 1750 rpm

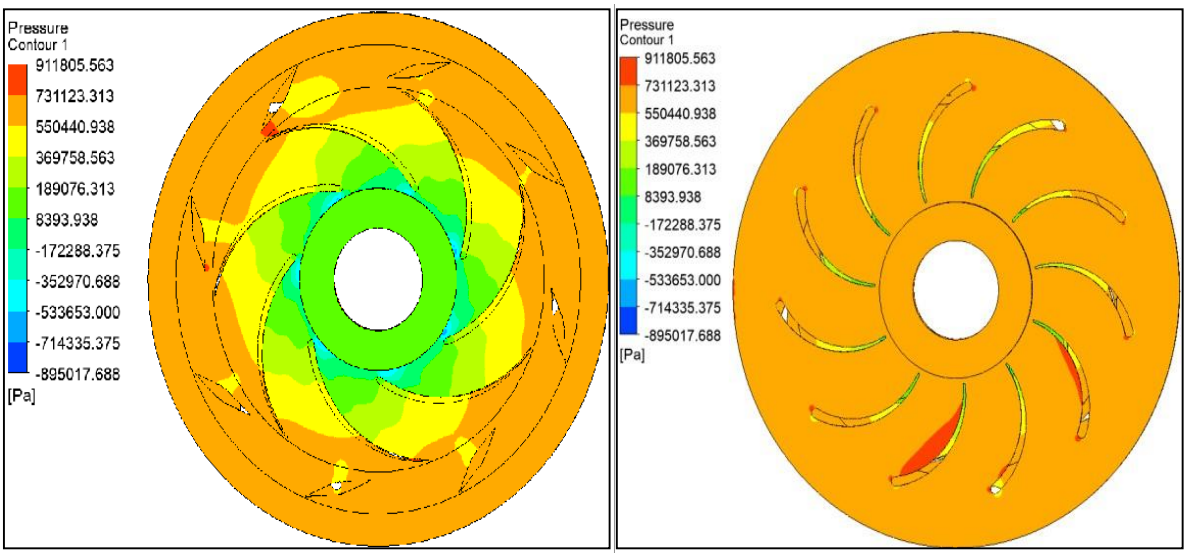

(a) (b)

Fig. 7.45 Pressure contour for single stage pump with 7 blades at 1900 rpm

7.5 OUTCOMES OF SINGLE STAGE CENTRIFUGAL PUMP

The flow simulation for a single-stage pump has been carried out at four different speeds for the pump having three different impellers of 5, 6, and 7 blades. From the above performance charts,velocity streamlines, and pressure contours, it has been observed that as speed and number of blades increase, the performance parameters increase. It is investigated that the single-stage pump running at a speed of 1900 rpm gives greater performance among all remaining speeds.

7.6 RSM RESULTS

A second-order polynomial equations (2) and (3) obtained from RSM analysis were used, as shown below, to identify the responses, such as the head coefficient (H^*) and flow coefficient (ψ), which are functions of the design variables (rotational speed, number of blades, and flow rate).

$$H^* = 9.97863 - 1.50117A - 0.006372B - 0.004486C + 0.000810AB + 0.000750AC - 4.19689 * 10^{-6}BC - 0.011611A^2 + 1.52680 * 10^{-6}B^2 - 5.37287 * 10^{-6}C^2 \quad (7.10)$$

$$\psi = -18.78094 + 1.25178A + 0.021236B + 0.000228C + 0.000011AB + 0.000255AC - 1.00031 * 10^{-6}BC - 0.086717A^2 - 5.30595 * 10^{-6}B^2 + 1.21688 * 10^{-6}C^2 \quad (7.11)$$

Table 7.4 Analysis of Variance ANOVA for Quadratic Model [89]

Variable	**Head Coefficient**			**Flow Coefficient**		
	Mean square	**F values**	**p values**	**Mean square**	**F values**	**p values**
Intercept	167.42	880.29	<0.0001	52.42	308.70	<0.0001
Main effect						
Z	227.15	1194.30	<0.0001	213.91	1259.77	<0.0001
N	1167.05	6136.15	<0.0001	209.76	1235.37	<0.0001
Q	69.91	367.56	<0.0001	22.05	129.87	<0.0001
Interaction effect						
zN	34.44	181.11	<0.0001			
zQ	1.19	6.23	0.0316	.0052	8.11	0.0173
NQ	1.58	8.33	0.0162			
Quadratic effect						
z^2	2.68	14.07	0.0038	.0207	18.24	0.0016
N^2				.0392	36.26	0.0001
Q^2						
Lack of fit	0.0162	0.3393	0.8697	.0008		
R^2	0.9681			.9968		
Adjusted R^2	0.9394			.9939		

In order to evaluate the degree of fit and the predictive accuracy of the model, the p-value of the model, alongside the coefficient of determination (R^2), the adjusted coefficient of determination (R^2 adj), and the predictive coefficient of determination (R^2pre), were scrutinized to authenticate the model[90]. The p-value serves as a statistical tool to assess the significance of each parameter within the model. When the p-value falls below the established significance threshold (commonly set at 0.05), it signifies that the variable exerts a substantial influence on the model. R^2 and R^2adj represent metrics of the fitting precision of the regression equation, exhibiting values that span from 0 to 1. Values that approach 1 suggest a superior fit of the model to the data. R^2pre acts as a metric employed to evaluate the predictive capacity of the model. Typically, a discrepancy of 0.2 or less between R^2adj and R^2 pre suggests that the model demonstrates commendable predictive performance. The findings derived from the variance analysis pertaining to the regression equations of the model are delineated in Table 9. The p-values associated with each response variable fall below the threshold of 0.0001, thereby underscoring the substantial significance of the model. The adjusted R^2 values for head and efficiency are recorded at 0.9658 and 0.8318, respectively, which suggests a favorable alignment of the regression equations. The disparity between the pre-adjusted R^2 and the adjusted R^2 for head and efficiency is quantified at 0.0352 and 0.0674, respectively. This observation denotes a commendably high degree of fitting accuracy, implying that the model possesses the capability to effectively predict the internal performance metrics of the centrifugal pump. Fig.7.46 provides a visual comparison between the actual and anticipated values of head and efficiency. The X-axis delineates the actual values corresponding to the design points, whereas the Y-axis illustrates the simulated values associated with these design points. The color blue denotes lower levels, whereas the color red signifies higher levels. A majority of the design points depicted in the graph are positioned in proximity to the line of equality (X = Y), thereby indicating that the reliability of the predictions has been satisfactorily established. The response surface model has been validated to ensure that it accurately represents the true relationship between the input factors and the response. This involves checking for model adequacy, lack of fit, and statistical significance of model terms. The analysis demonstrated that the linear effect of rotation ($p \leq 0.05$) was subsequently followed by the linear effect of blade count and discharge, along with the interaction effect between blade count and rotation, succeeded by blade count and discharge, and the association of rotations per minute with discharge, in addition to the quadratic effect of blade count, which were classified as variables with effects ranked from largest to smallest on the head coefficient. Thus, the final models incorporated the significant terms. The model fits well, as shown by the lack of fit test ($P > 0.05$) being insignificant for the head. Table 7.4 shows that the variables with the largest to smallest effects on the efficiency were

the linear effect of blade numbers, rotation per minute, and discharge, and the interaction effect between number of blades and flow rate, and the quadratic effect of blade numbers and rotation per minute, respectively ($p \leq 0.01$). The interaction effect between the blade numbers and rotation per minute, rotation per speed, and discharge, and the quadratic effect of the discharge had no impact on the efficiency. The findings demonstrated that the model fits well and that the lack of fit test ($P > 0.05$) was not relevant for efficiency. In Design-Expert software under the Analysis of Variance (ANOVA) function, the approximate model was examined by using R-squared (R^2=0.9681), shown by eq^n 7.12, Adjusted R-squared (Adj.R2 =0.9394), shown by eq^n 7.13, and Predicted R-squared (Pred. R^2 =0.9060)[73].

$$R^2 = 1 - \frac{\sum_{i=1}^{n}(y_i - \bar{y})^2}{\sum_{i=1}^{n}(y - y_i)^2} \tag{7.12}$$

$$Adj.R^2 = 1 - \frac{n-1}{n-k-1}(1 - R^2) \tag{7.13}$$

According to equation (7.13), n denotes the size of the sample; k denotes the number of independent factors. The Predicted R^2 of 0.9060 and the Adjusted R^2 of 0.9394 are reasonably in accord, i.e., the difference is < 0.2, which shows that there is a very close range between actual optimization objectives and parameters & the regression equations (7.10) and (7.11) are important to anticipate the head and efficiency. The Design Expert software's optimization module was used for predicting optimum impeller parameters. The head and efficiency of the centrifugal pump were evaluated in this investigation using the greatest and lowest values, respectively. To get a high-efficiency impeller with a suitable head, set both the efficiency and head optimization conditions to "maximize."

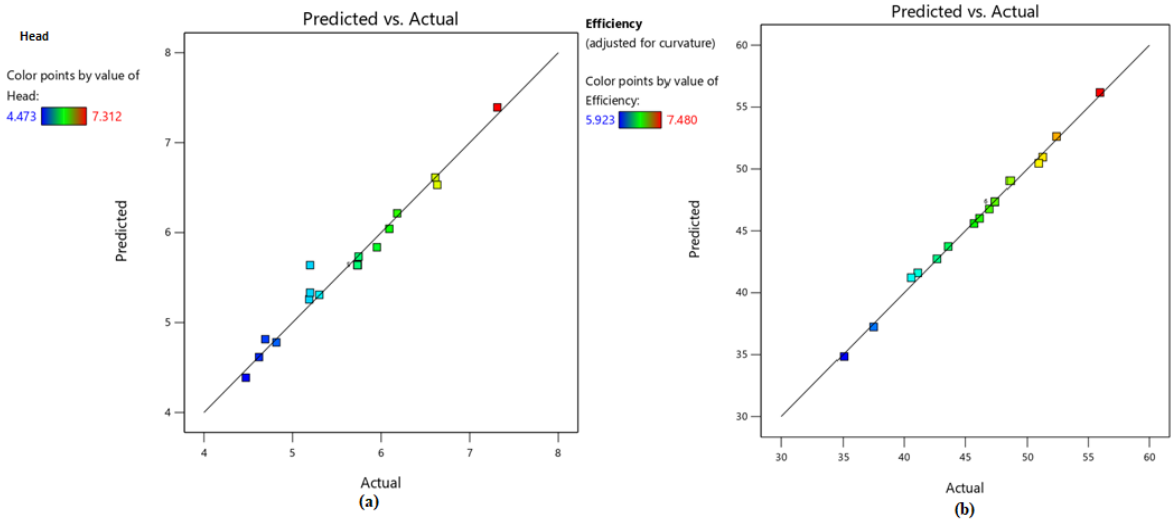

Fig. 7.46 Predicted vs. Actual values plot for (a) head, and (b) efficiency using RSM.

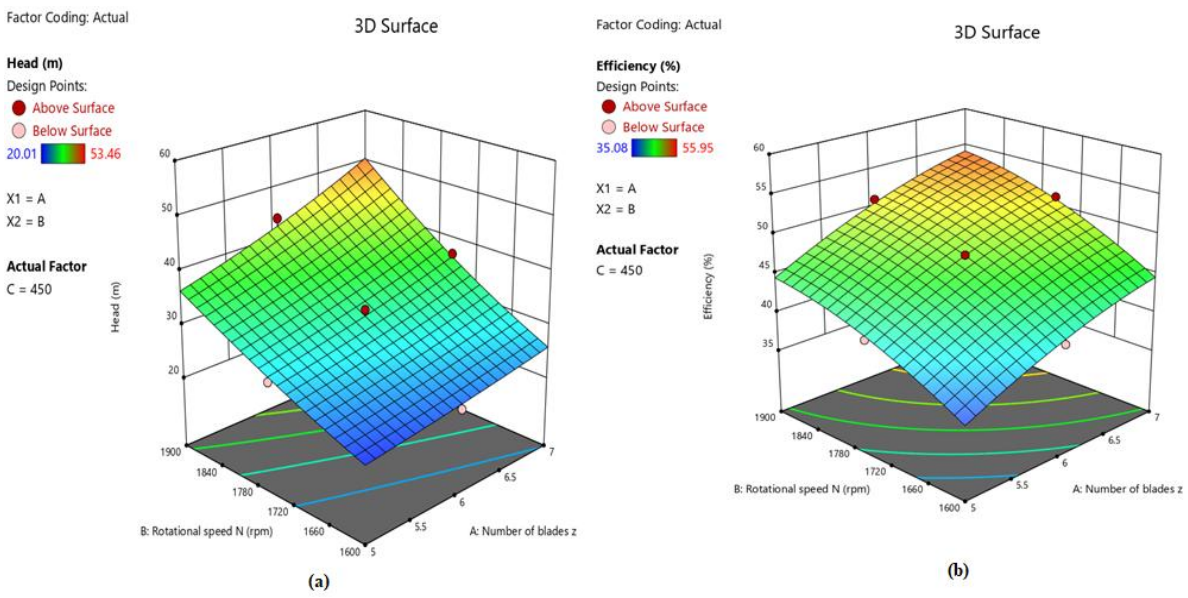

Fig. 7.47 Response surface and contour plots of the interaction between rotational speed and number of blades for (a) Head and (b) Efficiency of single-stage centrifugal pump.

Fig. 7.46 shows the plot between predicted versus actual values of experiments for head and efficiency. To comprehend the dominant influencing parameters, the effect of variables on the responses is investigated. Figure 10 shows the variation in predicted and actual values of experiments for head and efficiency for different numbers of blades, respectively. It shows the dominating influence of the input parameter, i.e., the number of blades, on the responses (head and efficiency). Fig. 7.47 represents the response surface and contour plots of the interaction between rotational speed and number of blades for (a) Head and (b) Efficiency of single-stage centrifugal pump. It shows that as we increase the number of blades from 5 to 7 and the rotational speed from 1600 rpm to 1900 rpm, the head and efficiency increase significantly. But the effect of the number of blades is lower than that of the rotational speed. Thus, rotational speed has the dominant effect on the head and efficiency of the pump. The validated response surface model was used to identify the optimal factor levels that maximize or minimize the response variable. This involves finding the settings that result in maximum yield, minimum cost, or optimal product quality.

Fig. 7.48 shows (a) streamline pattern for optimized single-stage pump in impeller and diffuser with 7 blades, and (b) return passage at 1900 rpm, and Fig. 7.49 shows the pressure contour for the optimized single-stage pump with 7 blades at 1900 rpm.

A confirmation experiment was conducted using the optimal factor levels identified by the response surface model to validate the predicted results and ensure that the optimum has been achieved, which is shown in Table 7.5 and Fig. 7.49.

7.6.1. Streamline Velocity for Optimized Single Stage with Seven Impeller Blades

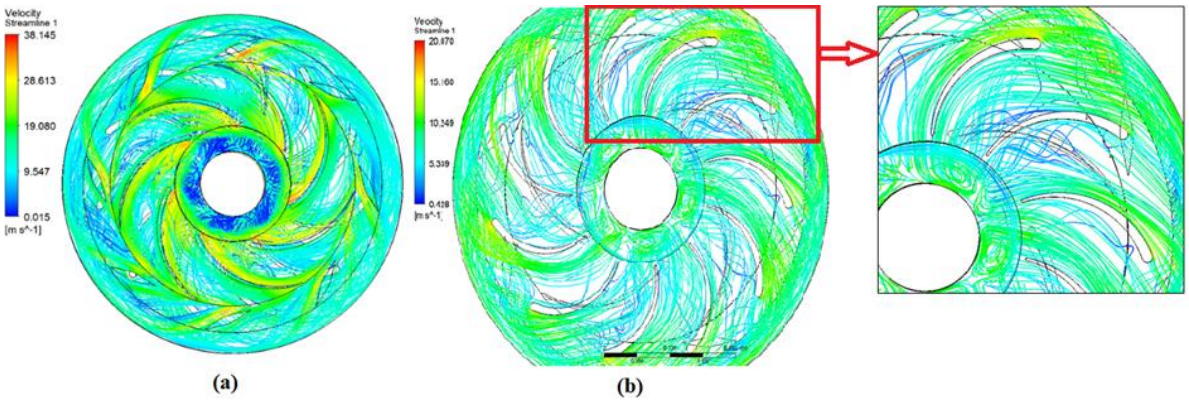

Fig. 7.48 (a) Streamline pattern for optimized single-stage pump in impeller and diffuser with 7 blades, and (b) return passage at 1900 rpm.

7.6.2. Pressure Contour for Optimized Single Stage with Seven Impeller Blades

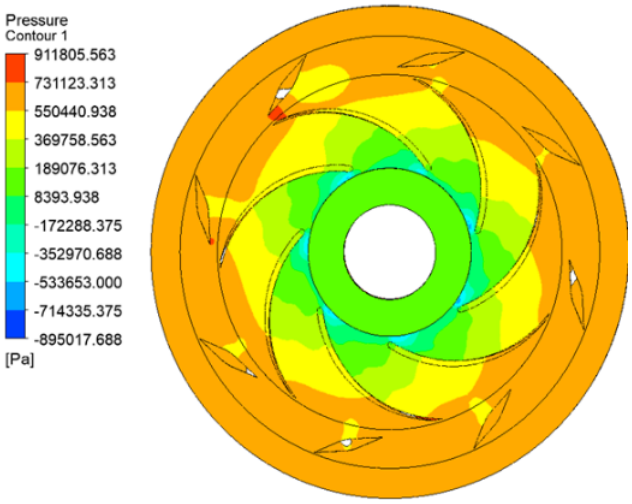

Fig.7.49 Pressure contour for the optimized single-stage pump with 7 blades at 1900 rpm.

Table 7.5 Comparison of numerically simulated results and selected solution from RSM

Results	Number of blades z	Rotation N (rpm)	Flow rate Q (m^3/h)	Head H (m)	Efficiency η (%)
Simulated Results	7	1900	450	49.34	54.65
RSM Results	7	1900	450	53.24	55.78

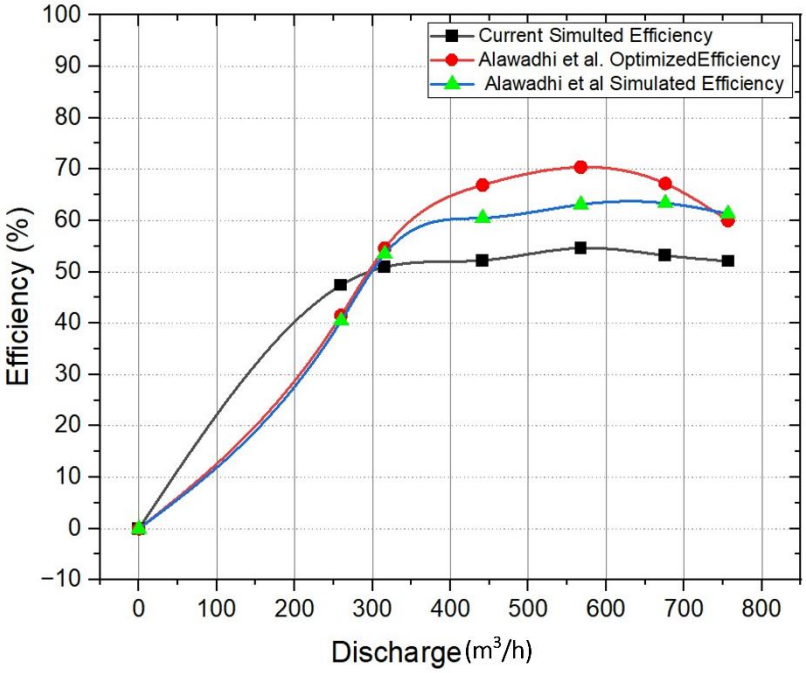

Fig. 7.50 Comparison of Alawadhi et al. results and Current simulated results [27].

7.7 VALIDATION OF RESULTS

To validate the results obtained from RSM, we create the 3D model using the parameters from Table 7.5 to obtain the optimized impeller for the entire computational domain. The optimal pump model is then estimated in CFX 2022R1 to confirm the optimization findings. The head and efficiency calculated from the numerical simulation are 49.34m and 54.65% with deviations of 7.90% and 2.06% respectively, as shown in Table 7.5. This is because RSM takes into account a wider range of operating parameters and their interactions. Numerical simulations often focus on a limited set of parameters and assume linear relationships between them, which may not accurately capture the complex interactions that occur in a real pump system. RSM, on the other hand, uses statistical techniques to model the relationships between multiple variables and optimize the design based on these interactions. Numerical simulations typically assume idealized conditions and do not consider factors such as fluctuations in fluid properties, changes in system resistance, or variations in operating temperatures. RSM, however, can incorporate these uncertainties into the optimization process, leading to a design that performs well under a wider range of real-world conditions. Table 7.5 shows the numerical simulation results of the optimized single-stage pump. Fig. 7.50 shows the comparison of Alawadhi et al.[27] work results with the current simulated results. It shows that the current simulated work follows the trend of the characteristics curve of Alawadhi et al.[27] work with a reasonable deviation.

This shows that the efficiency goes on increasing as we increase the flow rate, and after a certain discharge, it decreases as we increase the discharge. Because of the following high discharge rates, the pump may operate at a lower head and flow rate than its design point, leading to reduced efficiency. This is because the pump may be operating away from its optimal operating conditions, where it is designed to perform most efficiently.

7.8 STUDY OF FLOW SIMULATION FOR TWO STAGE MULTISTAGE PUMP

After the study of numerical flow simulation for single-stage pumps and finding the best pump that gave the best performance, it's now time to carry out flow analysis for a two-stage multistage pump. The analysis of a two-stage multistage centrifugal pump will be carried out for a speed of 1900 rpm, and the mass flow rate is kept constant for all, i.e., 128.88 kg/s. So, the flow simulation for 3 two stage pump which will have impeller with 5, 6, and 7 blades.

7.8.1 Two Stage with Five Impeller Blades

The CFD simulation investigation has been done for a two-stage centrifugal pump, which has two impellers with five blades surrounded by a stationary diffuser with 8 DFV, the 1st stage return passage with 11 DFV, and the last stage return passage with an outlet pipe. The performance of a two-stage pump is represented graphically for parameters like head, efficiency, and power with respect to speed. The velocity streamline pattern and pressure contourare represented below. The data result for the same is shown in Table 7.6.

Table 7.6 Data result for two-stage pumps of impeller with 5 blades

Speed (rpm)	Values
P_1 (pa)	263785
P_2 (pa)	1162840
H (m)	91.64
P_{out} (W)	115798.28
P_{in}(W)	205762.35
η (%)	56.27

7.8.2 Two Stage with Six Impeller Blades

The flow analysis is now carried out for a two-stage pump, which has two impellers with six blades. The data result for the same is shown in Table 7.7.

Table 7.7 Data result for two-stage pump of impeller with 6 blades

Speed (rpm)	Values
P_1 (pa)	231758
P_2 (pa)	1257730
H (m)	104.58
P_{out} (W)	132145.19
P_{in}(W)	222307.87
η (%)	59.44

7.8.3 Two Stage with Seven Impeller Blades

The flow analysis is now carried out for a two-stage pump which has two impellers with seven blades, and the data results for this are shown in Table 7.8.

Table 7.8 Data result for two-stage pump of impeller with 7 blades

Speed (rpm)	Values
P_1 (pa)	223856
P_2 (pa)	1333400
H (m)	62.14165
P_{out} (W)	142909.2672
P_{in}(W)	229973.3907
η (%)	62.14165

7.9 STREAMLINE VELOCITY OF TWO-STAGE PUMP

In a two-stage pump, the streamline pattern is represented. Looking towards the streamlines, it is observed that the whirl velocity (Cu1) at the inlet of both impellers is nearly equal to zero, which satisfies the pump condition. The function of the return passage guide vane was to deswirl the flow before entering the next stage, and this is achieved for the two-stage simulation.

7.9.1 Streamline Velocity for Two Stage with Five Impeller Blades

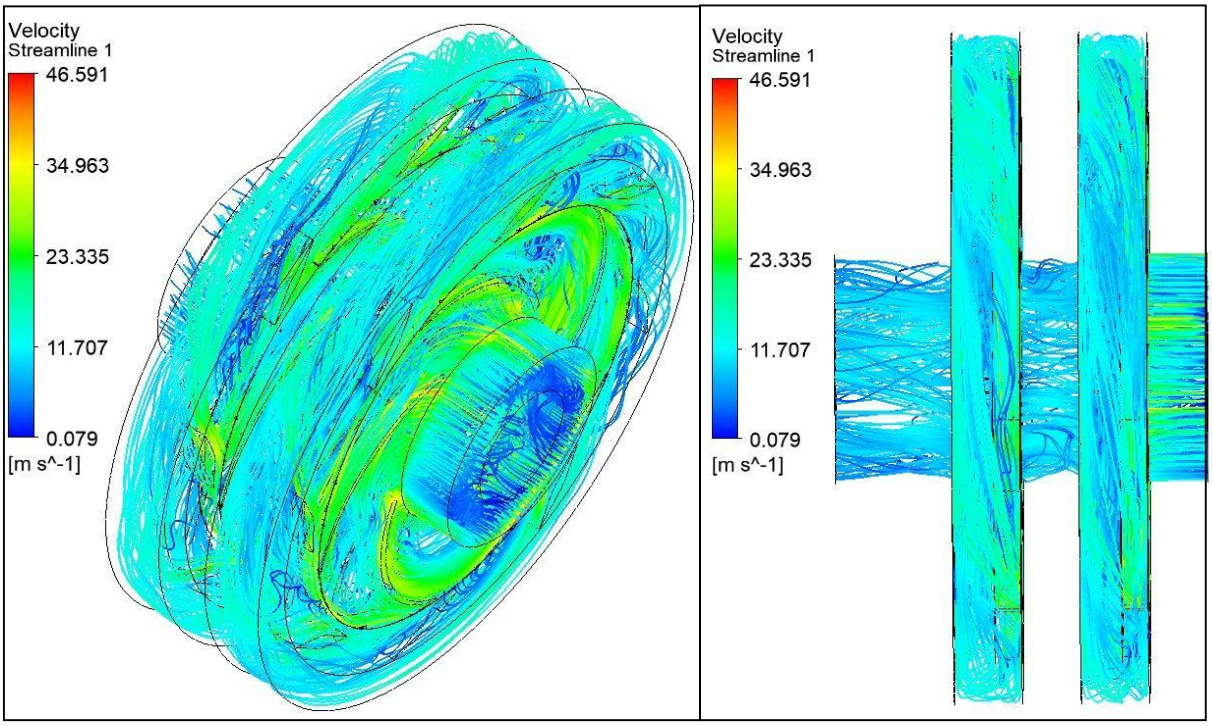

Fig. 7.51 3D view Streamlinespattern for two-stage pump with 5 blades at 1900 rpm

The maximum velocity for the two-stage pump domain with an impeller having 5 blades was found to be 46.591m/s, as shown in Fig.7.51.

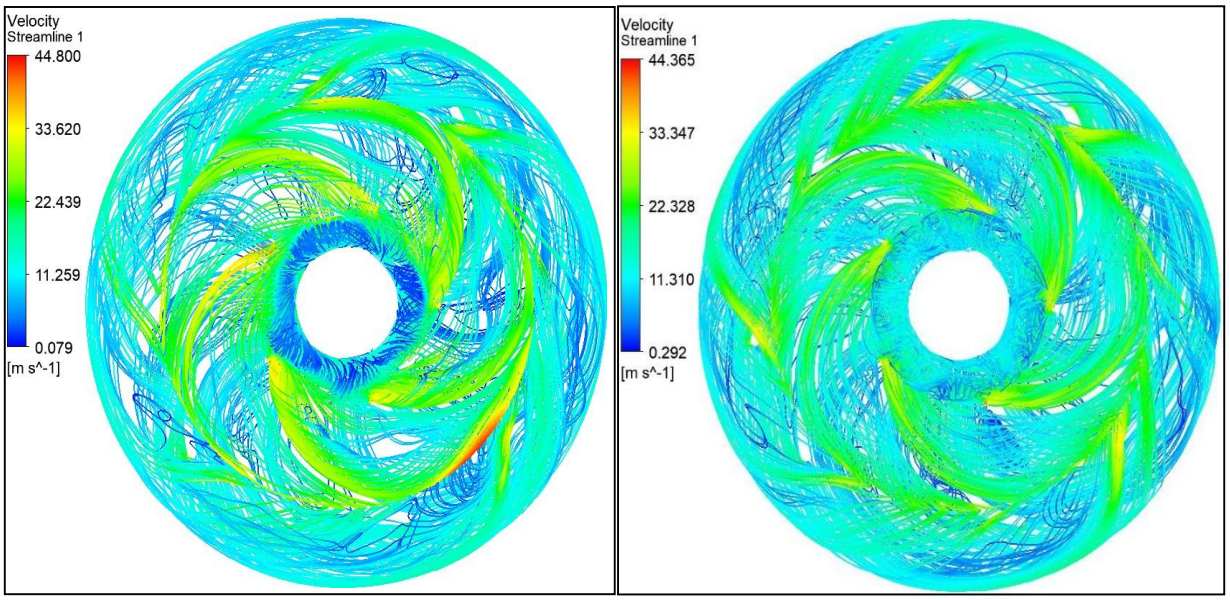

Fig. 7.52 Streamlines pattern of 1st stage and 2nd stage for impeller with 5 blades

In 1st stage, the highest velocity value was found to be 44.80m/s at the impeller outlet. In the 2nd stage, the maximum velocity value was found to be 44.365 m/s at the impeller exit, as shown in Fig. 7.52.

7.9.2 Streamline Velocity for Two Stage with Six Impeller Blades

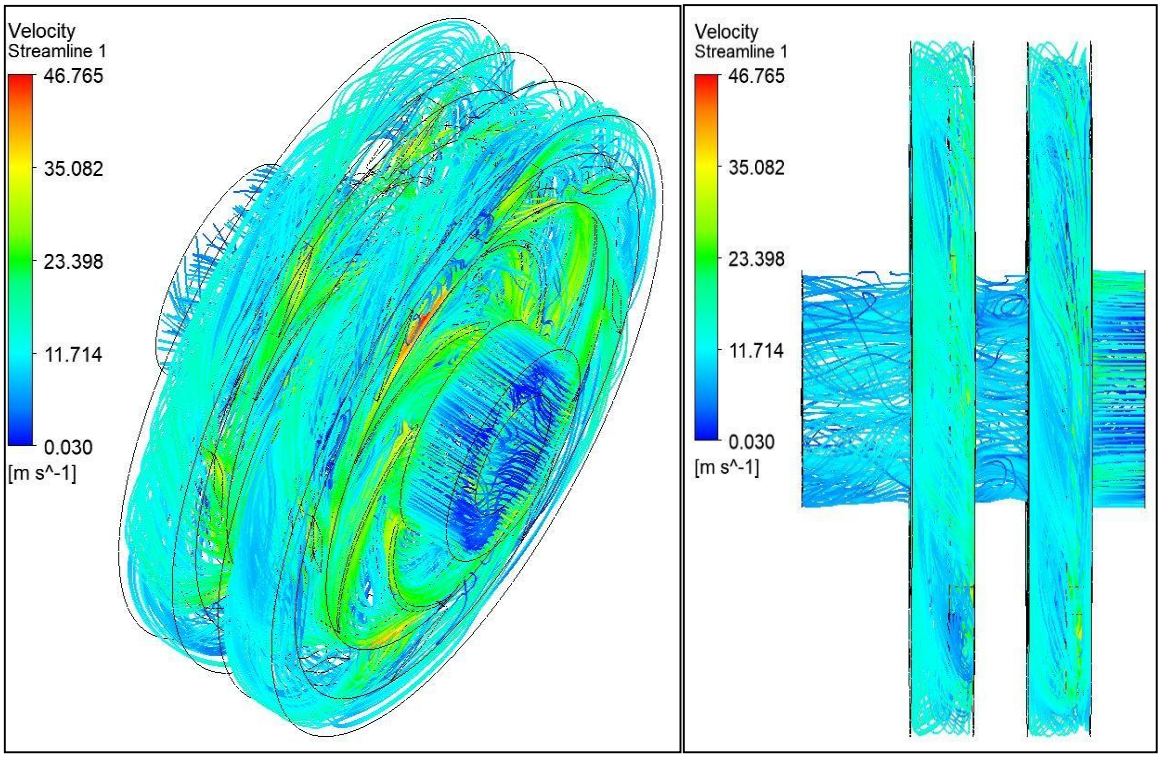

Fig. 7.53 3D view Streamlinespattern for two-stage with 6 blades at 1900 rpm

The maximum velocity for a two-stage pump domain with an impeller having 6 blades was foundto be 46.765m/s, as shown in Fig. 7.53.

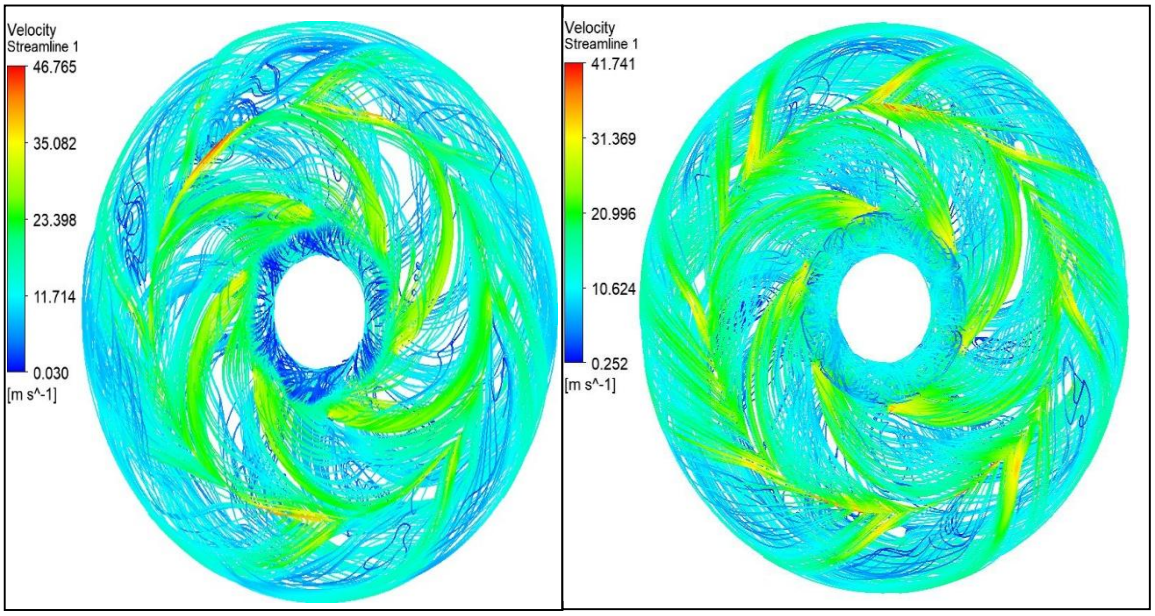

Fig. 7.54 Streamlines pattern of 1st stage and 2nd stage for impeller with 6blades

In 1st stage, the highest velocity value was found to be 46.765m/s at the impeller outlet. In the 2nd stage, the maximum velocity value was found to be 41.741m/s at the impeller exit, as shown in Fig. 7.54.

7.9.3 Streamline Velocity for Two Stage with Seven Impeller Blades

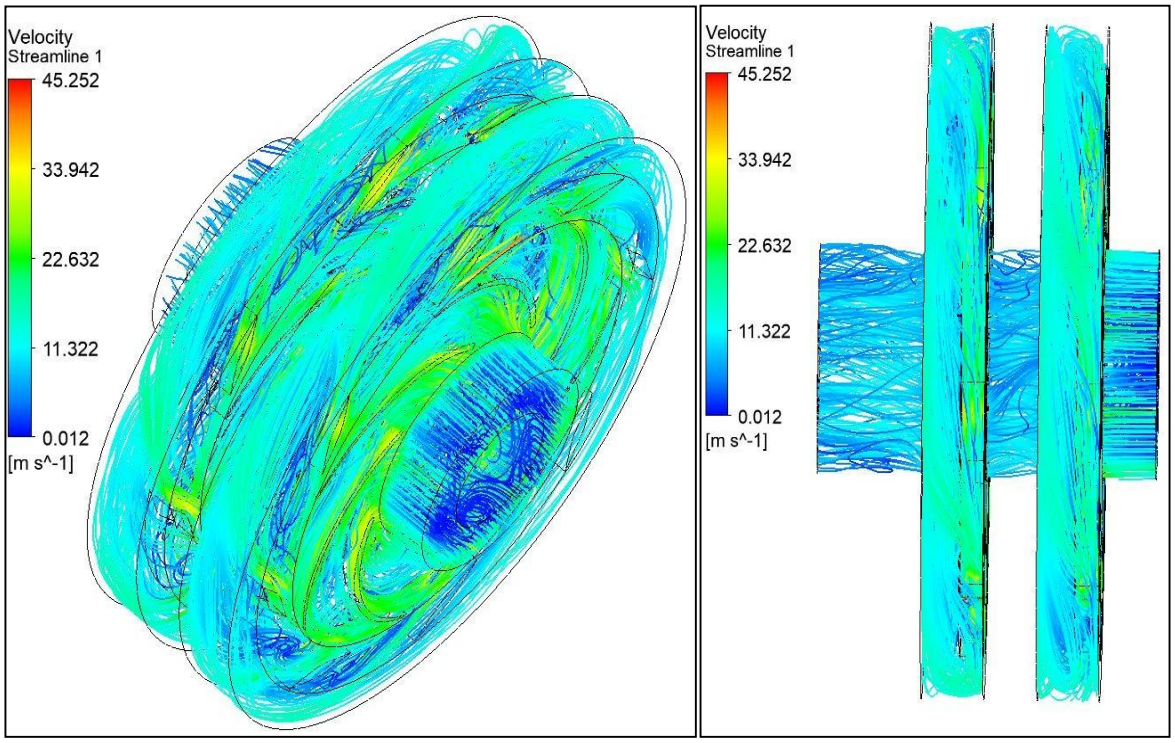

Fig. 7.55 3D view Streamlinespattern for two-stage with 7 blades at 1900 rpm

The maximum velocity for a two-stage pump domain with an impeller having 6 blades was found to be 45.252m/s is shown in Fig. 7.55.

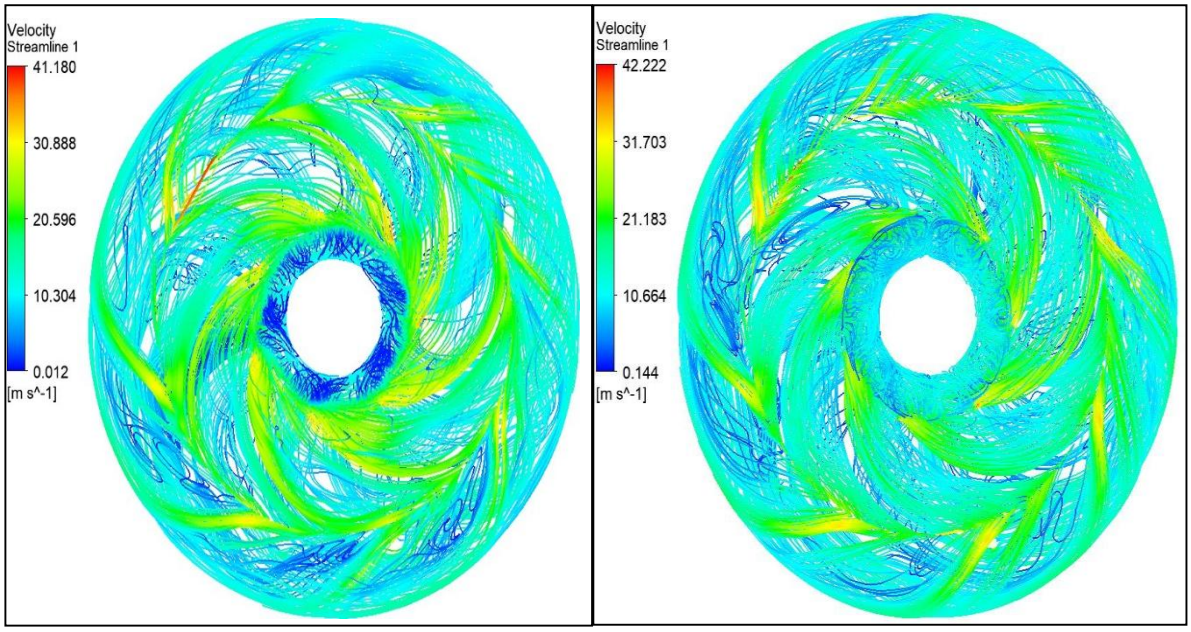

Fig. 7.56 Streamlines pattern of1st stage and 2nd stage for impeller with 7 blades

In 1st stage, the highest velocity value was found to be 41.180m/s at the impeller outlet. In the 2nd stage, the maximum velocity value was found to be 42.222m/s at the impeller exit, as shown in Fig. 7.56.

7.10 PRESSURE DISTRIBUTION FOR TWO-STAGE CENTRIFUGAL PUMP

The pressure distribution for a two-stage pump with impellers having 5,6, and 7 no. of blades isfound. It was investigated that the pressure increases from one stage to the next stage, and thus, the pressure at the outlet is more than that of the single-stage pump. The head generated by a two-stage pump is double that of a single-stage one. The figures below show the pressure contours for a constant mass flow rate of 128.88kg/s for the 1900 rpm rotational speed.

7.10.1 Pressure Contour for Two Stage with Five Impeller Blades

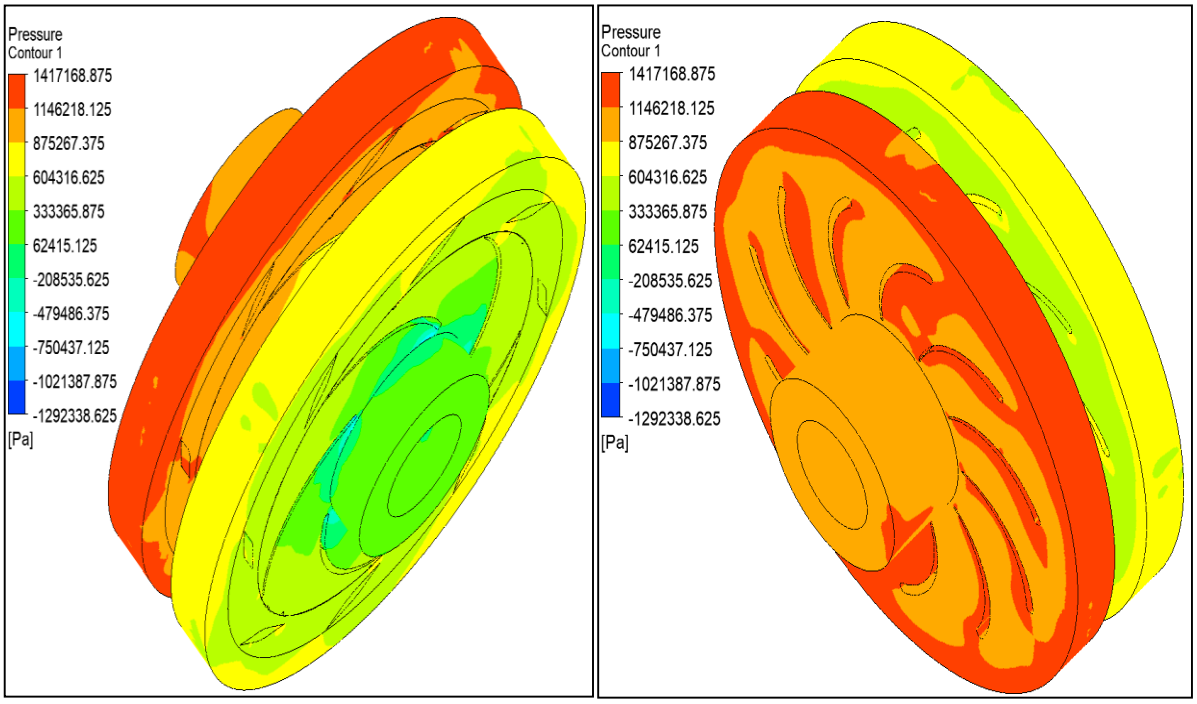

Fig. 7.57 3D view of pressure contour for a two-stage pump with 5 blades

From the above figure, Fig. 7.57, it is concluded that the pressure goes on rising from one stage tothe next stage. The total pressure at the inlet of the pump is 263785 pa, and at the outlet 1162840 pa.The hydraulic head (H) generated is equal to 91.64m.

Fig. 7.58 shows the pressure distribution in blade-to-blade view for the 1st and 2nd stage impeller and diffuser. The pressure variation in the return passage is not so much

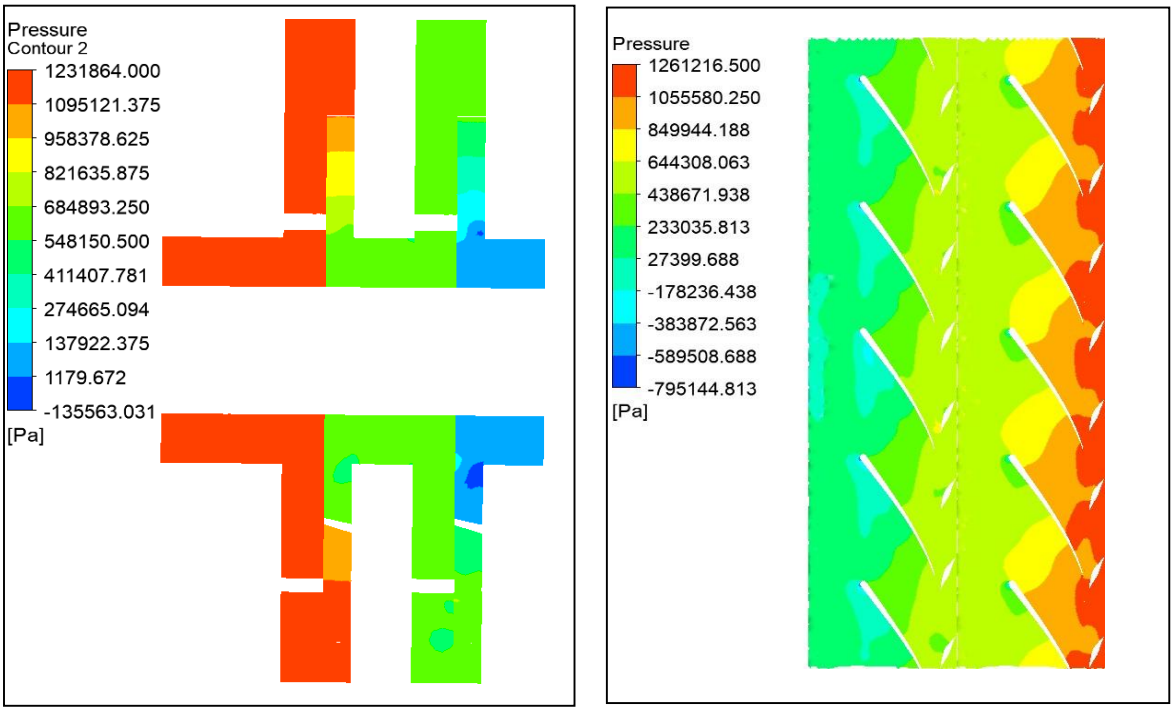

(a) (b)

Fig. 7.58 (a) Sectional view (b) Pressure contours on the blade to blade in impeller and diffuser for a two-stage pump with 5 blades

7.10.2 Pressure Contour for Two-Stage with Six Impeller Blades

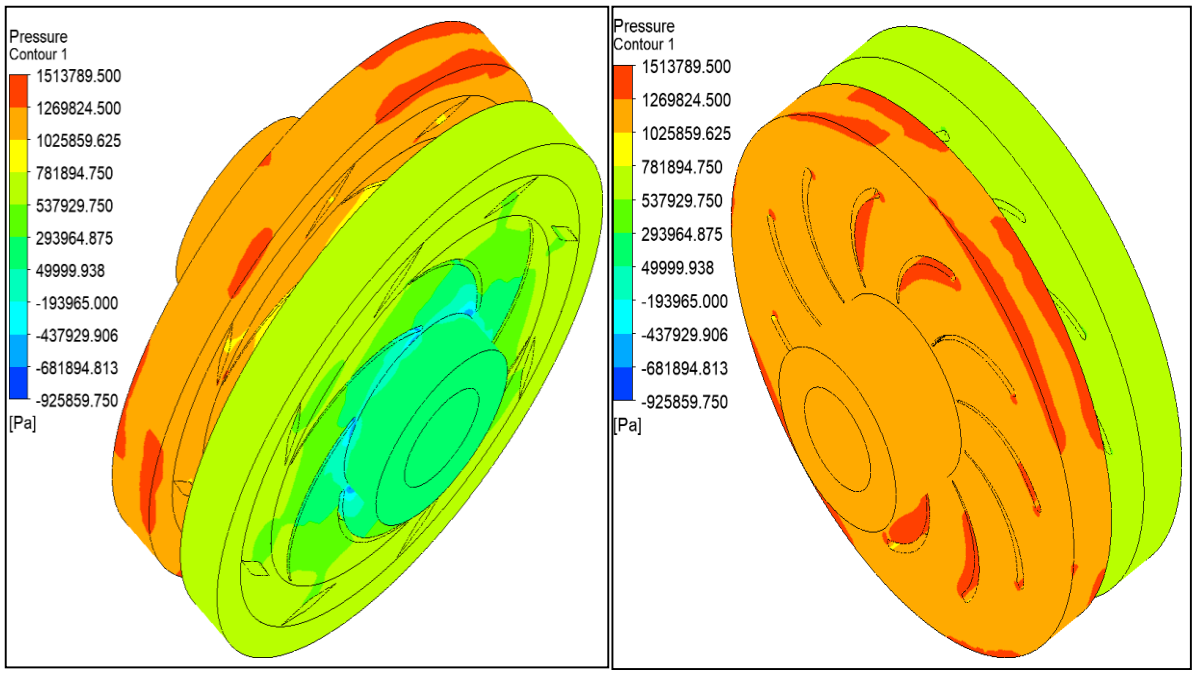

Fig. 7.59 3D view of pressure contour for a two-stage pump with 6 blades

From the above figures, Fig.7.58 and Fig. 7.59, it is concluded that the pressure goes on rising fromone stage to the next stage. The total pressure at the inlet of the pump is 231758 pa, and at the outlet,1257730 pa. The hydraulic head (H) generated is equal to 104.58m.

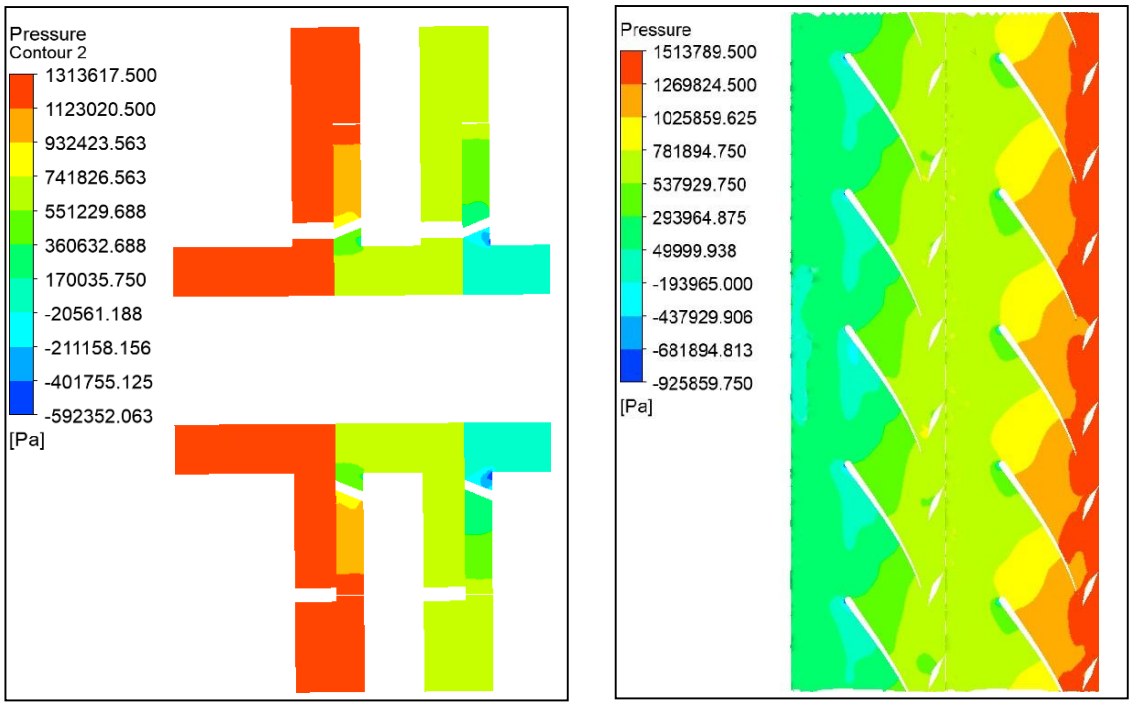

(a) (b)

Fig. 7.60 (a) Sectional view (b) Pressure contours on the blade-to-blade in the impeller and diffuser for a two-stage pump with 5 blades

7.10.3 Pressure Contour for Two Stage with Seven Impeller Blades

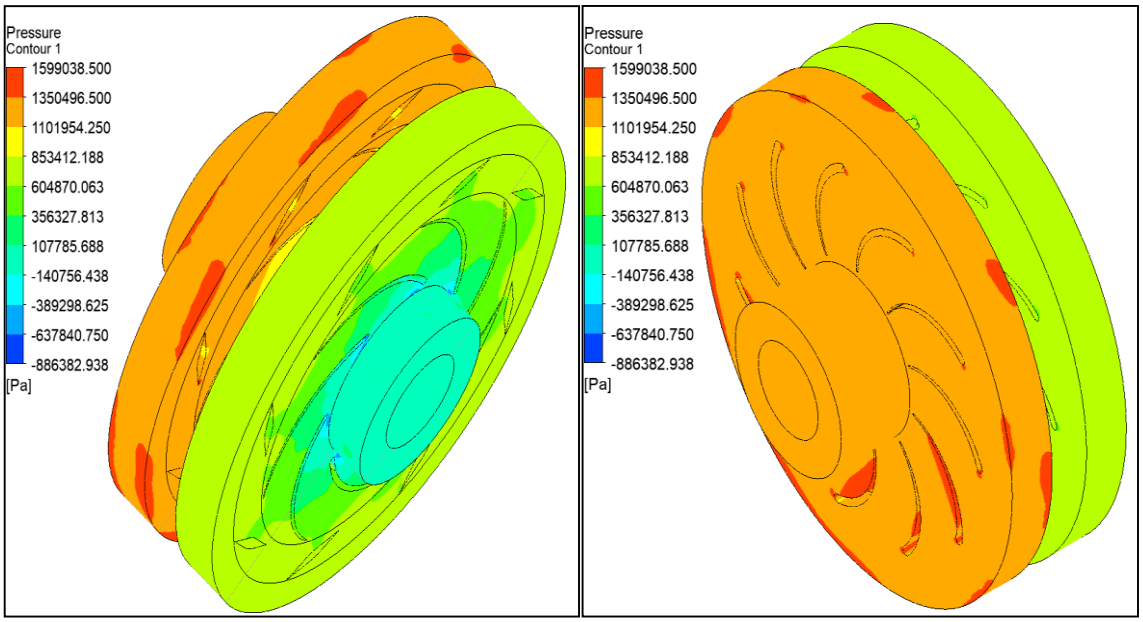

Fig. 7.61 3D view of pressure contour for a two-stage pump with 7 blades

From the figures Fig. 7.60 and Fig. 7.61, it is concluded that the pressure goes on rising from one stage tothe next stage. The total pressure at the inlet of the pump is 223856 pa, and at the outlet, 1333400 pa.The hydraulic head (H) generated is equal to 113.10m.

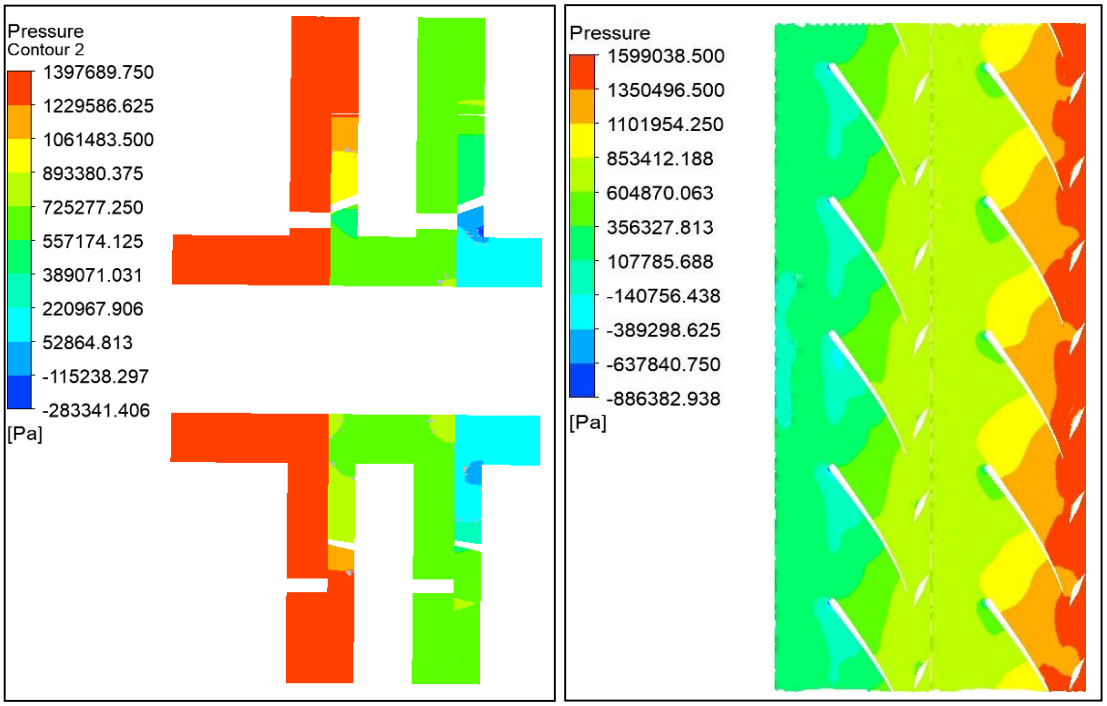

(a) (b)

Fig. 7.62 (a) Sectional view (b) Pressure contours on the blade-to-blade in the impeller and diffuser for a two-stage pump with 7 blades

7.11 HYDRAULIC LOSSES IN TWO-STAGE CENTRIFUGAL PUMP

In a centrifugal pump, when the flow is directed from one stage to another stage or from one part to another, that is, from the impeller to the diffuser, from the diffuser to the return passage, there are some losses. Head losses in multistage centrifugal pumps occur due to various factors such as friction losses, leakage losses, and losses due to impeller clearance.

Friction losses occur due to the flow of fluid through the impellers, diffusers, return passages, and other components. These losses increase with the square of the flow rate and are proportional to the length of the flow path. Leakage losses occur due to the clearance between the impeller and the casing, which allows some fluid to bypass the impeller and flow directly from the suction to the discharge. These losses can be minimized by maintaining tight clearances between the impeller and casing. Losses due to impeller clearance occur when the clearance between the impeller and casing is too large, allowing fluid to recirculate within the pump. This results in a reduction in head and efficiency. Therefore, losses in the stationary parts, that is, the diffuser and return passage of the 1st stage and 2nd stage, are calculated and tabulated in Table 7.9 and shown in Fig. 7.63.

Table 7.9 Head loss in stationary parts

Pump with impeller blades no.	Head loss in 1st stage diffuser (m)	Head loss in 2nd stage diffuser (m)	Head loss in 1st stage return passage (m)	Head loss in 2nd stage return passage (m)
5	4.085	4.034	8.035	9.634
6	4.672	4.725	8.743	11.236
7	4.653	5.227	8.602	10.632

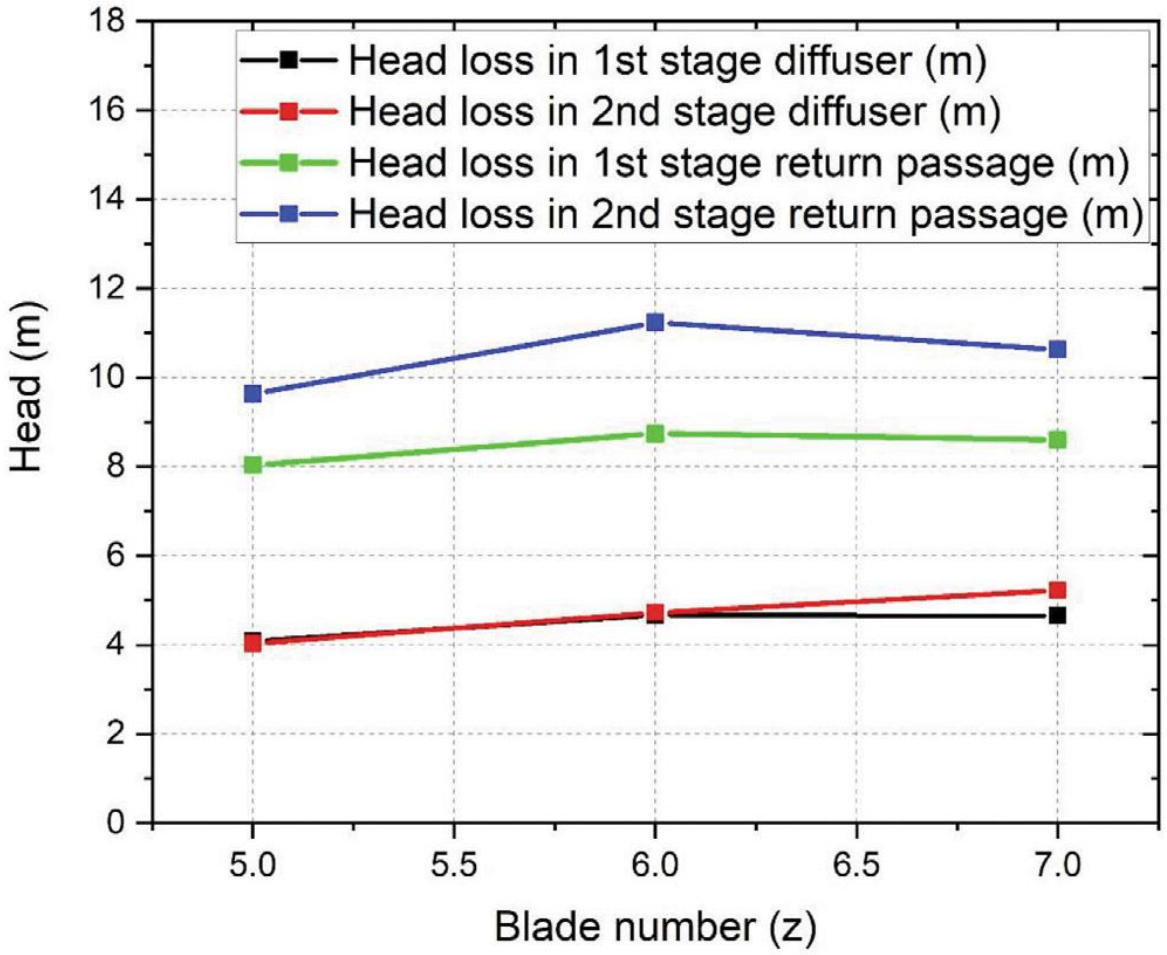

Fig. 7.63 Head loss versus number of impeller blades plot.

From the data given in Table 7.9 and from Fig. 7.63, it is seen that the head loss in the 1st stage diffuser and 1st stage return passage is nearly the same for all three cases, while the head loss in the 2nd stage diffuser and 2nd stage return channel varies a little bit. The losses in the return guide vane of the 1st and 2nd stages of a centrifugal pump can be different because their designs and operating conditions may not be the same. The return guide vane is located after the diffuser, and its main function is to redirect the flow of fluid to the next stage of the pump.

The design of the return guide vane can vary depending on the specific pump application, and factors such as the angle of the vanes, the number of vanes, and the curvature of the vanes can all affect the losses in this component. In addition, the operating conditions of the 1st and 2nd stages may also differ, which can impact the losses in the return guide vane. For example, if the flow rate or pressure of the fluid changes between the two stages, this can affect the performance of the return guide vane and lead to different losses. Overall, while the diffusers in the 1st and 2nd stages of a centrifugal pump are designed to serve a similar purpose and therefore have similar losses, the design and operating conditions of other components, such as the return guide vane, can lead to differences in losses between stages. The head loss (Δh) in a diffuser and return passages is calculated by $\mathbf{\Delta h} = \frac{(P_1 - P_2)}{\rho g}$.

7.12 STUDY OF FLOW SIMULATION FOR THREE RETURN GUIDE VANE OF SINGLE-STAGE CENTRIFUGAL PUMP

The simulation of the three return guide vanes (mixed return guide vane, radial return guide vane, and distorted return guide vane) is carried out by assuming the specifications of the single-stage model except for the return channel. To demonstrate the effectiveness of the design, Fig. 7.63 shows the velocity streamlines within the guide vanes.

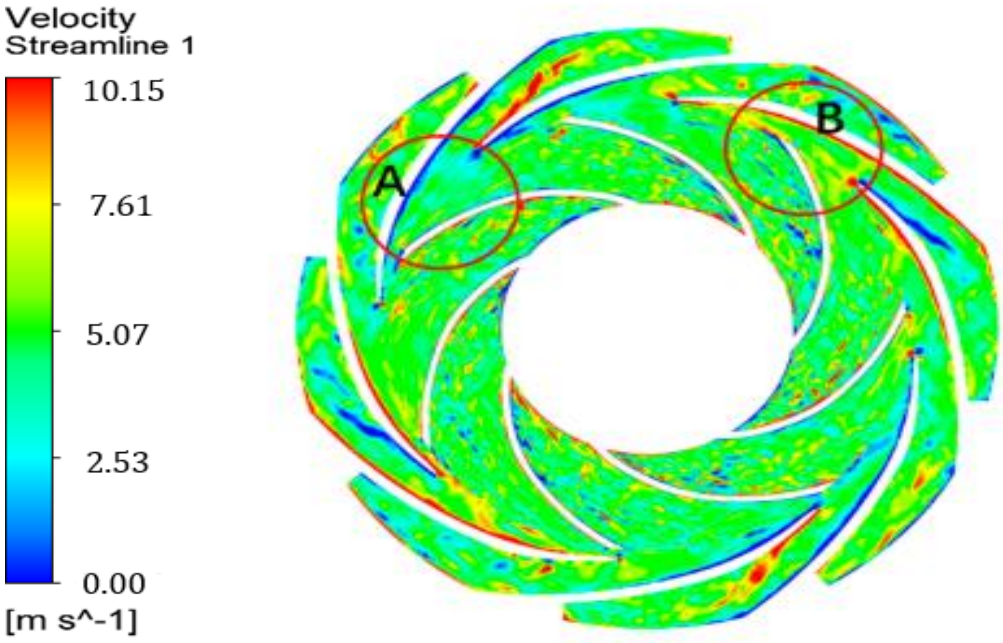

Fig. 7.64: 2D view of streamlines pattern of Mixed Return Guide Vane

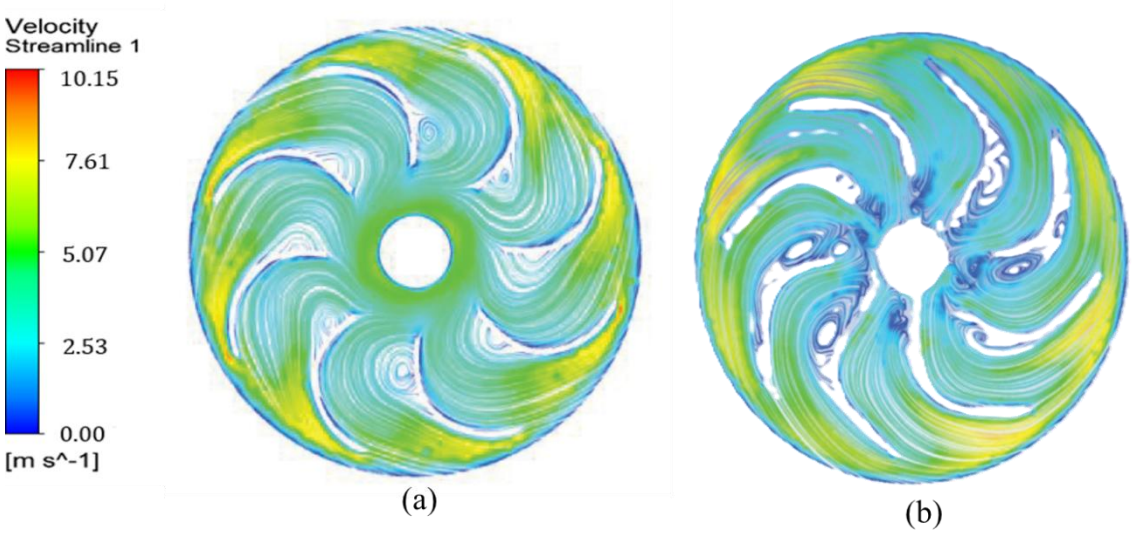

Fig. 7.65: 2D view of streamlines pattern of (a) Radial RGV and (b) Distorted RGV

The flow within the impeller section is anticipated to remain uniform. In the return channel region, deswirls are significantly reduced. By evenly spreading the vane's curvature throughout the entire geometry, flow separation on the pressure sides is eliminated.

The rotational flow exiting the impeller must pass through the guide vanes to achieve uniformity. Because the guide vane path is extended, friction loss from wall shear increases, which is necessary to prevent flow separation. To explore the impact of different return guide vanes, a series of CFD analyses were performed, and the results are summarized in Table 7.10.

Table 7.10: Total pump head, overall guide vane efficiencies, and Loss coefficient of Mixed, Radial, and Distorted RGV

Parameters	**Values**		
	Total Head (m)	Vane Efficiency	Loss coefficient
Mixed	38.11	0.87	0.47
Radial	41.23	0.91	0.45
Distorted	39.56	0.89	0.59

The highest efficiency is achieved with the radial return guide vane, despite experiencing a slight loss in head and higher loss coefficients compared to the mixed and distorted return guide vanes. However, data in Table 7.10 reveal that variations in the shape of the return guide vane impact the pump head more significantly than guide vane efficiency. As depicted in Figure 7.65, although a minor loss in velocity occurs at the trailing edges of the return vane with smaller outlet angles, the flow remains uniform within the channels.

7.13 STUDY OF FLOW SIMULATION OF RADIAL RETURN GUIDE VANE WITH VARYING OUTLET VANE ANGLE

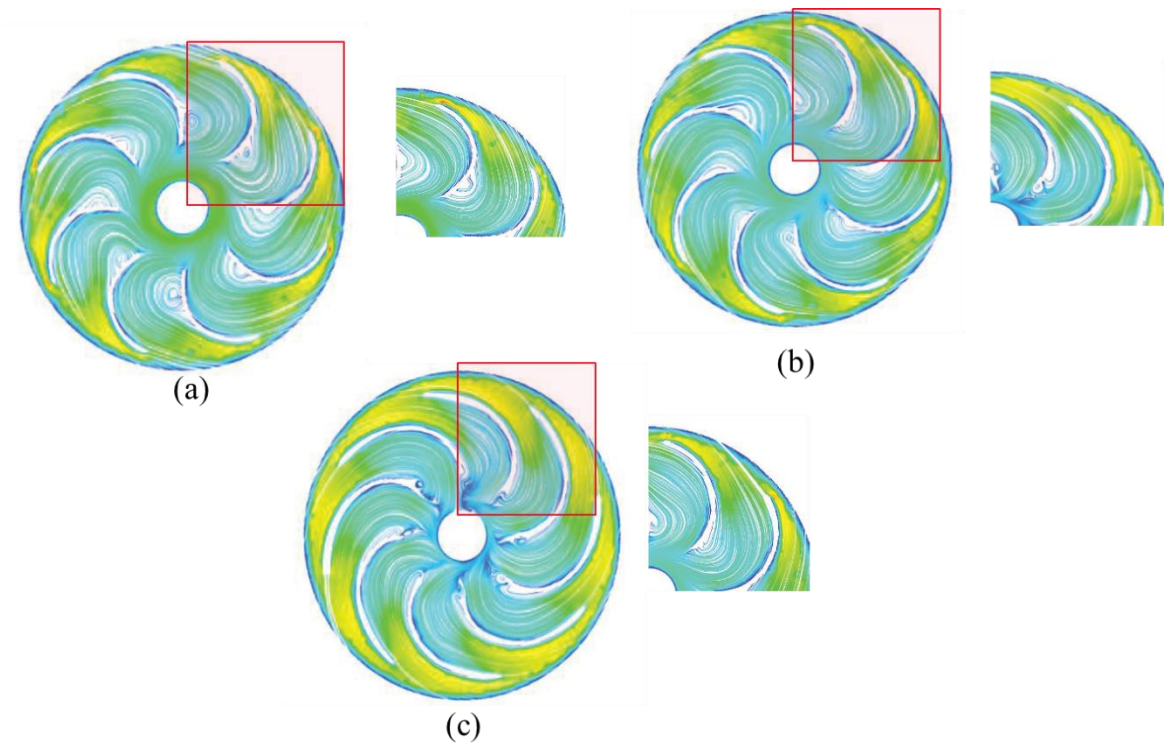

Fig. 7.66: 2D view of streamlines pattern of Radial RGV with outlet angle of (a) 20◦ (b) 25◦ (c) 30◦

Table 7.11: Total pump head and overall guide vane efficiencies for variation in outlet blade angles

Outlet blade Angle (◦)	Values		
	Total Head (m)	Guide Vane Efficiency	Loss Coefficient
20	39.87	0.89	0.59
25	43.01	0.90	0.46
30	41.23	0.91	0.45

Data in Table 7.11 indicates that changes in vane outlet angle have a more significant impact on the pump head than on guide vane efficiency. The small travel length differences of flow between vanes do not significantly affect the tangential energy, which causes inefficiency in guide vanes. Efficiencies are observed to be highest between 25 and 30 degrees of vane outlet angles, with minimal loss in the head and similar loss coefficients, except at 20 degrees.

As shown in Fig. 7.66, although small velocity drops occur at the trailing edges of guide vanes with smaller outlet angles, the flow remains uniform within the channels. No flow

recirculation is observed in the return channels for any outlet angle. This demonstrates that forming a smooth, curved vane is crucial for eliminating recirculation in channels.

Summary

1. **The function of the return passage guide vanes is to deswirl the fluid before entering the next stage, which results in an undistorted flow into the following impeller and the ability to draw more fluid into it.**
2. **While designing the return channel guide vanes, it should be noted that the guide vanes must have a large radius of curvature to have a minimum head loss.**
3. **The flow simulation for a single-stage pump has been carried out at four different speeds for the pump having three different impellers of 5, 6, and 7 blades.**
4. **From the above performance charts, velocity streamlines, and pressure contours, it has been observed that as speed and number of blades increase, the performance parameters such as efficiency, head, and output power increase.**
5. **It is investigated that the single-stage pump running at a speed of 1900 rpm gives greater performance among all remaining speeds.**
6. **The circumferential velocity at the inlet of the 1st stage and 2nd stage was found to be nearly equal to zero, which satisfies the theoretical concept of velocity triangle C_{U1} = -0.00137 m/s and C_{U3} = -0.59985 m/s**
7. **It was investigated that the pressure increases from one stage to the next stage, and thus the pressure at the outlet is more than that of the single-stage pump. The head generated by a two-stage pump is more than double that of a single stage.**

CHAPTER 8.

CONCLUSION, FUTURE SCOPE, AND SOCIAL IMPACT

This chapter discusses the conclusions inferred from the above results and discussions, the future scope, industrial relevance, and the social impact of the thesis.

8.1 Conclusions

The study of CFD flow simulation for a single-stage multistage pump is carried out first at different numbers of blades and rotational speeds. It has been investigated that the number of blades and the different effect performance of the pump, resulting in the fact that as the number of impeller blades and the rotational speed increase, the pump performance also increases. On thebasis of single-stage analysis, the best results were selected, and further flow analysis of a two-stage multistage is being carried out for different numbers of blades at constant speed. The following conclusions have been drawn from the results and discussion:

- The single-stage pump having an impeller with 5 blades, 8 diffuser vanes, and 11 return passage guide vanes is analyzed for constant Q = 0.1288m^3/s and different rotational speeds. It is observed that as speed changes from 1450 rpm to 1900 rpm, the head and efficiency of the pump increase. The maximum head of 35m and efficiency of44.58% were obtained for 1900 rpm.
- For a single-stage pump with 6 impeller blades, the flow simulation has been obtained for constant Q = 0.1288 m3/s, and the speed has been varied from 1450 rpm to 1900 rpm. The maximum head developed was 44.01m and the maximum hydraulic efficiency was 50.93%for the 1900 rpm.
- When the impellers with 7 blades were used for the same discharge, the speed was varied from1450 rpm to 1900 rpm. The highest head produced by the pump was 49.34m, and the highest efficiency was 54.65% for 1900 rpm speed.
- The whirl velocity C_{u1} at the inlet of the pump is nearly equal to zero, which satisfies pump theory.
- The total pressure and total pressure in the stationary frame were observed to be exactly equal.
- From the above three cases, it was found that the single-stage pump gave good performance for1900 rpm, and then, while considering this speed, a flow simulation for two-stage pumps has been carried out for different no. of impeller blades.
- The pressure increases from one stage to the next stage.
- For two-stage pumps having an impeller with 5 blades, the flow was simulated for Q =

0.1288m^3/s at 1900 rpm rotational speed. The maximum head developed by the pump is 91.64m, and the hydraulic efficiency was found to be 56.27.

- The two-stage pump with 6 impeller blades for the same discharge and speed was studied, the head given by the pump is 104.58m, and the efficiency was 59.44 %.
- For two-stage pumps with 7 impeller blades for the same Q and speed, the head obtained is 113.01m, and the efficiency is 62.14%.
- The return passage guide vane directs the flow before fluid enters the next stage, so the whirl velocity at the inlet of the next stage is nearly equal to zero.
- The head loss for two-stage pumps in the diffuser and return passage was found to be nearly the same for 1st stage, while for the 2nd stage, it was a little bit varied.
- The highest efficiency is achieved with the radial return guide vane, despite experiencing a slight loss in head and higher loss coefficients compared to the mixed and distorted return guide vanes.
- The changes in vane outlet angle have a more significant impact on pump head than on guide vane efficiency. The small travel length differences of flow between vanes do not significantly affect the tangential energy, which causes inefficiency in guide vanes.
- Efficiencies are observed to be highest between 25 and 30 degrees of vane outlet angles, with minimal loss in head and similar loss coefficients, except at 20 degrees.
- A small velocity drops occur at the trailing edges of guide vanes with smaller outlet angles, and the flow remains uniform within the channels.
- No flow recirculation is observed in the return channels for any outlet angle. This demonstrates that forming a smooth, curved vane is crucial for eliminating recirculation in channels.

8.2 Future Scope

- The further performance can be improved by increasing the outlet width of the diffuser and by increasing the return passage casing height.
- The return passage at the periphery of the casing can be made into a circular shape, i.e., eliminating sudden sharpness.
- The model can be analyzed for various mass flow rates.
- The radius of curvature of diffuser vanes can be increased.

8.3 Industrial Relevance and Social Impact

The optimized 7-blade impeller at 1900 rpm achieved nearly a **10% efficiency gain** corresponding to ~5 kW energy savings for a 50 kW pump, or about **30 MWh annually** in continuous operation. Such improvements are highly relevant for applications like **boiler**

feed, mine dewatering, and pressure boosting, where sustained energy efficiency translates directly into significant cost savings. Considering the widespread use of such pumps, even modest efficiency improvements can collectively translate into significant reductions in **electricity consumption and operating costs**, thereby contributing to national goals of energy conservation and sustainability. Moreover, reduced energy demand directly lowers **carbon emissions**, aligning with global efforts to mitigate climate change. In sectors like irrigation and municipal water supply, efficiency improvements also help deliver water more reliably and affordably, enhancing community well-being. Thus, the thesis not only advances pump technology but also supports broader **economic, environmental, and social sustainability objectives**.

REFERENCES

[1] B.R. Rode, R. Khare, Numerical Simulation for Design Improvement in Diffuser of Multistage Centrifugal Pump, in: Lect. Notes Civ. Eng., Springer Science and Business Media Deutschland GmbH, 2023: pp. 153–163. https://doi.org/10.1007/978-981-19-3371-4_14.

[2] B.R. Rode, R. Khare, A review on development in design of multistage centrifugal pump, Adv. Comput. Des. 6 (2021) 43–53. https://doi.org/10.12989/acd.2021.6.1.43.

[3] M.N. Hawas, A.A. Mohammed, A.H. Al-Abbas, Improving the efficiency and performance of centrifugal pump through model development and numerical analysis for the pump impeller, Int. J. Mech. Eng. Robot. Res. 9 (2020) 60–65. https://doi.org/10.18178/ijmerr.9.1.60-65.

[4] Y. Wang, L. Zhou, M. Han, L. Shen, Performance Prediction of an Optimized Centrifugal Pump with High Efficiency, Fluid Dyn. Mater. Process. 19 (2023) 2215–2228. https://doi.org/10.32604/fdmp.2023.027188.

[5] H. Liu, Z. Cheng, Z. Ge, liang dong, cui dai, Collaborative improvement of efficiency and noise of bionic vane centrifugal pump based on multi-objective optimization, Adv. Mech. Eng. 13 (2021). https://doi.org/10.1177/1687814021994976.

[6] L. Zhang, X. Wang, P. Wu, B. Huang, D. Wu, Optimization of a centrifugal pump to improve hydraulic efficiency and reduce hydro-induced vibration, Energy 268 (2023). https://doi.org/10.1016/j.energy.2023.126677.

[7] D. Zhu, Z. Hu, Y. Chen, C. Wang, Y. Yang, J. Lu, X. Song, R. Tao, Z. Wang, W. Ma, Improvement Design of a Two-Stage Double-Suction Centrifugal Pump for Wide-Range Efficiency Enhancement, Water (Switzerland) 15 (2023). https://doi.org/10.3390/w15091785.

[8] C. Wang, Y. Yao, Y. Yang, X. Chen, H. Wang, J. Ge, W. Cao, Q. Zhang, Automatic optimization of centrifugal pump for energy conservation and efficiency enhancement based on response surface methodology and computational fluid dynamics, Eng. Appl. Comput. Fluid Mech. 17 (2023). https://doi.org/10.1080/19942060.2023.2227686.

[9] C. Wu, K. Pu, C. Li, P. Wu, B. Huang, D. Wu, Blade redesign based on secondary flow suppression to improve energy efficiency of a centrifugal pump, Energy 246 (2022) 123394. https://doi.org/10.1016/J.ENERGY.2022.123394.

[10] M.W. Heo, S.B. Ma, H.S. Shim, K.Y. Kim, High-efficiency design optimization of a centrifugal pump, J. Mech. Sci. Technol. 30 (2016) 3917–3927. https://doi.org/10.1007/s12206-016-0803-4.

[11] K. Wang, G. Luo, Y. Li, R. Xia, H. Liu, Multi-condition optimization and experimental verification of impeller for a marine centrifugal pump, Int. J. Nav. Archit. Ocean Eng. 12 (2020) 71–84. https://doi.org/10.1016/J.IJNAOE.2019.07.002.

[12] Y. Zhang, S. Hu, J. Wu, Y. Zhang, L. Chen, Modeling and multi-objective optimization of double suction centrifugal pump based on Kriging meta-models, Springer Proc. Math. Stat. 95 (2015) 251–261. https://doi.org/10.1007/978-3-319-08377-3_25.

[13] L. Zhou, W. Shi, S. Wu, Performance optimization in a centrifugal pump impeller by orthogonal experiment and numerical simulation, Adv. Mech. Eng. 2013 (2013). https://doi.org/10.1155/2013/385809.

[14] J. Feng, F. Benra, H.J. Dohmen, Numerical Study on Impeller-Diffuser Interactions with Radial Gap Variation Chair of Turbomachinery, 2006.

[15] M. Miyano, T. Kanemoto, D. Kawashima, A. Wada, T. Hara, K. Sakoda, Return Vane Installed in Multistage Centrifugal Pump, Int. J. Fluid Mach. Syst. 1 (2008) 57–63. https://doi.org/10.5293/ijfms.2008.1.1.057.

[16] S. Chakraborty, K.M. Pandey, Numerical Studies on Effects of Blade Number Variations on Performance of Centrifugal Pumps at 4000 RPM, 2011. https://doi.org/10.7763/ijet.2011.v3.262.

[17] Q. Zhang, W. Shi, Y. Xu, X. Gao, C. Wang, W. Lu, D. Ma, A new proposed return guide vane for compact multistage centrifugal pumps, Int. J. Rotating Mach. 2013 (2013). https://doi.org/10.1155/2013/683713.

[18] N. La Roche-Carrier, G. Dituba Ngoma, W. Ghie, Numerical investigation of a first stage of a multistage centrifugal pump: Impeller, diffuser with return vanes, and casing, ISRN Mech. Eng. 2013 (2013). https://doi.org/10.1155/2013/578072.

[19] A. Bowade, C. Parashar, A Review of Different Blade Design Methods for Radial Flow Centrifugal Pump, 3 (2014) 2347–3878. www.ijser.in.

[20] N. Zhang, D. Li, J. Jiang, B. Gao, D. Ni, A.A. Alubokin, W. Zhang, Experimental Investigation on Velocity Fluctuation in a Vaned Diffuser Centrifugal Pump Measured by Laser Doppler Anemometry, Energies 16 (2023). https://doi.org/10.3390/en16073223.

[21] Y. Duan, G. Li, J. Ge, H. Zou, W. Jiang, X. Zhu, Mechanism study on half vaned diffuser to improve efficiency of centrifugal pump, Phys. Fluids 36 (2024). https://doi.org/10.1063/5.0213884.

[22] K.M. Guleren, Automatic optimization of a centrifugal pump based on impeller–diffuser interaction, Proc. Inst. Mech. Eng. Part A J. Power Energy 232 (2018) 1004–1018. https://doi.org/10.1177/0957650918766688.

[23] A. Ichinose, N.K.M. Yoshimura, T. Hayashi, K. Miyagawa, Investigation of interaction

between tip leakage flow generated by unshrouded impeller and diffuser internal flow, Am. Soc. Mech. Eng. Fluids Eng. Div. FEDSM 3 (2018). https://doi.org/10.1115/FEDSM2018-83502.

[24] D. Khoeini, E. Shirani, M. Joghataei, Improvement of Centrifugal Pump Performance by Using Different Impeller Diffuser Angles with and Without Vanes, J. Mech. 35 (2019) 577–589. https://doi.org/10.1017/jmech.2018.39.

[25] P.V. Rao, G.V.R. Murty, G.V. Rao, CFD analysis of impeller-diffuser interaction in a centrifugal compressor with twisted vaned diffuser, Lect. Notes Mech. Eng. (2017) 911–922. https://doi.org/10.1007/978-81-322-2743-4_86.

[26] Q. Si, P. Dupont, A.C. Bayeul-Lainé, A. Dazin, O. Roussette, S. Yuan, An experimental study of the flow field inside the diffuser passage of a laboratory centrifugal pump, J. Fluids Eng. Trans. ASME 137 (2015). https://doi.org/10.1115/1.4029671.

[27] K. Alawadhi, B. Alzuwayer, T.A. Mohammad, M.H. Buhemdi, Design and optimization of a centrifugal pump for slurry transport using the response surface method, Machines 9 (2021). https://doi.org/10.3390/machines9030060.

[28] A.R. Al-Obaidi, Monitoring the performance of centrifugal pump under single-phase and cavitation condition: A CFD analysis of the number of impeller blades, J. Appl. Fluid Mech. 12 (2019) 445–459. https://doi.org/10.29252/jafm.12.02.29303.

[29] Z. ming Tong, J. ge Xin, S. guang Tong, Z. qin Yang, J. yun Zhao, J. hua Mao, Internal flow structure, fault detection, and performance optimization of centrifugal pumps, J. Zhejiang Univ. Sci. A 21 (2020) 85–117. https://doi.org/10.1631/jzus.A1900608.

[30] K.W. Cheah, T.S. Lee, S.H. Winoto, Z.M. Zhao, Numerical flow simulation in a centrifugal pump at design and off-design conditions, Int. J. Rotating Mach. 2007 (2007). https://doi.org/10.1155/2007/83641.

[31] O. Babayigit, O. Kocaaslan, M.H. Aksoy, K.M. Guleren, M. Ozgoren, Numerical identification of blade exit angle effect on the performance for a multistage centrifugal pump impeller, EPJ Web Conf. 92 (2015). https://doi.org/10.1051/epjconf/20159202003.

[32] M.N. Patil, G.S. Joshi, V.R. Naik, Validation in the improved performance of Centrifugal pump using CFD, Int. Res. J. Eng. Technol. (2017). www.irjet.net.

[33] D.G. Mentzos, M. D.; Margaris, D. P.; Papanikas, A numerical simulation of the impeller volute interaction in a centrifugal pump, 2004.

[34] R. Kumar Singh, Performance Enhancement and Numerical Simulation of Inter-Stage of Multistage Centrifugal Pump by varying number of blades Using CFD, (2023).

[35] L. Zhai, C. Lu, J. Guo, Z. Zhu, B. Cui, Flow Characteristics and Energy Loss of a Multistage Centrifugal Pump with Blade-Type Guide Vanes, J. Mar. Sci. Eng. 10 (2022).

https://doi.org/10.3390/jmse10020180.

[36] M.M. Shamsuddeen, S. Ma, S. Kim, J. Yoon, K. Lee, C. Jung, J. Kim, Flow Field Analysis and Feasibility Study of a Multistage Centrifugal Pump Designed for Low-Viscous Fluids, Appl. Sci. (2021).

[37] S.A.I. Bellary, A. Husain, A. Samad, R.A. Kanai, Performance optimization of centrifugal pump for crude oil delivery, J. Eng. Res. 15 (2018) 88–101. https://doi.org/10.24200/tjer.vol15iss1pp88-101.

[38] Y. Lin, X. Li, Z. Zhu, X. Wang, T. Lin, H. Cao, An energy consumption improvement method for centrifugal pump based on bionic optimization of blade trailing edge, Energy 246 (2022) 123323. https://doi.org/10.1016/j.energy.2022.123323.

[39] J. Pei, W. Wang, M.K. Osman, X. Gan, Multiparameter optimization for the nonlinear performance improvement of centrifugal pumps using a multilayer neural network, J. Mech. Sci. Technol. 33 (2019) 2681–2691. https://doi.org/10.1007/s12206-019-0516-6.

[40] Y. Shi, L. Tang, Y. Tan, W. Luo, Optimization of the Structural Parameters of a Plastic Centrifugal Pump, Fluid Dyn. Mater. Process. 18 (2022) 713–736. https://doi.org/10.32604/fdmp.2022.018434.

[41] X. Yang, D. Tian, Q. Si, M. Liao, J. He, X. He, Z. Liu, Flow Loss Analysis and Optimal Design of a Diving Tubular Pump, Machines 10 (2022). https://doi.org/10.3390/machines10030175.

[42] W. Wang, J. Sun, J. Liu, J. Zhao, J. Pei, J. Wang, Introducing Non-Hierarchical RSM and MIGA for Performance Prediction and Optimization of a Centrifugal Pump under the Nominal Condition, Processes 10 (2022). https://doi.org/10.3390/pr10081529.

[43] A.M. S[l], J.M. Issac, II METHODOLOGY 2.1.1 specification of the pump, 2015. www.ijser.in.

[44] O. Petit, H. Nilsson, Numerical investigations of unsteady flow in a centrifugal pump with a vaned diffuser, Int. J. Rotating Mach. 2013 (2013). https://doi.org/10.1155/2013/961580.

[45] W. Li, H. Li, M. Liu, L. Ji, R.K. Agarwal, S. Jin, Energy dissipation mechanism of tip-leakage cavitation in mixed-flow pump blades, Phys. Fluids 36 (2024). https://doi.org/10.1063/5.0183540.

[46] L. Zhou, Y. Yang, W. Shi, W. Lu, D. Ye, Influence of outlet edge position of diffuser vane on performance of deep-well centrifugal pump, Paiguan Jixie Gongcheng Xuebao/Journal Drain. Irrig. Mach. Eng. 34 (2016) 1028–1034. https://doi.org/10.3969/j.issn.1674-8530.16.0232.

[47] R. Barrio, J. Parrondo, E. Blanco, Numerical analysis of the unsteady flow in the near-tongue region in a volute-type centrifugal pump for different operating points, Comput. Fluids 39

(2010) 859–870. https://doi.org/10.1016/j.compfluid.2010.01.001.

[48] L. Zhang, X. Wang, P. Wu, B. Huang, D. Wu, Optimization of a centrifugal pump to improve hydraulic efficiency and reduce hydro-induced vibration, Energy 268 (2023) 126677. https://doi.org/10.1016/J.ENERGY.2023.126677.

[49] Y. Wang, X. Huo, Multiobjective Optimization Design and Performance Prediction of Centrifugal Pump Based on Orthogonal Test, Adv. Mater. Sci. Eng. 2018 (2018). https://doi.org/10.1155/2018/6218178.

[50] B. Jafarzadeh, A. Hajari, M.M. Alishahi, M.H. Akbari, The flow simulation of a low-specific-speed high-speed centrifugal pump, Appl. Math. Model. 35 (2011) 242–249. https://doi.org/10.1016/j.apm.2010.05.021.

[51] B.R. Chakraborty, Sujoy KM Pandey, Numerical Analysis on Effects of Blade Number Variations on Performance of Centrifugal Pumps with Various Rotational Speeds, 2012. http://inpressco.com/category/ijcet.

[52] E.M. Ofuchi, H. Stel, T. Sirino, T.S. Vieira, F.J. Ponce, S. Chiva, R.E.M. Morales, Numerical investigation of the effect of viscosity in a multistage electric submersible pump, Eng. Appl. Comput. Fluid Mech. 11 (2017) 258–272. https://doi.org/10.1080/19942060.2017.1279079.

[53] D. Arumugam, K. Sivasailam, Pressure fluctuation study in the stages of a multistage pump at best efficiency points under various operating speeds, J. Eng. Res. 10 (2022) 227–247. https://doi.org/10.36909/jer.10257.

[54] A. Ali, J. Yuan, F. Deng, B. Wang, L. Liu, Q. Si, N.A. Buttar, Research progress and prospects of multi-stage centrifugal pump capability for handling gas–liquid multiphase flow: Comparison and empirical model validation, Energies 14 (2021). https://doi.org/10.3390/en14040896.

[55] Y. Bai, F. Kong, B. Xia, Y. Liu, Effect of blade number matching of impeller and diffuser in high-speed rescue pump, Adv. Mech. Eng. 9 (2017). https://doi.org/10.1177/1687814017703595.

[56] T. Goel, D.J. Dorney, R.T. Haftka, W. Shyy, Improving the hydrodynamic performance of diffuser vanes via shape optimization, Comput. Fluids 37 (2008) 705–723. https://doi.org/10.1016/j.compfluid.2007.10.002.

[57] S. Derakhshan, M. Pourmahdavi, E. Abdolahnejad, A. Reihani, A. Ojaghi, Numerical shape optimization of a centrifugal pump impeller using artificial bee colony algorithm, Comput. Fluids 81 (2013) 145–151. https://doi.org/10.1016/j.compfluid.2013.04.018.

[58] Q. Si, S. Yuan, J. Yuan, C. Wang, W. Lu, Multiobjective optimization of low-specific-speed multistage pumps by using matrix analysis and CFD method, J. Appl. Math. 2013 (2013). https://doi.org/10.1155/2013/136195.

[59] Y. Lin, L. Li, S. Yang, X. Chen, X. Li, Z. Zhu, Performance prediction and optimization of hydrogenation feed pump based on particle swarm optimization–least squares support vector regression surrogate model, Eng. Appl. Comput. Fluid Mech. 18 (2024). https://doi.org/10.1080/19942060.2024.2315985.

[60] K. Seeniappan, S. Kaliappan, M.D. Rajkamal, D. Balamurali, Numerical analysis of centrifugal pump impeller for performance improvement Analysis View project Renewable energy resources View project NUMERICAL ANALYSIS OF CENTRIFUGAL PUMP IMPELLER FOR PERFORMANCE IMPROVEMENT, 2016. https://www.researchgate.net/publication/305444111.

[61] S. Kim, K.Y. Lee, J.H. Kim, J.H. Kim, U.H. Jung, Y.S. Choi, High performance hydraulic design techniques of mixed-flow pump impeller and diffuser, J. Mech. Sci. Technol. 29 (2015) 227–240. https://doi.org/10.1007/s12206-014-1229-5.

[62] H. Zhao, Neural network with data augmentation in multi-objective prediction of multi-stage pump, (2020). http://arxiv.org/abs/2002.02402.

[63] W. Li, Y. Long, L. Ji, H. Li, S. Li, Y. Chen, Q. Yang, Effect of circumferential spokes on the rotating stall flow field of mixed-flow pump, Energy 290 (2024). https://doi.org/10.1016/j.energy.2024.130260.

[64] H. Zhao, Neural network with data augmentation in multi-objective prediction of multi-stage pump, 2020. http://arxiv.org/abs/2002.02402.

[65] S. Srivastava, A.K. Roy, K. Kumar, Design analysis of Mixed flow pump impeller blades using ANSYS and prediction of its parameters using artificial neural network, in: Procedia Eng., Elsevier Ltd, 2014: pp. 2022–2031. https://doi.org/10.1016/j.proeng.2014.12.445.

[66] C. Wang, W. Shi, X. Wang, X. Jiang, Y. Yang, W. Li, L. Zhou, Optimal design of multistage centrifugal pump based on the combined energy loss model and computational fluid dynamics, Appl. Energy 187 (2017) 10–26. https://doi.org/10.1016/j.apenergy.2016.11.046.

[67] N. Condition, Introducing Non-Hierarchical RSM and MIGA for Performance Nominal Condition, (2022).

[68] S. Thakkar, H. Vala, V.K. Patel, R. Patel, Performance improvement of the sanitary centrifugal pump through an integrated approach based on response surface methodology, multi-objective optimization and CFD, J. Brazilian Soc. Mech. Sci. Eng. 43 (2021). https://doi.org/10.1007/s40430-020-02753-0.

[69] W. Jiang, J. Pei, W. Wang, S. Yuan, Optimization for First Stage of Multistage Pump Based on Response Surface Methodology, IOP Conf. Ser. Earth Environ. Sci. 627 (2021). https://doi.org/10.1088/1755-1315/627/1/012017.

[70] G. Pavesi, Impeller Volute and Diffuser Interaction, n.d.

http://www.rto.nato.int/abstracts.asp.

[71] H.-W. Oh, Hydrodynamic Characteristics of Vaned-Diffuser and Return-Channel for a Multistage Centrifugal Pump, J. Fluid Mach. 14 (2011) 54–60. https://doi.org/10.5293/kfma..2011.14.6.054.

[72] D. Yadav, C. Parashar, Design and Performance analysis of Crossflow turbine Using CFD, Maulana Azad National institute of Technology, Bhopal, 2019.

[73] D. Yadav, R.K. Singh, K. Manjunath, Response surface method-based hydraulic performance optimization of a single-stage centrifugal pump, Int. J. Numer. Methods Fluids (2024). https://doi.org/10.1002/fld.5332.

[74] Q.H. Zhang, Y. Xu, W.D. Shi, W.G. Lu, Research and development on the hydraulic design system of the guide vanes of multistage centrifugal pumps, IOP Conf. Ser. Earth Environ. Sci. 15 (2012). https://doi.org/10.1088/1755-1315/15/3/032030.

[75] D. Yadav, R.K. Singh, M. Kumarswamy, Numerical simulation of inter-stage of multistage centrifugal pump by varying number of blades, Can. J. Chem. Eng. 102 (2024) 2921–2935. https://doi.org/10.1002/cjce.25231.

[76] A.S. Thomareis, G. Dimitreli, Techniques used for processed cheese characterization, in: Process. Cheese Sci. Technol. Ingredients, Manuf. Funct. Qual. Regul., 2022: pp. 295–349. https://doi.org/10.1016/B978-0-12-821445-9.00007-8.

[77] L. Wang, Z. Luo, A. Shahbazi, Optimization of simultaneous saccharification and fermentation for the production of ethanol from sweet sorghum (Sorghum bicolor) bagasse using response surface methodology, Ind. Crops Prod. 42 (2013) 280–291. https://doi.org/10.1016/j.indcrop.2012.06.005.

[78] M.R.I. Shishir, W. Chen, Trends of spray drying: A critical review on drying of fruit and vegetable juices, Trends Food Sci. Technol. 65 (2017) 49–67. https://doi.org/10.1016/j.tifs.2017.05.006.

[79] W.R. Myers, Response Surface Methodology, in: Encycl. Biopharm. Stat., 2010: pp. 1171–1179. https://doi.org/10.3109/9781439822463.187.

[80] S.J.M. Breig, K.J.K. Luti, Response surface methodology: A review on its applications and challenges in microbial cultures, Mater. Today Proc. 42 (2021) 2277–2284. https://doi.org/10.1016/j.matpr.2020.12.316.

[81] L. Vera Candioti, M.M. De Zan, M.S. Cámara, H.C. Goicoechea, Experimental design and multiple response optimization. Using the desirability function in analytical methods development, Talanta 124 (2014) 123–138. https://doi.org/10.1016/j.talanta.2014.01.034.

[82] A. Weremfo, S. Abassah-Oppong, F. Adulley, K. Dabie, S. Seidu-Larry, Response surface methodology as a tool to optimize the extraction of bioactive compounds from plant sources,

J. Sci. Food Agric. 103 (2023) 26–36. https://doi.org/10.1002/jsfa.12121.

[83] A.T. Nair, A.R. Makwana, M.M. Ahammed, The use of response surface methodology for modelling and analysis of water and wastewater treatment processes: A review, Water Sci. Technol. 69 (2014) 464–478. https://doi.org/10.2166/wst.2013.733.

[84] A.A. Khalid, A.M. Gora, A.D. Rafindadi, S.I. Haruna, Y.E. Ibrahim, Response Surface Methodology Approach for the Prediction and Optimization of the Mechanical Properties of Sustainable Laterized Concrete Incorporating Eco-Friendly Calcium Carbide Waste, Infrastructures 9 (2024). https://doi.org/10.3390/infrastructures9110206.

[85] L.M.S. Pereira, T.M. Milan, D.R. Tapia-Blácido, Using Response Surface Methodology (RSM) to optimize 2G bioethanol production: A review, Biomass and Bioenergy 151 (2021). https://doi.org/10.1016/j.biombioe.2021.106166.

[86] Response Surface — Lesson 6 - ANSYS Innovation Courses. (2021, December 20). ANSYS Innovation Courses., (n.d.). https://courses.ansys.com/index.php/courses/plate-with-a-hole-optimization/lessons/response-surface-lesson-6/.

[87] S. Lamidi, N. Olaleye, Y. Bankole, A. Obalola, E. Aribike, I. Adigun, Applications of Response Surface Methodology (RSM) in Product Design, Development, and Process Optimization, Response Surf. Methodol. - Res. Adv. Appl. (2023). https://doi.org/10.5772/intechopen.106763.

[88] R. Meega, K. Rupak, Response surface methodology (RSM): An overview to analyze multivariate data, Indian J. Microbiol. Res. 2023 (2023) 18202.

[89] D. of Experiments, Response Surface Methodology, (2018).

[90] W. Cao, H. Wang, X. Yang, X. Leng, Optimization of Guide Vane Centrifugal Pumps Based on Response Surface Methodology and Study of Internal Flow Characteristics, J. Mar. Sci. Eng. 11 (2023). https://doi.org/10.3390/jmse11101917.

Research Publications from the thesis

List of Publications in International Journals

1. Durvesh Yadav, Raj Kumar Singh, Manjunath K. Numerical simulation of inter-stage of two stage multistage pump by varying impeller blades, **The Canadian Journal of Chemical Engineering,** Volume 102, 2024, 2921-2935 **https://doi.org/10.1002/cjce.25231**. **(SCIE, Published)**
2. Durvesh Yadav, Raj Kumar Singh, Manjunath K., Response Surface Method-Based Hydraulic Performance Optimization of a Single-Stage Centrifugal Pump, **International Journal for Numerical Methods in Fluids**, Volume 97, 2025, 20-43, **https://doi.org/10.1002/fld.5332 (SCIE, Published)**
3. Durvesh Yadav, Raj Kumar Singh, Manjunath K., Non-dimensionless Parametric Optimization of Hydraulic Performance of Centrifugal Pump using Response Surface Analysis. **Progress in Computational Fluid Dynamics, An Int. J.. (SCIE, Online)** . doi: 10.1504/PCFD.2025.10070078

List of Publications in International Conferences

1. "International Conference on Recent Advances in Fluid Mechanics", held at Manipal Institute of Technology, MAHE, Manipal, from 4 to 6th October 2022. Title of paper presented – Stress and Deformation Analysis of Impeller Blade of Mixed Flow Pump using ANSYS.

2. "International Conference on Recent Advances in Fluid Mechanics and Nanoelectronics", held at Manipal Institute of Technology, MAHE, Manipal, from 12 to 14th July 2023. Title of paper presented – Optimization of Single Stage Centrifugal Pump by Using Response Surface Methodology.

3. "International Conference on Emerging Aspects of Manufacturing, Thermal and Design Engineering" held at NIT Hamirpur, Himachal Pradesh, from 16th to 18th December 2024. Title of paper presented- Comparative Stress Analysis of a Mixed Flow Impeller Blade using different materials in ANSYS.

BRIEF PROFILE

I, Durvesh, completed B.Tech. in Mechanical Engineering from Uttar Pradesh Technical University, Lucknow, India, and M.Tech. in Hydropower Engineering from National Institute of Technology, Bhopal, India. Currently, I am working as a Research Scholar in the Department of Mechanical Engineering at Delhi Technological University, Delhi, India. I have enrolled for a Ph.D. in the Department of Mechanical Engineering at Delhi Technological University, Delhi-42, (India) under the supervision of Prof. Rajkumar Singh and Dr. Manjunath K. I have 2 SCI/SCIE published papers and 1 SCI/SCIE accepted papers in the reputed journals. I have a diverse educational background and expertise in Computational Fluid Dynamics (CFD), underscoring my proficiency in both Mechanical and Hydropower engineering domains. I have presented 3 conference papers at 3 international Conferences.